THE UNIVERSITY OF QUEENSLAND

SCHOOL OF
CIVIL ENGINEERING

REPORT CH79/10

TURBULENCE AND SEDIMENT PROCESSES IN THE TIDAL BORE OF THE GARONNE RIVER: FIRST OBSERVATIONS

AUTHOR: Hubert CHANSON, Pierre LUBIN, Bruno SIMON and David REUNGOAT

Turbulence and Sediment Processes in the Tidal Bore of the Garonne River: First Observations

by

Hubert CHANSON

Professor, School of Civil Engineering, The University of Queensland, Brisbane QLD 4072, Australia, Ph.: (61 7) 3365 3619, Fax: (61 7) 3365 4599, Email: h.chanson@uq.edu.au

Pierre LUBIN

Lecturer, Université de Bordeaux, IPB, CNRS UMR 8508, ENSCBP, 16 avenue Pey Berland, 33607 Pessac, France, E-mail: lubin@enscbp.fr

Bruno SIMON

Ph.D. candidate, Université de Bordeaux, CNRS UMR 8508, ENSCBP, 16 avenue Pey Berland, 33607 Pessac, France

and

David REUNGOAT

Lecturer, Université de Bordeaux, CNRS UMR 8508, ENSCBP, 16 avenue Pey Berland, 33607 Pessac, France, E-mail: reungoat@enscbp.fr

Tidal bore of the Garonne River at Arcins on 10 September 2010

ABSTRACT

A tidal bore is a series of waves propagating upstream as the tidal flow turns to rising, forming during spring tide conditions when the tidal range exceeds 4 to 6 m and the flood tide is confined to a narrow funnelled estuary. After the formation of the bore, there is an abrupt rise in water depth at the bore front that is discontinuity in the water depth, and pressure and velocity fields. To date, the field observations of tidal bores are very limited, and most studies were conducted with a very-coarse resolution in terms of temporal and spatial scales: it is challenging to analyse conclusively these data. In the present study, some detailed turbulence field measurements were conducted continuously at high-frequency (64 Hz) in the tidal bore of the Garonne River in September 2010. The turbulent velocity components were sampled with an acoustic Doppler velocimeter (ADV) with its sampling volume located 0.8 m beneath the free-surface. The tidal bore propagation in the Garonne River was observed on both 10 and 11 Sept. 2010. The tidal bore was undular as it passed in front of the sampling site. The passage of the tidal bore was characterised by a pseudo-chaotic wave motion lasting for several minutes after the bore. At the sampling location, the free-surface elevation rose very rapidly. The tidal bore Froude number was estimated from the channel bathymetry and tidal bore observations: it was equal to 1.30 and 1.20 on 10 and 11 Sept. 2010 respectively. The turbulent velocity data showed the marked impact of the tidal bore propagation. The longitudinal velocity component highlighted some rapid flow deceleration during the passage of the tidal bore, associated with a sudden rise in the free surface elevation, and a flow reversal after the tidal bore front passage. The observations were consistent with some earlier field and laboratory results. The tidal bore passage was further characterised by some large fluctuations of all three turbulent velocity components. The Reynolds stress data indicated some large and rapid turbulent stress fluctuations during the tidal bore and flood flow. The Reynolds stress magnitudes were significantly larger than during the ebb tide, and some substantial normal and tangential stress fluctuations were observed. The ADV backscatter intensity was calibrated in terms of the suspended sediment concentration in laboratory using the soft mud bed material. The results provided an unique characterisation of the turbulence and sediment flux beneath to the free-surface during the tidal bore. The arrival of the tidal bore was characterised by a rapid reversal in suspended sediment flux. Prior the tidal bore, the net sediment mass transfer per area was positive downstream. After the passage of the bore, the net sediment mass transfer per unit area was negative and its magnitude was 30 times larger than the ebb tide net flux. A striking feature of the present field data set was the large and rapid fluctuations in turbulent velocities and suspended sediment flux during the tidal bore and flood flow. This was not documented to date, but an important difference between the present ADV data set from earlier reported field measurements was that the present data were collected continuously at relatively high frequency (64 Hz) during a relatively long period (at least 2 hours).

Keywords: Tidal bore, Garonne River, Field measurements, Turbulence, Turbulent mixing, Suspended sediment concentration, Sediment processes, Acoustic Doppler velocimetry.

TABLE OF CONTENTS

APPENDICES

REFERENCES

LIST OF SYMBOLS

The following symbols are used in this report:

A   channel cross-section area (m^2);

A_1 initial channel cross-section area (m^2) immediately prior to the tidal bore passage;

A_2 channel cross-section area (m^2) immediately after to the tidal bore passage;

Ampl ADV signal amplitude (counts);

B   free-surface width (m);

B_1 initial free-surface width (m) immediately prior to the tidal bore passage;

BSI   backscatter intensity defined as:

$$BSI = 10^{-5} \times 10^{0.043 \times Ampl}$$

d   water depth (m);

d_1 initial water depth (m) immediately prior to the tidal bore passage;

Fr   Froude number;

Fr_1 tidal bore Froude number defined as:

$$Fr_1 = \frac{V_1 + U}{\sqrt{g \times d_1}}$$

g   gravity acceleration (m/s^2);

I_b acoustic backscatter intensity;

N   number of data points;

m   dimensionless exponent;

q_s instantaneous advective suspended sediment flux per unit area ($kg/m^2/s$) defined as:

$$q_s = SSC \times V_x$$

SSC   suspended sediment concentration (kg/m^3);

s   relative density of wet sediment;

t   time (s);

T   integration period (s);

U   tidal bore celerity (m/s) for an observer standing on the bank, positive upstream;

V   flow velocity (m/s);

V_1 initial flow velocity (m/s) immediately prior to the tidal bore passage;

V_x instantaneous longitudinal velocity component (m/s);

V_y instantaneous transverse velocity component (m/s);

V_z instantaneous vertical velocity component (m/s);

$\overline{V}$ variable interval time-averaged velocity (m/s)

v   instantaneous velocity fluctuation (m/s) : $v = V - \overline{V}$;

v_x instantaneous fluctuation (m/s) of V_x;

v_y instantaneous fluctuation (m/s) of V_y;

v_z instantaneous fluctuation (m/s) of V_z;

x   longitudinal distance (m) positive downstream;

y   transverse distance (m) positive towards the Arcins island;

z   vertical distance (m) positive upwards;

μ   effective viscosity (Pa.s);

ρ   water density (kg/m^3);

τ   shear stress (Pa);

τ_c apparent yield stress (Pa);

τ_o boundary shear stress (Pa);

$(\tau_o)_c$ critical boundary shear stress (Pa) for bed load motion;

Subscript

x   longitudinal direction positive downstream;

y   transverse direction positive towards the Arcins island;

z   vertical direction positive upwards;

1   flow property immediately prior to the tidal bore passage;

2   flow property immediately after the tidal bore passage;

Abbreviations

ADV   acoustic Doppler velocimeter;

BSI   acoustic backscatter intensity;

h   hour;

IGN   Institut National Géographique;

min.   minute;

Nb   number;

SSC   suspended sediment concentration;

Std   standard deviation;

s   second

VITA   variable-interval time average.

Note

All times are expressed in local French times (GMT + 1).

GLOSSARY

Aggradation: raise in channel bed elevation caused by deposition of sediment material. Another term is accretion.

Bed load: sediment material transported by rolling, sliding and saltation motion along the bed.

Bélanger equation: momentum equation applied across a hydraulic jump in a horizontal channel; the equation was named after Jean-Baptiste BÉLANGER (1841) (CHANSON 2009).

BERNOULLI: Daniel BERNOULLI (1700-1782) was a Swiss mathematician, physicist and botanist who developed the Bernoulli equation in his "Hydrodynamica, de viribus et motibus fluidorum" textbook (1st draft in 1733, 1st publication in 1738, Strasbourg).

BIDONE: Giorgio BIDONE (1781-1839) was an Italian hydraulician. His experimental investigations on the hydraulic jump were published between 1819 and 1826.

BORDA: Jean-Charles de BORDA (1733-1799) was a French mathematician and military engineer. He achieved the rank of *Capitaine de Vaisseau* and participated to the U.S. War of Independence with the French Navy. He investigated the flow through orifices and developed the Borda mouthpiece.

BOSSUT: Abbé Charles BOSSUT (1730-1804) was a French ecclesiastic and experimental hydraulician, author of a hydrodynamic treaty (BOSSUT 1772).

BRESSE: Jacques Antoine Charles BRESSE (1822-1883) was a French applied mathematician and hydraulician. He was Professor at the *Ecole Nationale Supérieure des Ponts et Chaussées*, Paris as the successor of J.B. BELANGER. His contribution to gradually-varied flows in open channel hydraulics is considerable (BRESSE 1860).

BUAT: Comte Pierre Louis George du BUAT (1734-1809) was a French military engineer and hydraulician. He was a friend of Abbé C. BOSSUT. Du BUAT is considered as the pioneer of experimental hydraulics. His textbook (BUAT 1779) was a major contribution to flow resistance in pipes, open channel hydraulics and sediment transport.

CARNOT: Lazare N.M. CARNOT (1753-1823) was a French military engineer, mathematician, general and statesman who played a key-role during the French Revolution.

CAUCHY: Augustin Louis de CAUCHY (1789-1857) was a French engineer from the *Corps des Ponts-et-Chaussées*. He devoted himself later to mathematics and he taught at *Ecole Polytechnique*, Paris, and at the *Collège de France*. He worked with Pierre-Simon LAPLACE and J. Louis LAGRANGE. In fluid mechanics, he contributed greatly to the analysis of wave motion.

CHÉZY: Antoine CHÉZY (1717-1798) (or Antoine de CHÉZY) was a French engineer and member of the French *Corps des Ponts-et-Chaussées*. He designed canals for the water supply of the city of Paris. In 1768 he proposed a resistance formula for open channel flows called the Chézy equation. In 1798, he became Director of the *Ecole Nationale Supérieure des Ponts et Chaussées* after teaching there for many years.

Conjugate depth: In open channel flow, the solution of the momentum equation at a transition between supercritical and subcritical flow gives two flow depths (upstream and downstream flow depths). They are called conjugate or sequent depths.

CORIOLIS: Gustave Gaspard CORIOLIS (1792-1843) was a French mathematician and engineer of the *Corps des Ponts-et-Chaussées* who first described the Coriolis force (i.e. effect of motion on a rotating body).

DARCY: Henri Philibert Gaspard DARCY (1805-1858) was a French civil engineer. He studied at *Ecole Polytechnique* between 1821 and 1823, and later at the *Ecole Nationale Supérieure des Ponts et Chaussées* (BROWN 2002). He performed numerous experiments of flow resistance in pipes (DARCY 1858) and in open channels (DARCY and BAZIN 1865), and of seepage flow in porous media (DARCY 1856a,b). He gave his name to the Darcy-Weisbach friction factor and to the Darcy law in porous media.

DUPUIT: Arsène Jules Etienne Juvénal DUPUIT (1804-1866) was a French engineer and economist. His expertise included road construction, economics, statics and hydraulics.

Estuary: water passage where the tide meets a river flow. An estuary may be defined as a region where salt water is diluted with fresh water and the effects of the tides are felt.

Éteules: French for whelps.

EYTELWEIN: Johann EYTELWEIN (1764-1848) was a German mathematician and engineer.

Fawer jump: undular hydraulic jump.

FROUDE: William FROUDE (1810-1879) was a English naval architect and hydrodynamicist who invented the dynamometer and used it for the testing of model ships in towing tanks. He was assisted by his son Robert Edmund FROUDE who, after the death of his father, continued some of his work, and he used REECH's law of similarity to study the resistance of model ships (FROUDE 1872).

Froude number: The Froude number is proportional to the square root of the ratio of the inertial forces over the weight of fluid. The Froude number is used generally for scaling free surface flows, open channels and hydraulic structures. Although the dimensionless number was named after William FROUDE, several French researchers used it before. BÉLANGER (1828), DUPUIT (1848) and BRESSE (1860) highlighted the significance of the number to differentiate the open channel flow regimes, and BAZIN (1865) confirmed experimentally the findings. Ferdinand REECH introduced the dimensionless number for testing ships and propellers in 1852 (REECH 1852). The number is called the Reech-Froude number in France.

Gradually varied flow: A gradually varied flow is characterised by relatively small changes in velocity and pressure distributions over a short distance (e.g. long waterway).

Hydraulic jump: stationary transition from a rapid, high-velocity flow to a slower fluvial flow motion.

LAGRANGE: Joseph-Louis LAGRANGE (1736-1813) was a French mathematician (CHANSON 2007). During the 1789 Revolution, he worked on the committee to reform the metric system. He was Professor of mathematics at the *École Polytechnique* from the start.

Left bank: looking downstream, towards the river mouth, the left bank is on the left.

Mascaret: French for tidal bore.

Mile: See nautical mile.

MONGE: Gaspard MONGE (1746-1818), Comte de Péluse, was a French mathematician who invented descriptive geometry and pioneered the development of analytical geometry. He was a prominent figure during the French Revolution, helping to establish the *Système métrique* and the *École Polytechnique*, and being Minister for the Navy and colonies between 1792 and 1793.

Nautical mile: a nautical mile equals 1,852 m.

PITOT: Henri PITOT (1695-1771) was a French mathematician, astronomer and hydraulician. He was a member of the French *Académie des Sciences* from 1724. He invented the Pitot tube to measure flow velocity in the Seine river, with the first presentation in 1732 at the *Académie des Sciences de Paris*.

POISSON: Siméon Denis POISSON (1781-1840) was a French mathematician and scientist. He developed the theory of elasticity, a theory of electricity and a theory of magnetism.

Pororoca: tidal bore of the Amazon river in Brazil.

Positive surge: a positive surge results from a sudden increase in flow depth. It is an abrupt wave front. The unsteady flow conditions may be solved as a quasi-steady flow situation and a positive surge is called a hydraulic jump in translation.

PRONY: Gaspard Clair François Marie Riche de PRONY (1755-1839) was a French mathematician and engineer. He succeeded A. CHÉZY as director general of the *Ecole Nationale Supérieure des Ponts et Chaussées*, Paris during the French Revolution.

Rapidly varied flow: open channel flow characterised by large changes over a short distance (e.g. sharp-crested weir, sluice gate, hydraulic jump).

REECH: Ferdinand REECH (1805-1880) was a French naval instructor who proposed first the Reech-Froude number in 1852 for the testing of model ships and propellers (REECH 1852).

Rapidly varied flow: A rapidly varied flow is characterised by large changes over a short distance (e.g. luice gate, hydraulic jump, tidal bore front).

Right bank: looking downstream, towards the river mouth, the right bank is on the right.

Roller: in hydraulic engineering, a series of large-scale turbulent eddies: e.g., the roller of a hydraulic jump.

Shock waves: in high-velocity, supercritical flows, a flow disturbance (e.g. change of direction, contraction) induces the development of shock waves propagating at the free-surface across the channel. Shock waves are called also lateral shock waves, oblique hydraulic jumps, Mach waves, cross-waves, diagonal jumps.

Sequent depth: in open channel flow, another name for conjugate depth.

Stilling basin: hydraulic structure for dissipating the energy of the flow downstream of a spillway, outlet work, chute or canal structure. In many cases, a hydraulic jump is used as the energy dissipator within the stilling basin.

Supercritical flow: open channel flow characterised by a Froude number greater than unity.

Tidal bore: positive surge of tidal origin developing in an estuary as the tide turns to rising.

Undular hydraulic jump: stationary hydraulic jump characterised by steady free-surface undulations downstream of the jump and by the absence of a formed roller. An undular jump flow is called a Fawer jump in homage to Carlos FAWER's (1937) work.

Weak jump: A weak hydraulic jump is characterised by a marked roller, no free-surface undulation and low energy loss. It is usually observed after the disappearance of undular hydraulic jump with increasing upstream Froude numbers.

Whelps: waves behind the leading edge of the tidal bore front. For an observer standing on the bank, the whelps are the wave trains (incl. secondary waves) seen after the surge front passage.

TIDAL BORE VOCABULARY

Language	Positive surge of tidal origin	Local bore names	Undular waves	Chaotic wave motion
English	tidal bore		undulations whelps	
French	*mascaret*	*barre* ou *flot* (Seine) *montant* (Garonne)	*éteules*	*éteules* *ressac*
Portuguese (Brazil)	*pororoca*	*pororoca* (Amazon, Guama, Araguari ...)		
Spanish		*burro* (Colorado)		
Gallic	*aegir* (or *eagre*)			
Malay	*benak*			
Papua	*ibua*	*ibua*		
Bengali (Bangladesh)		*ban*		
India	*bahu*			

Language	Low freshwater inflow conditions	Spring tides	Neap tides	Tidal range
English		spring tides	neap tides	tidal range
French	*étiage*	*grandes marées*	*mortes eaux*	*marnage*

Language	Dam break wave
English	dam break wave
French	*onde de rupture de barrage*
German	*Dammbruchwellen*

1. INTRODUCTION

1.1 PRESENTATION

A tidal bore is a series of waves propagating upstream as the tidal flow turns to rising. It forms during spring tide conditions when the tidal range exceeds 4 to 6 m and the flood tide is confined to a narrow funnelled estuary. With time, the leading edge of the flood tidal wave becomes steeper and steeper until it forms a wall of water: i.e., the tidal bore. After the formation of the bore, there is an abrupt rise in water depth at the bore front that is discontinuity in the water depth, and pressure and velocity fields. Figure 1-1 shows the tidal bore of the Qiantang River in China, of the Dordogne River in France and of the Sélune River in the Baie du Mont Saint Michel in France.

A tidal bore induces a strong turbulent mixing in the estuarine zone, and the effects may be felt along considerable distances. For example, the Hooghly bore (India) may propagate more than 80 km flowing past the port of Calcutta. All the observations suggest that the tidal bores have a significant effect on the natural waterways and their ecology. The arrival of the tidal bore is associated with some intense mixing and upstream advection of the suspended material (BRANNER 1884, TESSIER and TERWINDT 1990, WOLANSKI et al. 2001,2004). The evidences of turbulent mixing induced by tidal bores are challenging (KJERFVE and FERREIRA 1993, TULL 1997, CHEN 2003). The tidal bore affected estuaries are the natural habitats of several fish species and aquatic life forms (RULIFSON and TULL 1999, CHANSON and TAN 2010). These estuaries are the natural habitat, the feeding zone and breeding grounds of several forms of wildlife. In Sumatra, for example, the Rokan River estuary is renowned for its abundance of fish, the organic matter being continually brought by the river while the turbulent mixing and aeration induced by the tidal bore contribute to the growth of many species of finfish and shrimps (BUTCHER 2004). A tidal bore is also an integral part of the cultural heritage in many regions: the Qiantang River bore in China, the Severn River bore in UK, the Dordogne River in France for example.

To date, the field observations of tidal bores are very limited (Table 1-1). Table 1-1 lists a few field experiments. Most studies were conducted with a very-coarse resolution in terms of temporal and spatial scales, and it is challenging to analyse conclusively the data. The data sets cannot give a complete description of the whole flow field, and more detailed informations are needed.

(A) Tidal bore of the Qiantang River (China) on 23 July 2009 (Courtesy Jean-Pierre GIRARDOT) - The bore front advances from top left to bottom right

(B) Tidal bore of the Dordogne River at Port de Saint Pardon (France) on 11 Sept. 2010 at 07:11 (sunrise) - Bore propagation from left to right

(C) Breaking tidal bore of the Sélune River downstream of Pointe du Grouin du Sud on 24 Sept. 2010 at 19:29 - Bore propagation from right to left at sunset - Note the Mont Saint Michel in the background left and an old WWII German truck in the foreground right

Fig. 1-1 - Photographs of tidal bores

1.2 TIDAL BORES IN FRANCE

A number of French rivers and estuaries are affected by a tidal bore process (Fig. 1-2A). A famous tidal bore was the *mascaret* of the Seine River (MALANDAIN 1988). It had had a sinister reputation because its height could reach up to 7.3 m and the bore front travelled at a celerity of about up to 10 m/s (BAZIN 1865, TRICKER 1965). In the Baie du Mont Saint Michel, several tidal bore processes are experienced in rivers and creeks (TESSIER and TERWINDT 1994, CHANSON 2004,2008) (Fig. 1-1C). There, the largest bores are those of the Couesnon, Sélune and Sée Rivers, although the Couesnon River bore is now affected by major works ([1]) in 2007-2011 with the destruction of part of the digue and of the barrage, and the completion of a new flushing system in 2009. In Brittany (*Bretagne*), smaller tidal bores are observed in the Baie de la Frênaye, in the Baie de l'Arguenon and at Saint Briac sur Mer (CHANSON 2008). In the South-West of France, some large tidal bores are observed in the Gironde estuary, and the Dordogne and Garonne Rivers. In the Gironde Estuary, a tidal bore develops during spring tides and continues upstream into the Dordogne and Garonne Rivers. Surfers and kayakers regularly ride the Dordogne and Garonne River tidal bores (Fig. 1-1B), and this has been the topic of several television documentaries.

---

[1] Travaux de Rétablissement du Caractère Maritime du Mont-Saint-Michel (LEFEUVRE and BOUCHARD 2002).

Table 1-1 - Field observations of tidal bores

Reference	Initial flow V_1 m/s	d_1 m	Instrument	Channel geometry	Remarks
(1)	(2)	(3)	(4)	(5)	(6)
LEWIS (1972)	0 to +0.2	0.9 to 1.4	Hydro-Products type 451 current meter	Dee River (UK) near Saltney Ferry footbridge. Trapezoidal channel	Field experiments between March and September 1972.
KJERFVE and FERREIRA (1993)			Interocean S4 electro-magnetic current meters (sampling: 1-2 Hz)	Rio Mearim (UK)	Field experiments on 19-22 Aug. 1990 & 28 Jan.-2 Feb. 1991.
NAVARRE (1995)	0.65 to 0.7	1.12 to 1.15	Meerestechnik-Electronik GmbH model SM11J acoustic current meter (sampling 10Hz)	Dordogne River (France) at Port de Saint Pardon. Width ~ 290 m	Field experiments on 25 & 26 April 1990.
WOLANSKI et al. (2001)	--	0.45	Analite nephelometer	Ord River (East Arm) (Australia). Width ~ 380 m	Field experiments in August 1999.
CHEN (2003)	--	--	--	North Branch of the Changjiang River Estuary (China)	Experiments in April 2001.
SIMPSON et al. (2004)	0.1	~0.8	ADCP (1.2 0 MHz) (sampling rate:1 Hz)	Dee River (UK) near Saltney Ferry Bridge. Trapezoidal channel (base width ~ 60 m)	Field experiments in May and September 2002.
WOLANSKI et al. (2004)	0.15	1.5 to 4	Nortek Aquadopp ADCP (sampling rate:2 Hz)	Daly River (Australia). Width ~ 140 m	Field experiments in July and September 2002, and on 2 July 2003.
Present study			ADV Nortek Vector (6 MHz) (sampling: 64 Hz)	Arcins channel, Garonne River (France) Width ~ 76 m	Both studies were conducted at the same location.
	0.33	1.40			10 Sept. 2010.
	0.30	1.43			11 Sept. 2010.

Notes: d_1: initial water depth; V_1: initial flow velocity; (--): information not available.
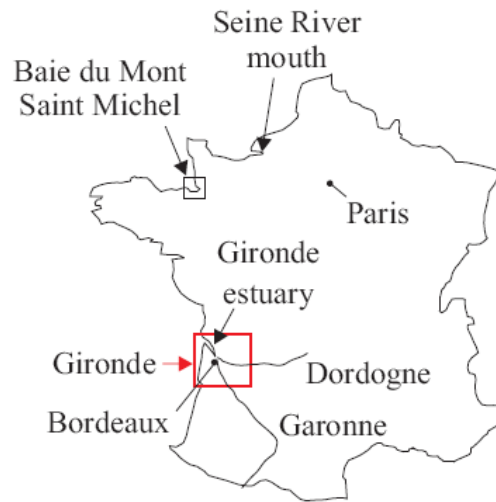
(A) Map of France and tidal-bore affected estuaries
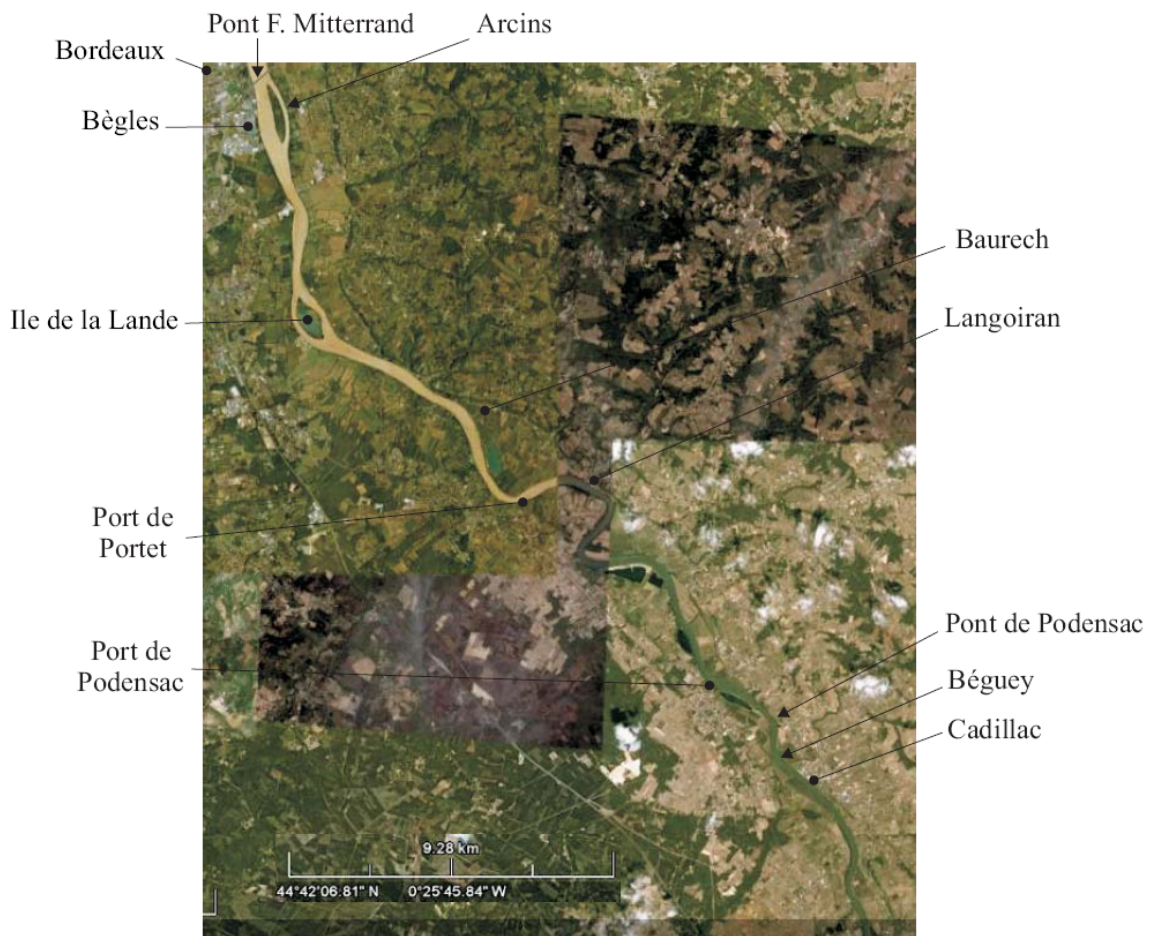
(B) Aerial photograph of the Garonne River between Bordeaux and Cadillac (Google Earth[TM] on 29 Sept. 2008) - At the bottom right, the scale corresponds to 9.28 km

Fig. 1-2 - Map of France and aerial photograph of the Garonne River estuarine zone

The Gironde estuary flows northwest between Bec d'Ambès at the confluence of the Garonne and Dordogne Rivers, and the Pointe de Grave for about 72 km. It is navigable for oceangoing vessels up to Bordeaux, despite sandbanks and strong tides. Its funnel shape and bathymetry amplifies the

tidal range. For example, when the tidal range is 5.25 m at Pointe de Grave, at the mouth of Gironde, the tidal range at Bordeaux is 6.59 m ([2]). The Garonne River is 575 km long excluding the Gironde Estuary and is affected by the tides from the confluence with the Dordogne River at Bec d'Ambès up to Castets. Its catchment area is 56,000 km^2 with its spring in the Spanish central Pyrenees. The tidal bore of the Garonne River occurs typically between Pont F. Mitterand in Bordeaux and upstream of Cadillac (Fig. 1-2B). A number of visual observations highlighted the rapid evolution of the tidal bore shape and appearance in response to the estuarine bathymetry (CHANSON 2008). In regions of deeper water, the bore may disappear, while it may strengthen in regions of shallow waters and sand banks.

1.3 STRUCTURE OF THE REPORT

In the present study, some detailed turbulence field measurements were conducted continuously at high-frequency (64 Hz) prior to, during and after the tidal bore of the Garonne River in September 2010. An acoustic Doppler velocimeter (ADV) was fixed on a large, heavy pontoon and the instrument sampled the turbulent velocity components about 0.8 m beneath the free-surface. The ADV backscatter intensity was calibrated in terms of the suspended sediment concentration in laboratory using the soft mud bed material. The results provided an unique characterisation of the turbulence and sediment flux close to the free-surface during a tidal bore event. The field investigation and instrumentation are described in section 2. The main results are presented in sections 3 to 5, and summarised in section 6. Appendix A lists the field work participants. Appendix B shows a number of photographs of the field study. Appendices C and D present respectively the ADV system configurations and the experimental calibration of the ADV system in terms of suspended sediment concentration. Appendix E shows the Reynolds stress tensor results and Appendix F gives a complete derivation of the continuity and momentum principles applied to a tidal bore in an irregular channel.

---

[2] Predicted tidal ranges on 10 Sept. 2010.

2. FIELD INVESTIGATION AND INSTRUMENTATION

2.1 FIELD INVESTIGATION AND SAMPLING SITE

The field study was conducted in the Garonne River (France) in the *Bras d'Arcins* (Arcins channel) between *Île d'Arcins* (Arcins island) and the right bank close to Lastrene. The location (44°47'58"N, 0°31'07"W) is seen in Figure 1-2B (Top left). The Arcins channel is about 1.8 km long, 70 m wide and about 1.1 to 2.5 m deep at low tide (Fig. 2-1). Figure 2-1 shows some photographs of the channel and further photographs are presented in Appendix B. Figure 2-2 presents a cross-sectional survey conducted on 10 Sept. 2010 where z is the vertical elevation. In Figure 2-2, the details of the ADV sampling volume location are presented.

Although the tides are semi-diurnal, the tidal cycles have slightly different periods and amplitudes indicating some diurnal inequality (Fig. 2-3). Figure 2-3 presents the water elevation observations at Bordeaux that are compared with the water elevations recorded on-site prior to and shortly after the passage of the tidal bore on 10 and 11 Sept. 2010. The water elevations are presented in m NGF IGN69 ([3]).

The field measurements were conducted under spring tidal conditions on 10 and 11 September 2010. The tidal range data are summarised in Table 2-1 (column 2). During the study, the water elevations and some continuous high-frequency turbulence data were recorded prior to, during and after the passage of the tidal bore for a few hours each day. The start and end times are listed in Table 2-1 (columns 6 & 8) for each study.

(A) View from Arcins Island at low tide on 7 Sept. 2010 before the tidal bore between 14:34 and 15:33 - The ADV was on the extreme left of the right bank pontoon seen in the background

---

[3] The NGF IGN69 Datum is 1.84 m above the datum of the Bordeaux tidal gauge.

(B) Looking downstream at the tidal bore on 7 Sept. 2010 at 15:45

(C) Looking downstream at the tidal bore on 7 Sept. 2010 at 15:47

Fig. 2-1 - *Bras d'Arcins* (Arcins channel)
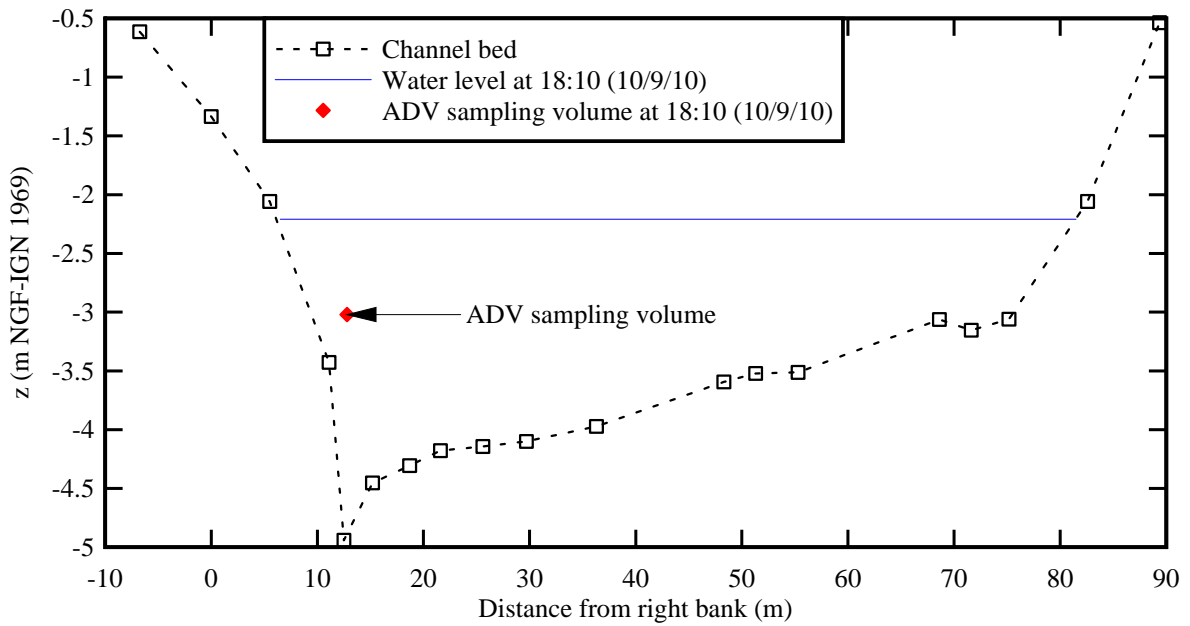
(A) Surveyed cross-section looking upstream
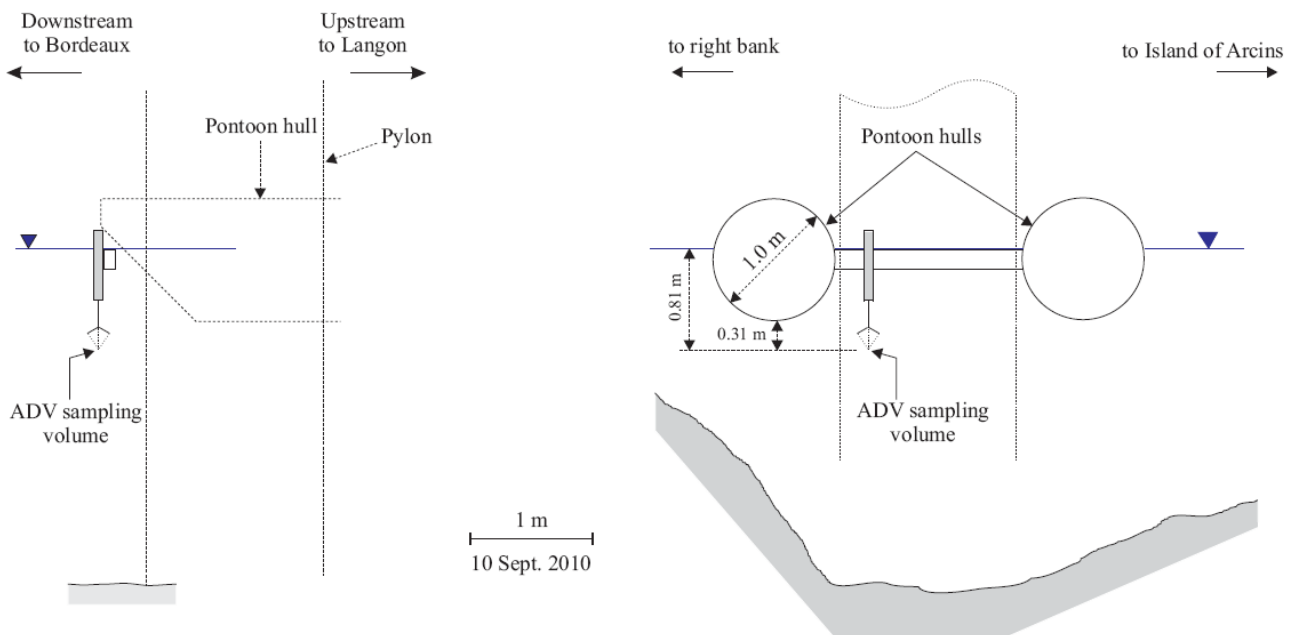
(B) Un-distorted sketch of the ADV mounting, sampling volume location and water surface 5 minutes prior to the tidal bore - Left: view from Arcins island - Right: looking upstream

Fig. 2-2 - Surveyed cross-section of Arcins channel with the low tide water level on 10 Sept. 2010 afternoon and the corresponding ADV sampling volume location

Fig. 2-3 - Measured water elevations at Bordeaux (44°52'N, 0°33'W) (Data: Vigicrue, Ministère de l'Environnement et du Développement Durable) and observations in the Arcins channel on 10 and 11 Sept. 2010

Table 2-1 - Tidal bore field measurements in the Arcins channel (Garonne River, France)

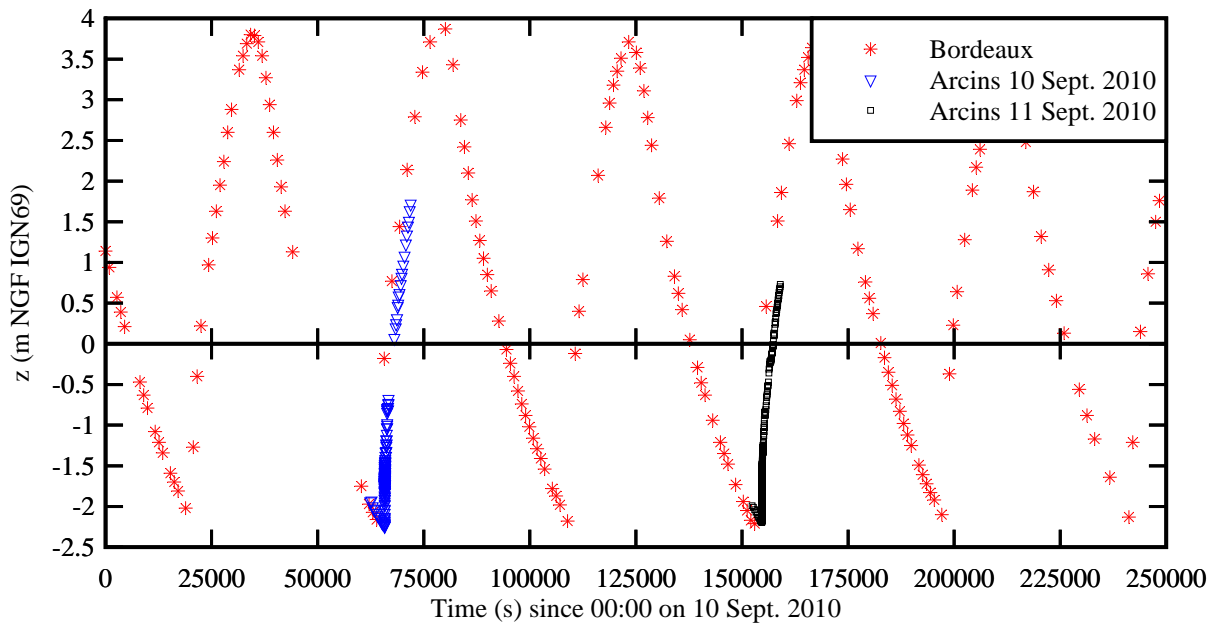| Date	Tidal range (m)	ADV system	Sampling rate (Hz)	Sampling duration	Start time	Tidal bore time	End time	Sampling volume
(1)	(2)	(3)	(4)	(5)	(6)	(7)	(8)	(9)
10/10/2010	6.03	Nortek Vector (6MHz)	64	2h 45 min	17:15	18:17	20:00	About 7 m from right bank waterline (at low tide), 0.81 m below water surface.
11/09/2010	5.89	Nortek Vector (6MHz)	64	2h 20 min	18:00	18:59	20:10	About 7 m from right bank waterline (at low tide), 0.81 m below water surface.

Notes: Tidal range: measured at Bordeaux; All times are in French local times (GMT+1).

2.2 INSTRUMENTATION

The free surface elevations were measured manually using a survey staff. During the passage of the tidal bore, a video camera recorded the water level and the data were collected frame by frame at 25 fps. The survey staff was mounted 1 m beside the ADV unit towards the right bank, to minimise any interference with the ADV sampling volume.

During the investigations, the turbulent velocities were measured with a Nortek™ Vector ADV (6 MHz, serial number VEC3332). The ADV system was equipped with a 3D downlooking head

(Head ID VEC4665) and the unit was self-logging. The system was fixed at the downstream end of a 23.55 m long heavy, sturdy pontoon. It was mounted vertically and the positive direction head was pointing downstream. Figure 2-2 shows the location of the ADV sampling volume in the surveyed cross-section. The probe was located between the hulls of the pontoon and the sampling volume was about 0.8 m below the free-surface (Table 2-1, column 9 & Fig. 2-2B). Further details on the ADV settings are reported in Appendix C. All the ADV data underwent a thorough post-processing procedure to eliminate any erroneous or corrupted data from the data sets to be analysed. The post processing was conducted with the software WinADV^{TM} version 2.026, and it included the removal of communication errors, the removal of average signal to noise ratio data less than 15 dB and the removal of average correlation values less than 60% (McLELLAND and NICHOLAS 2000). In addition, the phase-space thresholding technique developed by GORING and NIKORA (2002) was applied to remove spurious points.

Further observations were recorded with a digital camera Pentax^{TM} K-7, a digital video camera Canon^{TM} MV500i, a digital video camera JVC^{TM} GR-D225E and a HD digital video camera Canon^{TM} HF10E.

2.3 CHARACTERISATION OF THE BED MATERIAL

Some Garonne River bed material was collected at low tide on 11 September 2010 next to the pontoon on the right bank at Arcins. The soil sample consisted of fine mud and silt materials collected on the stream bed just above the low water mark ([4]), although the granulometry was not tested. A series of laboratory tests were conducted to characterise the bed material: some rheometry and acoustic backscatter experiments.

The rheological properties of mud samples were tested with a Rheometer TA-ARG2 (Serial 5L2980) equipped with a plane-cone setup ($\varnothing$ = 60 mm, cone angle: 20.005°). The gap truncation was 52 μm ([5]). The tests were performed under controlled strain rate for relatively short durations at constant temperature (20 Celsius). Between the sample collection and the tests, the mud was left to consolidate for 3 days. Prior to each rheological test, a small mud sample was placed carefully between the plate and cone (Fig. 2-4). The specimen was then subjected to a controlled strain rate loading and unloading between 0.01 s^{-1} and 1,000 s^{-1} with steady state flow steps. Figure 2-4 presents some photographs of the tests.

---

[4]The mud sample was soft and could be considered somehow as a form of mud cream (*crème de vase*).

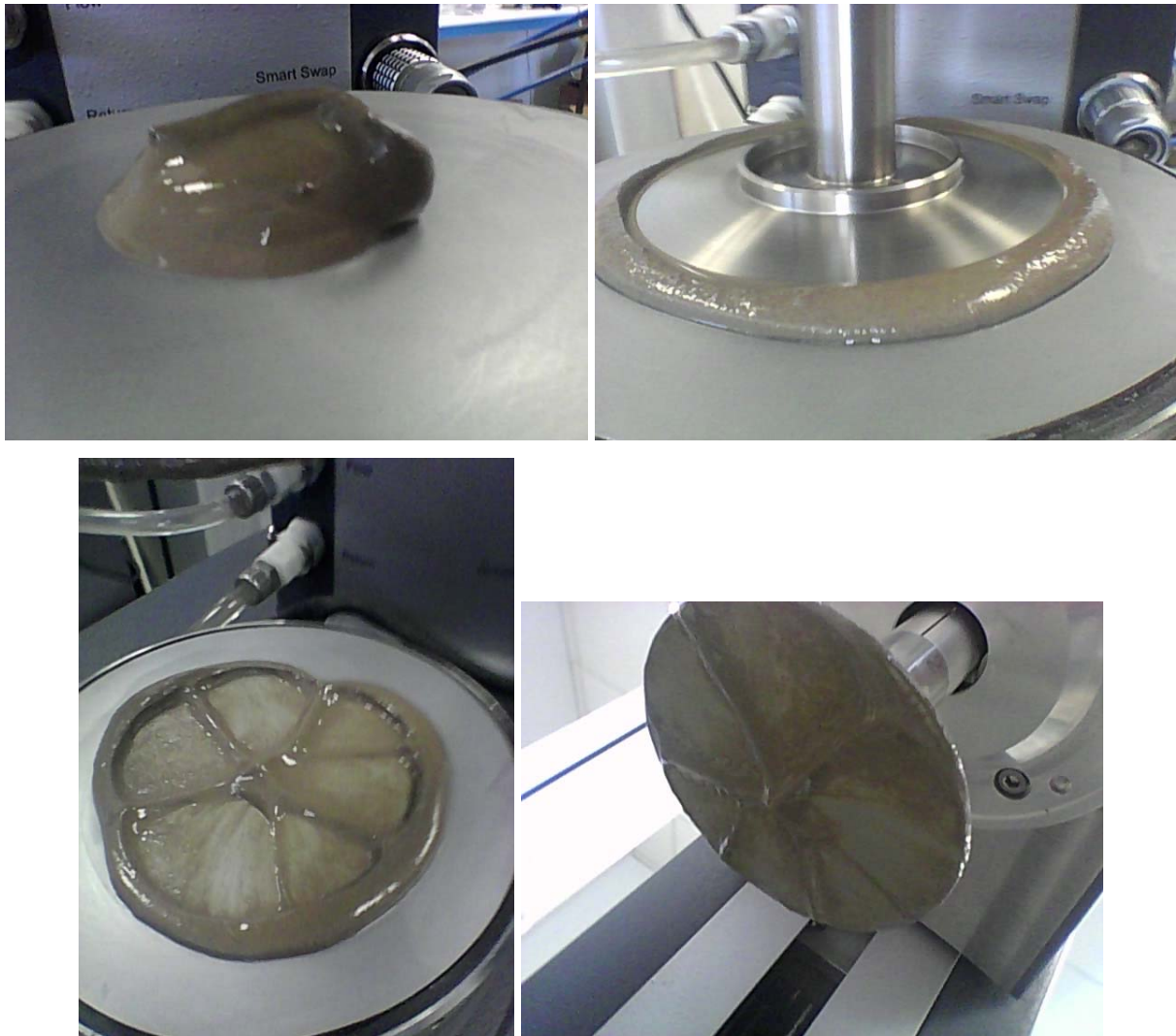[5]The gap was selected to be at least 10 times the mean particle size.

Fig. 2-4 - Photographs of the rheometry tests - From Top left, clockwise: mud sample on the plate prior to test, controlled strain rate test (loading), mud pattern on the plane at end of test, mud pattern on the lifted cone at end of test

The calibration of the ADV was accomplished by measuring the signal amplitude of known, artificially produced concentrations of material obtained from the bed material sample, diluted in tap water and thoroughly mixed. All the experiments were conducted within a couple of days from the sample collection. The laboratory experiments were conducted with the same Nortek™ Vector ADV (6 MHz, serial number VEC3332) system using the same settings as for the field observations on 10 and 11 Sept. 2010 (App. C).

For each test, a known mass of sediment was introduced in a water tank which was continuously stirred with two propeller mixers (Fig. 2-5). The propeller blades were located at 85 and 60 mm above the tank bottom while the ADV sampling volume was 57 mm above the bottom. In addition the tank was stirred manually during the most turbid water tests to check and prevent any sediment deposition on the tank bottom. The mass of wet sediment was measured with a Mettler™ Type

PM200 (Serial 86.1.06.627.9.2) balance, and the error was less than 0.01 g. The mass concentration was deduced from the measured mass of wet sediment and the measured water tank volume. During the tests, the suspended sediment concentrations ranged from less than 0.02 g/l to 74 g/l.

(A) SSC = 0 g/l (no added sediment) - The ADV system is in the middle with two water mixers on each side behind

(B, Left) SSC = 18.09 g/l

(C, Right) SSC = 60.8 g/l

Fig. 2-5 - Photographs of the laboratory experiments

The acoustic backscatter amplitude measurements were conducted with the ADV (6 MHz) system

using the same configuration employed in the field (pulse length, scan rate, velocity range) ([6]) (App. C). The ADV signal outputs were scanned at 64 Hz for 3 minutes for each test. The average amplitude measurements represented the average signal strength of the three ADV receivers. They were measured in counts ([7]). The backscatter intensity was deduced from the average amplitude as:

$$BSI = 10^{-5} \times 10^{0.043 \times Ampl} \tag{2-1}$$

where the backscatter intensity BSI is dimensionless and the average amplitude Ampl is in counts. The coefficient 10^{-5} is a value introduced to avoid large values of backscatter intensity (NIKORA and GORING 2002, CHANSON et al. 2008). Note that the ADV data were post-processed with the removal of average signal to noise ratio data less than 15 dB, average correlation values less than 60%, and communication errors. No further processing was performed.

2.4 REMARKS

2.4.1 ADV synchronisation

The water elevation measurements and ADV data were synchronised within a second. All cameras and digital video cameras were also synchronised together with the same reference time within a second.

2.4.2 Data accuracy

The accuracy on the ADV velocity measurements was 1% of the velocity range (± 2 m/s) (Nortek 2005). The accuracy of the water elevation was 0.5 cm prior to the tidal bore and 1-2 cm during the tidal bore passage.

The mass of wet sediment was measured with an accuracy of less than 0.01 g, and the SSC was estimated with an accuracy of less than 0.00025 g/l.

2.4.3 ADV settings and problem

The ADV settings are documented in Appendix C. The main difference between the two configurations was the control volume size: 3.5 mm on 10 Sept. 2010 and 6.6 mm on 11 Sept. 2010. The present experience showed that the original ADV settings on 10 Sept. 2010 yielded some very noisy and spiky velocity data, although the signal amplitude, SNR and backscatter data appeared to

---

[6]The tank was strongly agitated by two mixers. Typically the standard deviations of the velocity components were $v_x' \approx$ 0.25-1.0 m/s, $v_y' \approx$ 0.25-1.0 m/s, and $v_z' \approx$ 0.10-0.24 m/s depending upon the experimental conditions.

[7]One count equals 0.45 dB (Nortek 2005).

be correct. A spectral analysis of all velocity components indicated some unacceptable noise for frequencies larger than 0.02 to 0.1 Hz. While the exact cause of the problem remains unknown, it is thought that the ADV system on 10 Sept. 2010 was overloaded with the small control volume (App. C).

As a result, a slightly different set-up was selected on 11 Sept. 2010 with a 6.6 mm control volume size. The change yielded good quality data sets including for the turbulent velocity. In the section 4, only the velocity data set collected on 11 Sept. 2010 will be discussed. Some comparison between the signal outputs on 10 and 11 Sept. 2010 is presented in Appendix C.

3. GENERAL OBSERVATIONS

3.1 PRESENTATION

The tidal bore propagation in the Arcins channel was observed on both 10 and 11 Sept. 2010, and some similar patterns were seen. The tidal bore formed first at the downstream end of the channel about 4 min 45 s before it reached the sampling location (Fig. 3-1A & 3-2A). The tidal bore expanded rapidly across the entire channel width as a breaking bore (Fig. 3-1B & 3-2B). As the bore propagated upstream, its shape evolved in response to the local bathymmetry. About 200 m downstream of the sampling point, the bore became undular and its front was flatter (Fig. 3-1C & 3-2C). The tidal bore was undular as it passed in front of the sampling location, and the bore front is well marked by the surfer(s) riding ahead of the first wave crest in Figures 3-1D and 3-2D. Some basic tidal bore characteristics are summarised in Table 3-1. The bore continued to propagate up to the upstream end of the channel for another 4 minutes. Upstream of the sampling location, the tidal bore was undular (Fig. 3-1E & 3-2E).

The passage of the tidal bore was characterised by a pseudo-chaotic wave motion lasting for several minutes after the bore. At the sampling location, the free-surface elevation rose very rapidly by 0.50 m and 0.41 m in the first 5 seconds on 10 and 11 Sept. 2010 respectively. For the next 35 minutes, the water elevation rose further by 1.69 m and 1.59 m on 10 and 11 Sept. 2010 respectively. More details on the water elevation data are described in the next paragraphs.

Figures 3-1 and 3-2 present some photographs of the tidal bore propagation for each field study. Figures 3-1A to 3-1E, and 3-1A to 3-2E, show the tidal bore propagation in the channel. Figure 3-1F illustrates the Arcins channel about 105 minutes after the passage of the tidal bore.
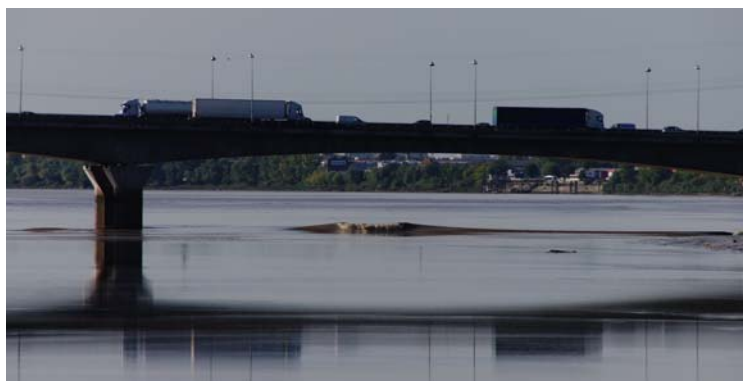
(A) Tidal bore formation at the channel downstream end at 18:13:00
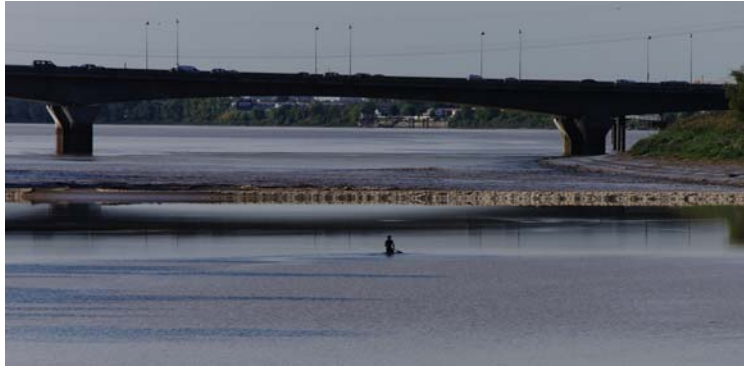
(B) Breaking tidal bore at 18:15:14

(C) Undular tidal bore downstream of the sampling location at 18:17:18- Frédéric DANEY surfed close to the Arcins island

(D) Undular tidal bore shortly after passing the ADV sampling location (Bottom right) at 18:17:42 - Pierre LUBIN held the survey staff used to record the water depth (bottom right corner)

(E) Undular tidal bore propagating upstream at 18:18:01 - The upstream end of the channel is seen in the background (Top left)

(F) Looking downstream at 19:58

Fig. 3-1 - Field study in *Bras d'Arcins* (Arcins channel) on 10 Sept. 2010
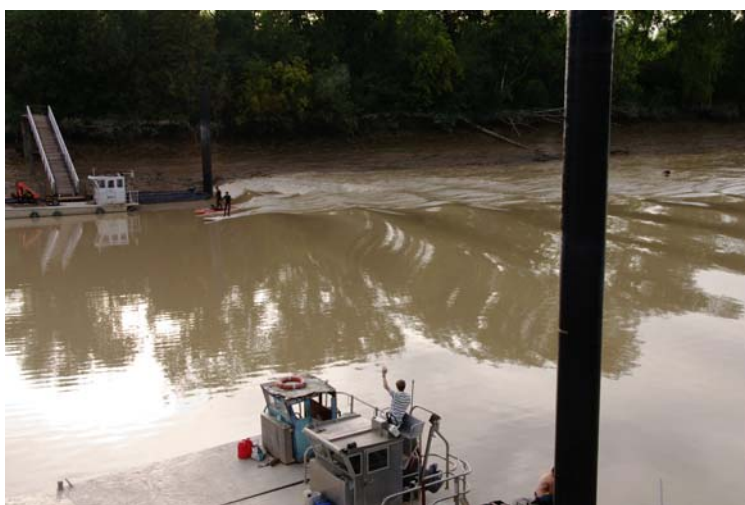
(A) Tidal bore formation at the channel downstream end at 18:54:42 - Note the Airbus Industry barge in the background starting its journey upstream to Langon behind the tidal bore

(B) Breaking tidal bore at 18:57:53

(C) Undular tidal bore downstream of the sampling location at 18:59:09

(D) Undular tidal bore shortly before passing the ADV sampling location (Bottom right) at 18:59:29

(E) Undular tidal bore propagating upstream at 19:00:10

Fig. 3-2 - Field study in *Bras d'Arcins* (Arcins channel) on 11 Sept. 2010

3.2 TIDAL BORE PROPERTIES

3.2.1 Tidal bore celerity and Froude number

A tidal bore is a hydrodynamic shock. The front is characterised by a sudden rise in free-surface elevation and a discontinuity of the pressure and velocity fields. In a tidal bore, the flow properties immediately before and after the bore front must satisfy the equations of conservation of mass and momentum (HENDERSON 1966, LIGGETT 1994, CHANSON 2004). In the system of reference in translation with the bore front, the integral form of the equations of conservation of mass and momentum gives a series of relationships between the flow properties in front of and behind the bore:

$$(V_1 + U) \times A_1 = (V_2 + U) \times A_2 \qquad (3\text{-}1)$$

$$\rho \times (V_1 + U) \times A_1 \times (\beta_1 \times (V_1 + U) - \beta_2 \times (V_2 + U)) = \iint_{A_2} P \times dA - \iint_{A_1} P \times dA \qquad (3\text{-}2)$$

where ρ is the water density, g is the gravity acceleration, U is the bore celerity for an observer standing on the bank, positive upstream, V is the cross-sectional averaged velocity positive downstream towards the river mouth, A is the flow cross-section, β is a momentum correction coefficient, P is the pressure, the subscript 1 refers to the initial flow conditions and the subscript 2 refers to the flow conditions immediately after the passage of the front. Equation (3-2) is based the assumptions of a quasi-horizontal channel bed and negligible friction losses, and the water density is assumed constant. In the right handside, the first term is the pressure force acting on the flow cross-section behind to the tidal bore, while the second term is the pressure force acting in front of the tidal bore.

The difference in pressure forces may be derived assuming a hydrostatic pressure distribution in front of and behind the tidal bore front. Neglecting the effect of the velocity correction coefficient

(i.e. $\beta \approx 1$), the solution of the momentum principle is:

$$\frac{A_2}{A_1} = \frac{1}{2} \times \frac{\sqrt{\left(2 - \frac{B'}{B}\right)^2 + 8 \times \frac{B'/B}{B_1/B} \times Fr_1^2} - \left(2 - \frac{B'}{B}\right)}{\frac{B'}{B}} \qquad (3-3)$$

where B_1 is the initial free-surface width, and the characteristic width B and B' are defined as:

$$B = \frac{A_2 - A_1}{d_2 - d_1} \qquad (3-4)$$

$$B' = \frac{\int\limits_{A_1}^{A_2} \int (d_2 - y) \times dA}{\frac{1}{2} \times (d_2 - d_1)^2} \qquad (3-5)$$

with d_2 and d_2 the initial and new flow depths respectively in front of and immediately behind the bore front, and y is the distance normal to the bed (Fig. 3-3) (App. F). The tidal bore Froude number Fr_1 is defined as:

$$Fr_1 = \frac{V_1 + U}{\sqrt{g \times \frac{A_1}{B_1}}} \qquad \text{Irregular channel} \quad (3\text{-}6a)$$

where A_1 is the initial flow cross-section and B_1 is the initial free-surface width (Fig. 3-3). The ratio A_1/B_1 represents an equivalent cross-sectional averaged water depth.
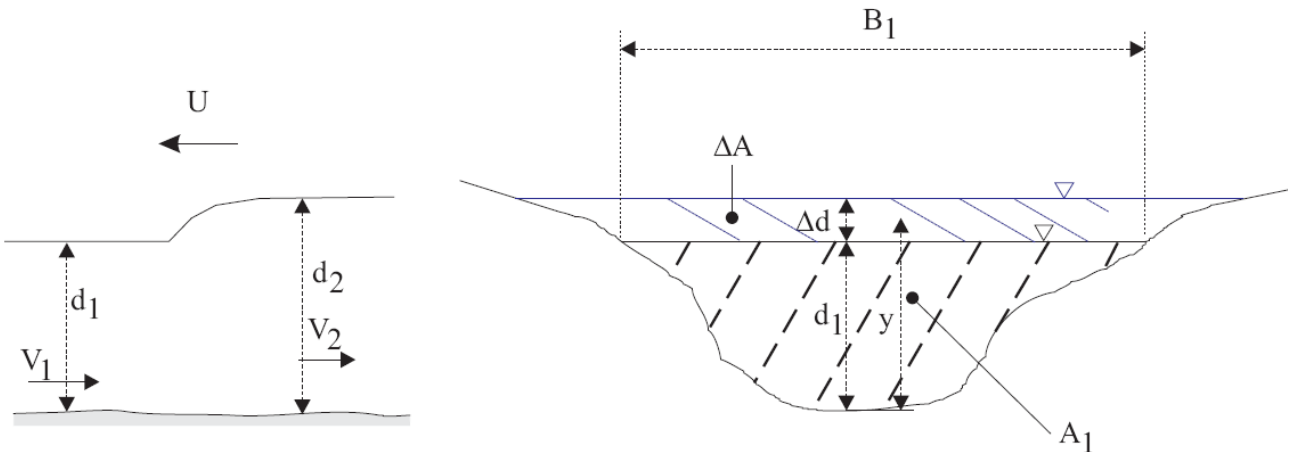

Fig.3-3 - Definition sketch of a tidal bore propagation in an irregular channel

For a rectangular horizontal channel, assuming some hydrostatic pressure distributions, Equations (3-1) and (3-2) yield the classical Bélanger equation:

$$\frac{d_2}{d_1} = \frac{1}{2} \times \left(\sqrt{1 + 8 \times Fr_1{}^2} - 1 \right) \tag{3-7}$$

that is a simplification of Equation (3-3). The tidal bore Froude number defined in the system of co-ordinates in translation with the bore front is simply:

$$Fr_1 = \frac{V_1 + U}{\sqrt{g \times d_1}} \qquad \text{Rectangular channel} \tag{3-6b}$$

In a tidal bore, the Froude number Fr_1 is always greater than unity. For $Fr_1 < 1$, the tidal wave cannot become a tidal bore. For $1 < Fr_1 < 1.5$ to 1.8, the tidal bore is undular, and a breaking bore is observed for $Fr_1 > 1.5$ to 1.8. For an observer travelling with the flow upstream of the tidal front at a downstream velocity V_1, the celerity of the bore relative to the upstream flow may be derived from some continuity and momentum considerations (App. F) ([1]):

$$U + V_1 = \sqrt{\frac{1}{2} \times \frac{g \times A_2}{A_1 \times B} \times \left(\left(2 - \frac{B'}{B} \right) \times A_1 + \frac{B'}{B} \times A_2 \right)} \tag{3-8}$$

Since $A_2 > A_1$, the relative bore celerity satisfies: $U + V_1 > \sqrt{g \times A_1 / B_1}$. For a small wave (i.e. $A_2 = A_1 + \delta A$), the relative celerity ($U + V_1$) tends to the celerity of a small disturbance $\sqrt{g \times A_1 / B_1}$ in an irregular channel.

Table 3-1 - Tidal bore properties in the Arcins channel (Garonne River, France) at the sampling location during the field experiments

Date	Tidal range	V_1 channel CL	U channel CL	d_1 next to ADV	A_1	B_1	A_1/B_1	Fr_1 Eq. (3-6b)	Remarks
	(m)	(m/s)	(m/s)	(m)	(m^2)	(m)	(m)		
(1)	(2)	(3)	(4)	(5)	(6)	(7)	(8)	(9)	(10)
10/10/2010	6.03	+0.33	4.5	1.77	106	75.4	1.40	1.30	Undular bore.
11/09/2010	5.89	+0.30	4.2	1.81	109	75.8	1.43	1.20	Undular bore.

Notes: Tidal range: measured at Bordeaux; A_1: channel cross-section area immediately prior to the bore passage; B_1: free-surface width immediately prior to the bore passage; d_1: water depth next to ADV immediately prior to the bore passage; Fr_1: tidal bore Froude number (Eq. (3-6b)); U: tidal bore celerity positive upstream on the channel centreline; V_1: downstream surface velocity on the

---

[1] For a rectangular channel, $A_1/B_1 = d_1$ and Equation (3-8) becomes:

$$U + V_1 = \sqrt{g \times d_1} \times \sqrt{\frac{1}{2} \times \frac{d_2}{d_1} \times \left(1 + \frac{d_2}{d_1} \right)}$$

channel centreline immediately prior to the bore passage.

During the present field experiments, the tidal bore was undular at the sampling location, and the tidal Froude number was estimated from the surveyed channel cross-section, water level observations and tidal bore celerity observations (Table 3-1). Equation (3-6a) yields $Fr_1 = 1.30$ and 1.20 for the field observations on 10 and 11 Sept. 2010 respectively.

Similarly the momentum considerations predict a bore celerity U (Eq. (3-8)) equals to 4.3 m/s on both 10 and 11 Sept. 2010 respectively, that is close to the field observations (Table 3-1, column 4).

### 3.2.2 Free-surface properties

The water depth was recorded using a survey staff placed about 1 m beside the ADV towards the right bank. The staff is visible in Figure 3-1D (bottom right). The data were recorded visually, using a video camera (25 fps) during the bore passage. Figure 3-4 presents the recorded water depth just beside the ADV for both field measurements. Figures 3-4A and 3-4B show the entire records and the horizontal axis corresponds to 10,000 s (2 h 47 min). Figures 3-4C and 3-4D highlight the 60 s period around the tidal bore front passage.

The water depth data showed consistently the same trends, qualitatively and quantitatively, for both field experiments. The water depth decreased slowly during the end of the ebb tide prior to the tidal bore arrival. The passage of the bore was associated with a very rapid rise of the water elevation (Fig. 3-4C & 3-4D) and some pseudo-chaotic wave motion shortly after. A frequency analysis showed no dominant wave frequency, but a superposition of a range of wave periods.
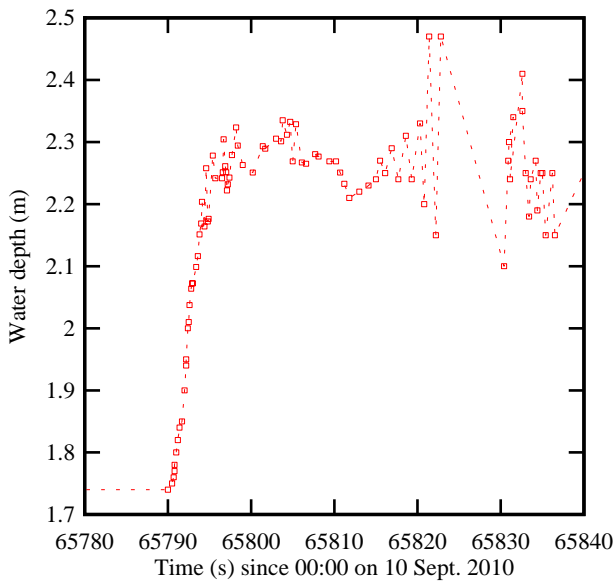
During the following flood flow, the water depth increased rapidly with time: i.e., nearly 3 m in 90 minutes.
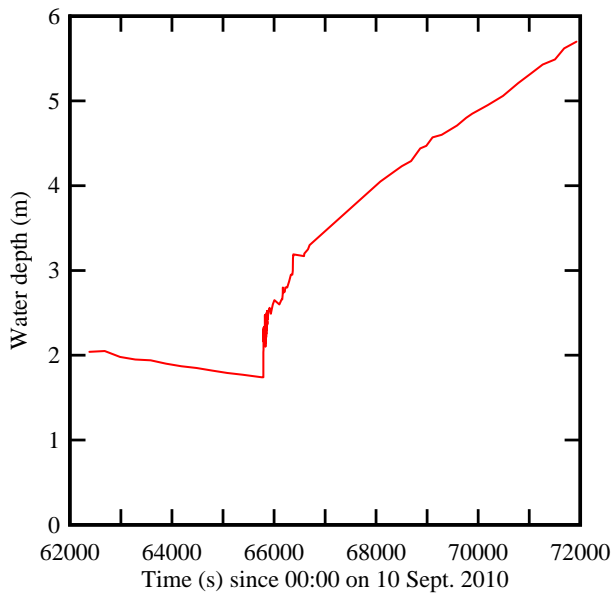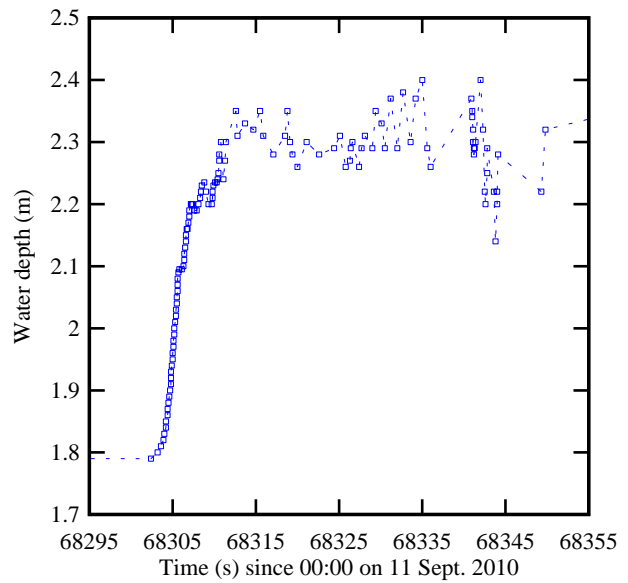
(A) On 10 Sept. 2010
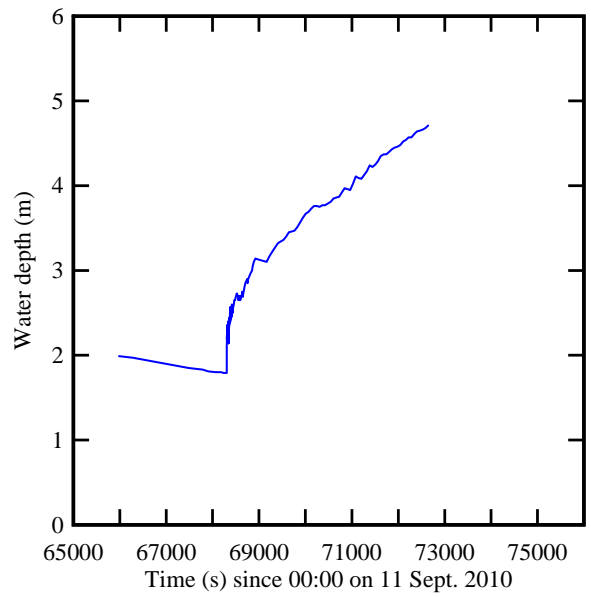
(B) On 11 Sept. 2010

(C) On 10 Sept. 2010

(D) On 11 Sept. 2010

Fig. 3-4 - Time variations of the water depth during the field experiments - Survey staff records

4. TURBULENCE CHARACTERISTICS

4.1 TURBULENT VELOCITY FIELD

On 11 Sept. 2010, the turbulent velocity data showed the marked impact of the tidal bore propagation (Fig. 4-1). Figure 4-1 presents the time-variations of the three velocity components, where the longitudinal velocity component V_x is positive downstream (towards Bordeaux), the transverse velocity component V_y is positive towards the Arcins island, and the vertical velocity component V_z is positive upwards. The time-variations of the water depth at the survey staff are shown together with the ADV sampling volume depth. The latter was deduced from the ADV pressure sensor assuming a hydrostatic pressure distribution. Some free-surface velocity observations are also included (Fig. 4-1A): these were recorded with stop watches using floating debris on the channel centreline and close to the right bank between the pontoon and the right bank. The turbulent velocity data showed the marked effect of the passage of the bore front at t = 68,302 s (Fig. 4-1). The longitudinal velocity component highlighted some rapid flow deceleration during the passage of the bore front. As the bore front reached the sampling volume (t = 68,302 s), a sudden rise in the free surface elevation took place associated with a sharp decrease in longitudinal velocity component and a flow reversal (Fig. 4-1). The observations were consistent with the earlier results of WOLANSKI et al. (2004) and SIMPSON et al. (2004) in the field, and HORNUNG et al. (1995), KOCH and CHANSON (2009) and CHANSON (2010) in laboratory. The tidal bore passage was further characterised by some large fluctuations of all three turbulent velocity components.

The longitudinal flow component changed from +0.3 m/s (oriented downriver) to -1 m/s (oriented upriver) immediately after the passage of the bore, with turbulent fluctuations between 0 to -2 m/s (Fig. 4-1A). The large velocity fluctuations lasted for the entire sampling duration. The longitudinal velocity results were consistent with the free-surface observations before and after the tidal bore passage, although the surface current was stronger on the channel centreline than close to the right bank. At times, the authors noted some recirculation patterns next the waterline mark on the right bank, where the surface velocity flowed at time downstream against the main flood flow direction.

After the passage of the bore, the transverse velocity data fluctuated between +0.6 and -1.1 m/s, and the time-averaged transverse velocity component was -0.28 m/s (Fig. 4-1B). The finding implied some net transverse circulation towards the right bank next to the free-surface. This flow pattern was linked possibly with the irregular channel cross-section and the existence of some secondary flow motion.

The vertical velocity data highlighted a marked effect of the tidal bore. After the bore passage, the vertical velocity fluctuated between +0.1 and -0.8 m/s, with a time-averaged value of about -0.28 m/s (Fig. 4-1C).

Note that the ADV sampling volume depth ranged from 0.7 to 0.9 m for the entire study duration (Fig. 4-1B). The velocity data characterised therefore the turbulence in the upper water column. Further the ADV was fixed to a pontoon. Although heavy and sturdy, the vertical motion of the pontoon cannot be ignored.
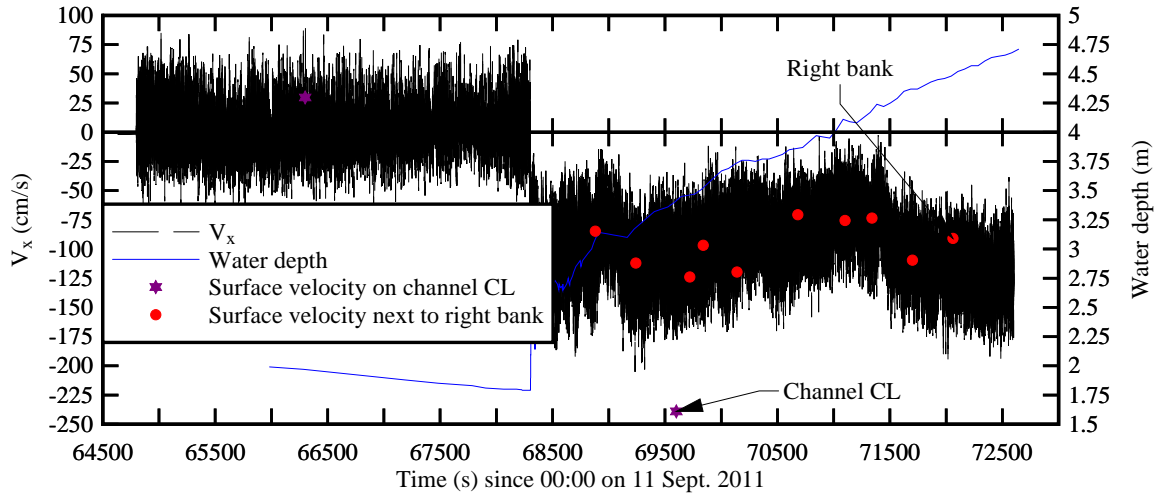
(A) Water depth, longitudinal velocity component V_x, and surface velocity on the channel centreline and next to right bank (between pontoon and right bank)
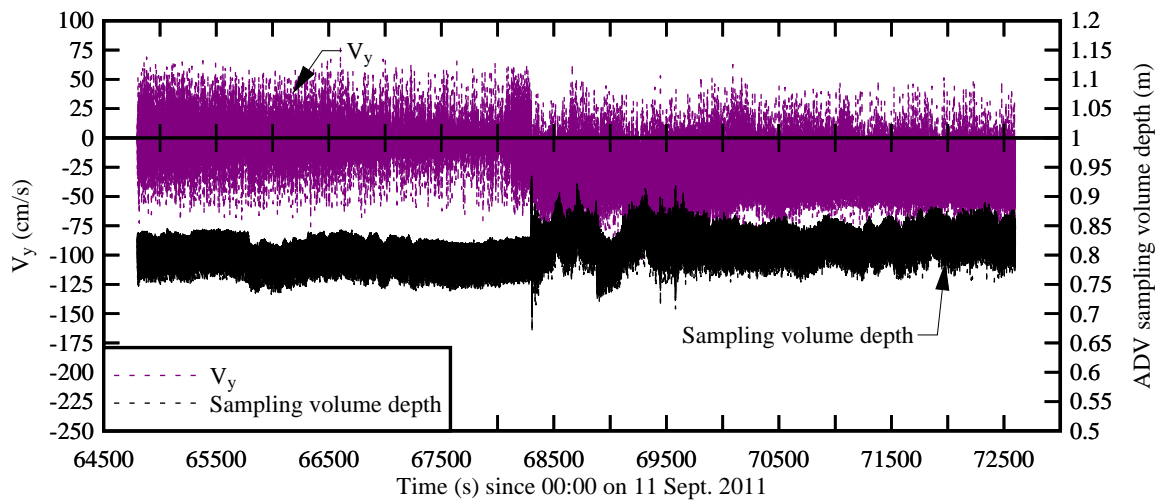
(B) ADV sampling depth below the free-surface and transverse velocity component V_y
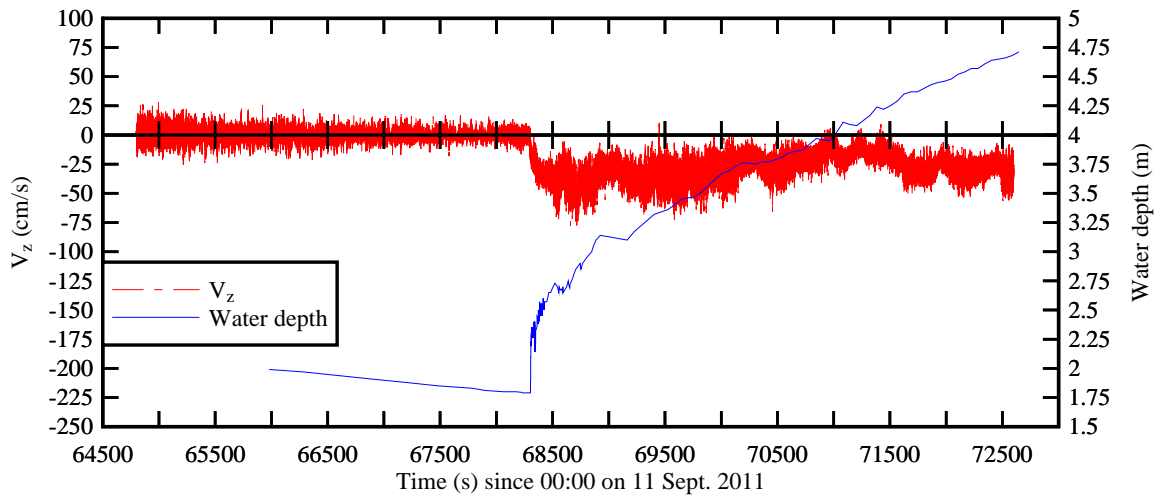
(C) Water depth and vertical velocity component V_z

Fig. 4-1 - Time variations of the water depth, ADV sampling volume depth below free-surface and turbulent velocity components in the tidal bore of the Garonne River on 11 Sept. 2010 - Post-processed ADV data, sampling rate: 64 Hz

Figure 4-2 presents further the dimensionless water depth and turbulent velocity components during the passage of tidal bore front. The data are dimensionalised in terms of the initial cross-sectional averaged depth A_1/B_1 (Table 3-1). The arrival of the bore was characterised with a gentle rise of the water elevation associated with a flow deceleration, the entire process lasting about 2-3 s. The sharp rise in water elevation was linked with large and rapid fluctuations of all three velocity components. These large and rapid fluctuations lasted several minutes after the bore passage.

Note that the vertical velocity data presented some quasi-periodic fluctuations with periods of about 1.2 s (Fig. 4-2B, right) starting about 400 s after the bore passage. These were believed to be linked with some free-surface waves, with a similar period, that were visually seen.

Discussion

The ADV sampling volume was located relatively close to the bank, and the flow patterns at this position might have been affected by the channel bank at low tide. This could be consistent with the comparison between the ADV data and surface velocity observations seen in Figure 4-1A. Some future studies may include several ADV systems located at different transverse locations.

A comparison between Figure 4-1C and Figures 4-1A and 4-1B indicates that the vertical velocity component V_z exhibited less fluctuation than the V_x and V_y velocity components. The reason remained unknown although a later field work experience suggested that this velocity component was less "noisy" than the other two.

27

4.2 TURBULENT SHEAR STRESSES

The turbulent Reynolds stresses characterise a transport effect resulting from turbulent motion induced by velocity fluctuations with its subsequent increase of momentum exchange and of mixing (BRADSHAW 1971, PIQUET 1999). A Reynolds stress is proportional to the product of two velocity fluctuations, where the turbulent velocity fluctuation is the deviation of the instantaneous velocity from an "average" velocity component $\overline{V}$. In an unsteady flow, $\overline{V}$ is the low-pass filtered velocity component, also called the variable interval time average VITA (PIQUET 1999). A VITA method was applied to the field data using a cut-off frequency derived upon a sensitivity analysis conducted between an upper limit of the filtered signal (herein 32 Hz, the Nyquist frequency) and a lower limit corresponding to a period of about 1-2 s of some residual undulations. The results yielded an optimum threshold of F_{cutoff} = 1 Hz, and the filtering was applied to all velocity components. Note that KOCH and CHANSON (2008) and DOCHERTY and CHANSON (2010) selected similarly a cutoff period $1/F_{cutoff}$ that was between the undulation period and half the undulation period, as in the present study.

The filtering was applied to all velocity components, and the turbulent Reynolds stresses were calculated from the high-pass filtered signals. Figure 4-3 presents some results in terms of normal and tangential Reynolds stresses, and the full data set is presented in Appendix E. The present data showed large and rapid turbulent Reynolds stress fluctuations below the tidal bore front and flood flow (Figure 4-3). The Reynolds stress levels were significantly larger than during the ebb tide, with normal stress magnitudes up to 400 Pa and tangential stress magnitudes up to 250 Pa. These values were significantly larger than previous laboratory data (KOCH and CHANSON 2009, CHANSON 2010). Furthermore some substantial normal and tangential stress fluctuations were observed.
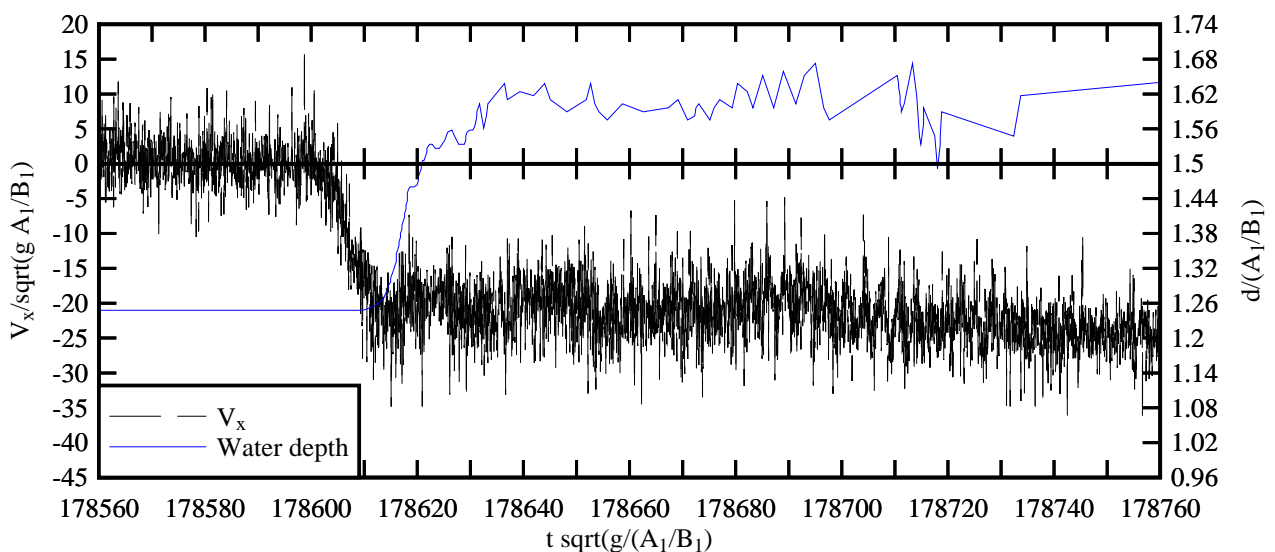
(A) Water depth and horizontal velocity component V_x
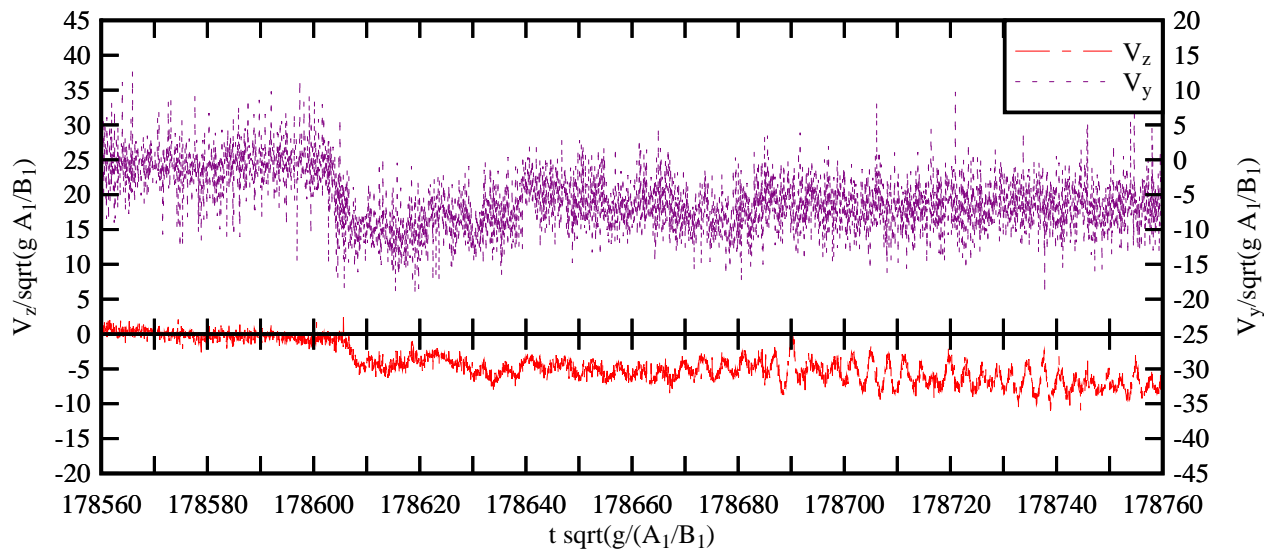
(B) Transverse and vertical velocity components (V_y, V_z)

Fig. 4-2 - Dimensionless water depth and turbulent velocity components during the tidal bore passage on 11 Sept. 2010 - Post-processed ADV data, sampling rate: 64 Hz

Discussion

The present field measurements demonstrated the intense turbulent mixing beneath the tidal bore. Some large magnitude and rapid fluctuations of turbulent Reynolds stresses were observed. For a non-cohesive sediment material, the Shields diagram gives a critical shear stress for sediment bed load motion about: $(\tau_o)_c = 0.1$ to 6 Pa for quartz particles with sizes between 0.1 and 10 mm (GRAF 1971, JULIEN 1995). Herein the instantaneous turbulent shear stress magnitudes ranged up to more than 400 Pa. The Reynolds stress levels were two to three orders of magnitude larger than the critical threshold for sediment motion and transport.

This comparison is limited however. First the bed material was cohesive (section 5) and had a thixotropic behaviour. Second, in a tidal bore, the large scale vortices play an important role in terms of sediment material pickup and upward advection (CHANSON 2001,2008). This type of sediment motion occurs by convection since the turbulent mixing length is much larger than the sediment distribution length scale. The validity of the Shields diagram and of the critical shear stress estimate is debatable.

Despite some differences in geometry and flow conditions, a comparison between field and laboratory data for comparable Froude number is pertinent. For an undistorted Froude similitude, the shear stress scaling ratio equals the geometric scaling ratio (LIGGETT 1994, CHANSON 2004). The geometric scaling ratio between the present field study and the experiments of KOCH and CHANSON (2009) was 17.5:1. The present shear stress magnitudes were typically 100 to 200 times

29

larger than the laboratory data, suggesting some limitations of the Froude similarity, although no systematic study was conducted to date to assess the scale effects affecting the turbulent mixing in tidal bore flows.
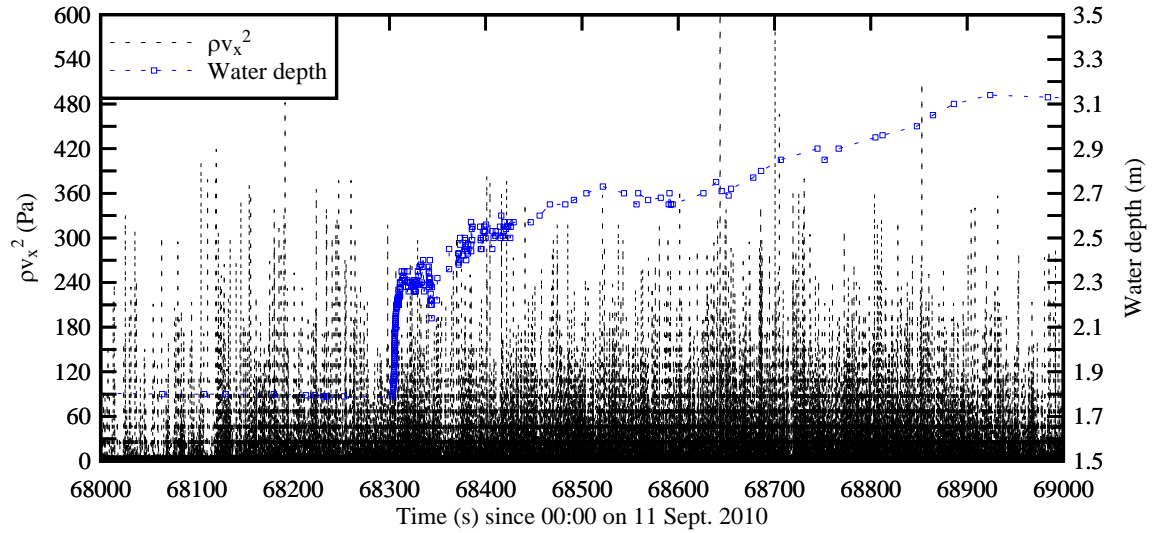
(A) $\rho \times v_x^2$
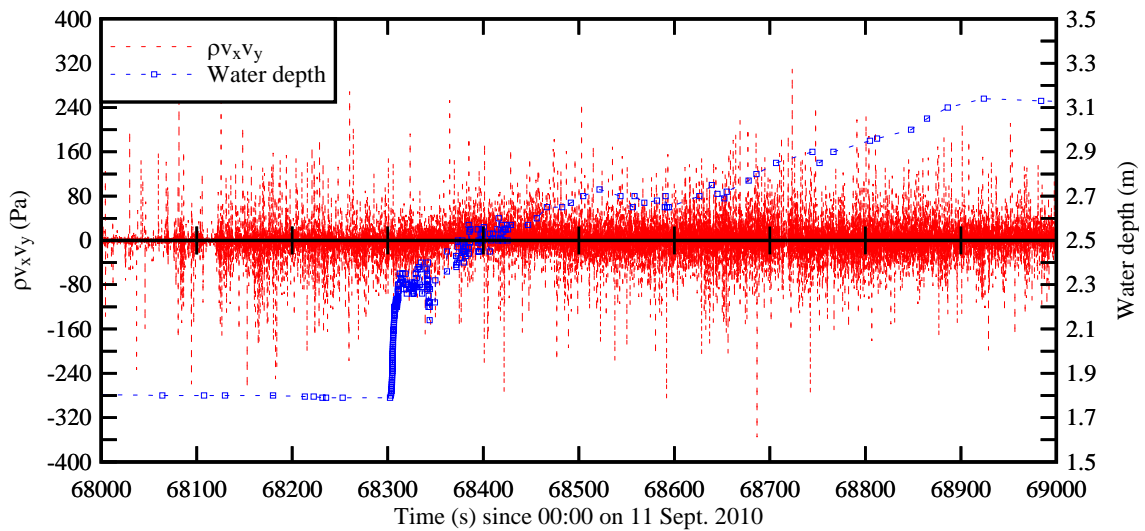
(B) $\rho \times v_x \times v_y$

Fig. 4-3 - Time-variations of Reynolds stresses and water depth during the tidal bore passage on 11 Sept. 2010 - Post-processed ADV data, sampling rate: 64 Hz

5. SEDIMENT PROPERTIES, SUSPENDED SEDIMENT CONCENTRATION AND SEDIMENT FLUXES

5.1 PRESENTATION

The bed sediment material was characterised by a series of laboratory experiments. The density of the wet sediment was **s** = 1.418. The bed material was a cohesive mud mixture but the granulometry was not tested.

The rheometry tests provided some information on the apparent yield stress of the fluid τ_c and the effective viscosity μ. Note that a more complete characterization of the rheological behaviour of such thixotropic material would require the determination of the parameters of a thixotropic model. Such a work was carried out successfully for a bentonite suspension (ROUSSEL et al. 2004). Within the frame of the present work, a more rapid but also more approximate characterization of the material was used. The yield stress and apparent viscosity were estimated during the unloading phase, to be consistent with earlier thixotropic experiments (ROUSSEL et al. 2004, CHANSON et al. 2006). The yield stress and viscosity results were derived by fitting the rheometer data with a Herschel-Bulkley model. In a Herschel-Bulkley fluid, the relationship between shear stress τ and shear rate $\partial V/\partial y$ is assumed to be:

$$\tau = \tau_c + \mu \times \left(\frac{\partial V}{\partial y} \right)^m \tag{5-1}$$

where $0 < m \leq 1$ (e.g. HUANG and GARCIA 1998, WILSON and BURGESS 1998). For m = 1, Equation (5-1) yields the Bingham fluid behaviour and μ is a material parameter.

The experimental results are presented in Figure 5-1. The behaviour of the mud material highlighted some differences between the loading and unloading sequence. The magnitude of the shear rate during unloading was smaller than the shear rate magnitude during loading for a given shear stress. For shear rates larger than 300 s^{-1}, the two tests gave close results, suggesting a conservation of the macroscopic structure possibly in the form of particle arrangement into thin layers. In average over the tests, the apparent viscosity was 0.1 Pa.s, the yield stress was about 223 Pa and m ~ 1.06.
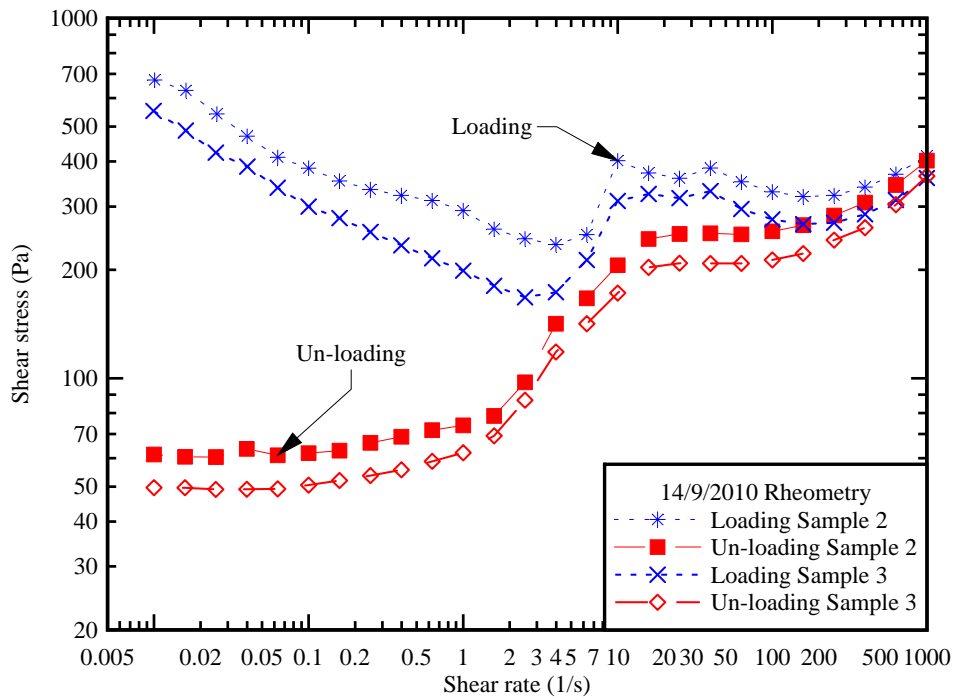
Fig. 5-1 - Mud rheometer test - Loading and unloading cycle in the TA-ARG2 Rheometer

Discussion

For future tests, it would be interesting to compare the particle concentration with another independent measurement system, like a laser LS to compare with the ADV data. Further information on the granulometry would be further valuable

Since there is a relationship between concentration and viscosity, it would be useful to know the real weight of the mud material (i.e. density of dry mud), assuming that the mud does not evolve during the drying process. Some information on the pH of the water at the time of the measurements would be valuable.

5.2 ACOUSTIC BACKSCATTER INTENSITY AND SUSPENDED SEDIMENT CONCENTRATION

5.1 Experimental calibration

The acoustic Doppler velocimeter (ADV) is designed to record the instantaneous velocity components at a single-point with relatively high frequency. Additionally the ADV signal strength, or acoustic backscatter strength, may be related to the instantaneous suspended sediment concentration (SSC) with proper calibration (KAWANISI and YOKOSI 1997, FUGATE and FRIEDRICHS 2002). Although the method was initially developed for non-cohesive sediments, it was recently extended successfully to cohesive materials (CHANSON et al. 2008, HA et al. 2009).

Some thorough experiments indicated that the acoustic backscatter intensity increased monotically with increasing SSC for relatively low suspended sediment loads (FUGATE and FRIEDRICHS 2002, CHANSON et al. 2008). For high suspended loads, the ADV backscatter intensity decreased with increasing SSC. The trend is believed to highlight some signal saturation linked to multiple scattering and associated sound absorption (HA et al. 2009).

Within the experimental conditions (section 2.3), the relationships between acoustic backscatter amplitude (Ampl), acoustic backscatter intensity (BSI) and suspended sediment concentrations (SSC) were tested systematically for SSCs between 0 and 74 g/l. The experimental results are summarised in Figure 5-2. The full data sets are reported in Appendix D.

First the results were independent of the ADV settings. No difference was observed between the ADV settings on 10 Sept. and 11 Sept. 2010. Second there was a good correlation between all the data showing two characteristic trends. For SSC ≤ 0.48 g/l, the data yielded a monotonic increase in suspended sediment concentration with increasing backscatter intensity. The relationships between SSC and amplitude, and SSC and BSI, were roughly linear. For larger SSCs (i.e. SSC > 0.48 g/l), the experimental results demonstrated a decreasing backscatter intensity with increasing SSC.

For the laboratory tests with low suspended loads (SSC ≤ 0.48 g/l), the best fit relationships were:

$$SSC = 0.0367 \times Ampl - 6.02 \qquad\qquad SSC \leq 0.48 \text{ g/l} \quad (5\text{-}2a)$$

$$SSC = 0.0019 \times BSI - 0.189 \qquad\qquad SSC \leq 0.48 \text{ g/l} \quad (5\text{-}2b)$$

where the suspended sediment concentration SSC is in g/l, and the amplitude Ampl is in counts and the backscatter intensity BSI is defined using Equation (2-1). Equations (5-2a) and (5-2b) were correlated with a normalised correlation coefficient of 0.886 and 0.915 respectively.

For large suspended sediment loads (i.e. SSC > 0.48 g/l), the data were best correlated by

$$SSC = 381.7 - 2.17 \times Ampl \qquad\qquad SSC > 0.48 \text{ g/l} \quad (5\text{-}3a)$$

$$SSC = 79.15 \times \exp(-0.010 \times BSI) \qquad\qquad SSC > 0.48 \text{ g/l} \quad (5\text{-}3b)$$

with a normalised correlation coefficient of 0.994 for both correlations. Equations (5-2) and (5-3) are compared with the data in Figure 5-2. For large suspended sediment concentration within 0.4 < SSC < 75 g/l, the results showed a good correlation between the acoustic backscatter strength and the SSC, although the ADV signal was saturated.

During the present field investigations, the authors observed that the Arcins channel waters were very turbid before, during and after the tidal bore. In the waters, they could not see their fingers below 1-3 cm from the water surface ([1]). In the Gironde estuary and Garonne River estuarine zone, the currents exceed the critical erosion except during neap tides (CANCINO and NEVES 1999). A

---

[1] Further, the people who went into the water got covered by fine sediment materials.

number of field measurements showed that, during low flow periods similar to the present investigations, the SSC in the upper Gironde estuary and lower Garonne River exceeded 1 g/l (SOTTOLOCHIO and CASTAING 1999). Recent SSC observations reported typically values from 0.5 to 2.5 g/l close to the surface (DOXARAN et al. 2009). Therefore Equations (5-3a) and (5-3b) were considered to be representative of the relationship between the suspended sediment concentration (SSC) and the acoustic backscatter intensity (BSI) in the Arcins channel on 10 and 11 Sept. 2010.
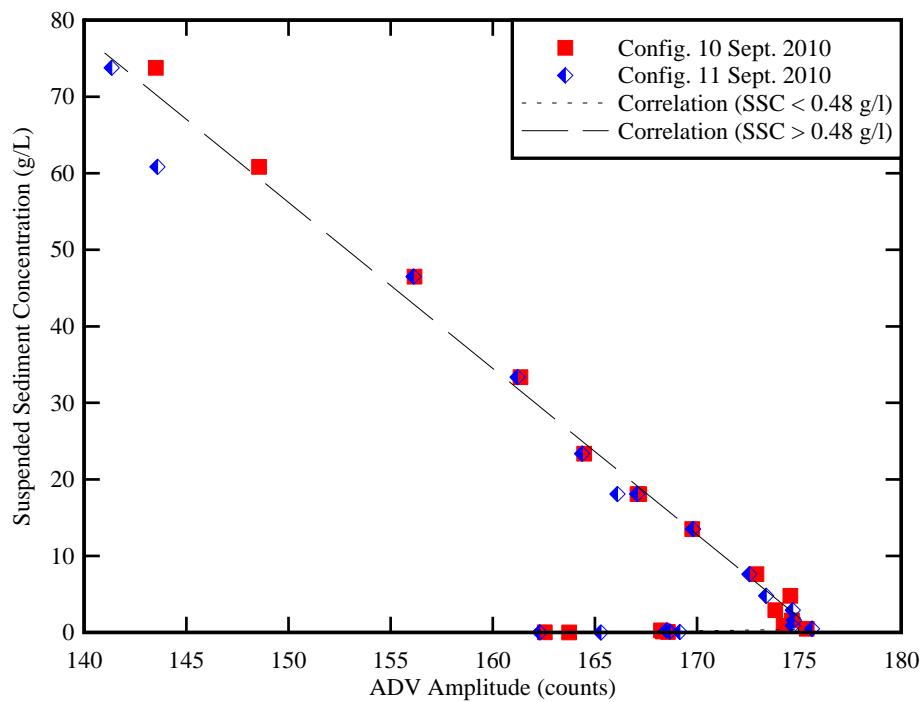
(A) Relationship between suspended sediment concentration (SSC in g/l) and acoustic signal amplitude (Ampl in counts)
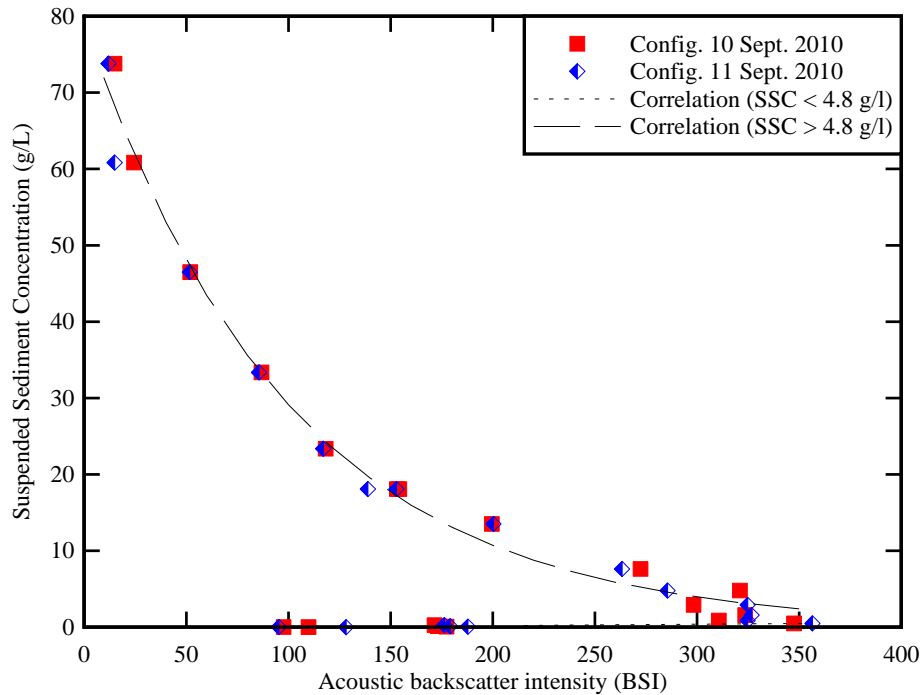
(B) Relationship between suspended sediment concentration (SSC in g/l) and acoustic backscatter intensity (BSI)

Fig. 5-2 - Relationship between suspended sediment concentration, acoustic signal amplitude and acoustic backscatter intensity with the sediment mud collected at Arcins - Comparison between the data and Equations (5-2) and (5-3)

5.2 Field observations

The time-variations of the acoustic backscatter amplitude, and the corresponding suspended sediment concentration (SSC) deduced from Equation (5-3a), are presented in Figure 5-3 for the field studies on 10 and 11 Sept. 2010. The water depth and longitudinal velocity data are reported also in Figure 5-3.

The complete data set showed some increase in SSC with decreasing water depth prior to the tidal bore arrival (Fig. 5-3). The trend could be linked with the larger depth-averaged shear stress in the shallower water column. The passage of the tidal bore was associated with large fluctuations of the backscatter amplitude and SSC including during the flood flow motion. Some unusual event was observed about 100 s after the tidal bore front on both days, lasting for more than 10 minutes (e.g. t = 68,400 to 69,000 s in Fig. 5-3B). The details are shown in Figure 5-4.

For both studies, the event details indicated a sharp decrease in SSC about 50-70 s after the bore front passage (e.g. t = 68,355 s in Fig. 5-3B), followed by a major event with large and rapid fluctuations in SSC: e.g., between t = 68,380 and 68,800 s in Figure 5-3B.

Visually, the authors observed some turbulent patches of mud flocs at the free-surface during the

35

flood flow during the two hours after the tidal bore. The waters were very murky and Figure 5-5 illustrates two examples on 10 September 2010.
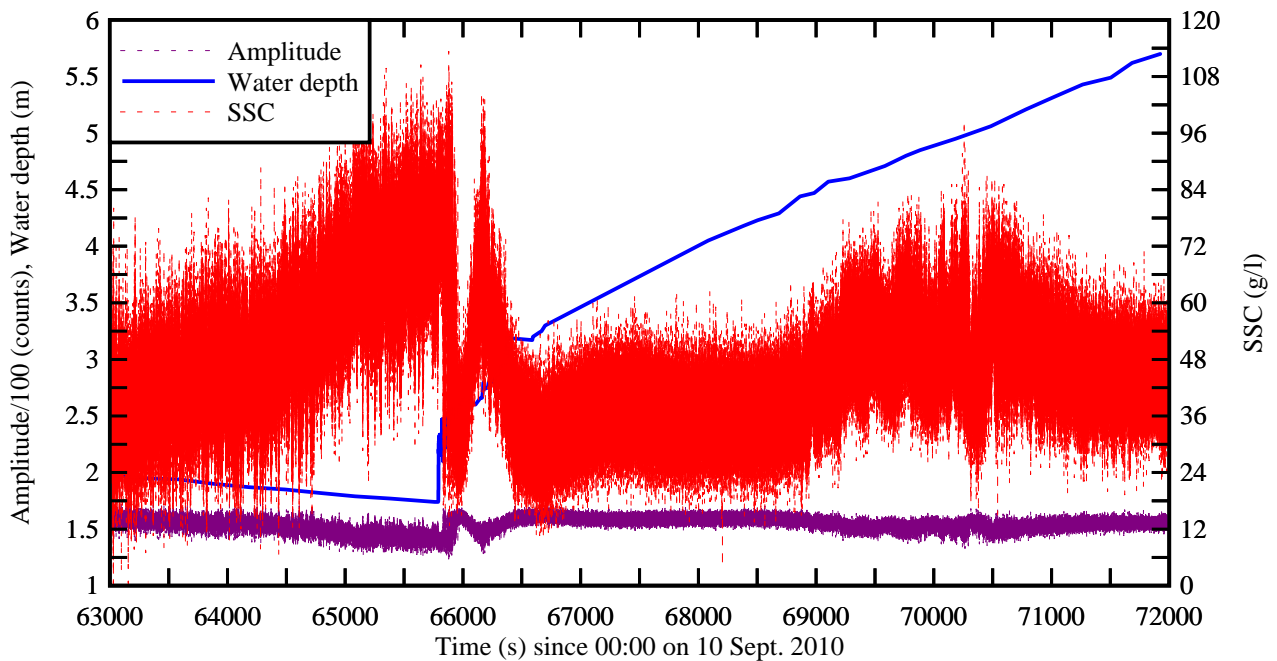
(A) Time variations of the water depth, acoustic backscatter amplitude and suspended sediment concentration (SSC) on 10 Sept. 2010
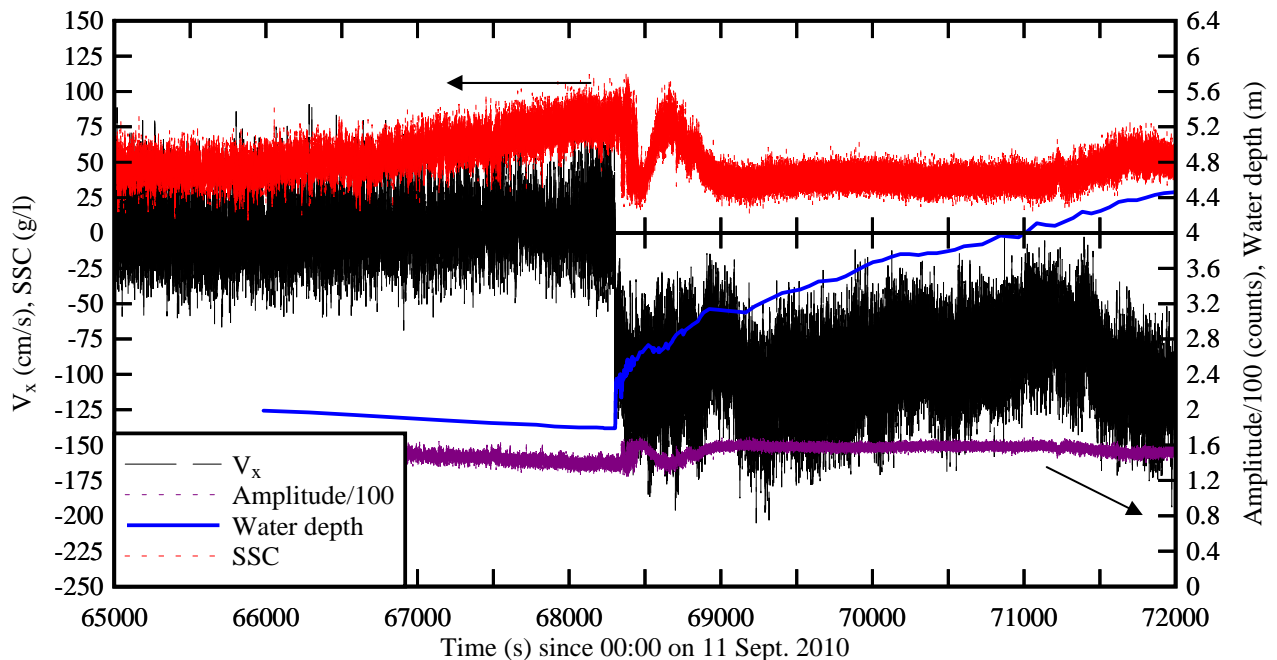
(B) Time variations of the water depth, longitudinal velocity component V_x, acoustic backscatter amplitude and suspended sediment concentration (SSC) on 11 Sept. 2010

Fig. 5-3 - Time variations of the suspended sediment concentration (SSC) on 10 & 11 Sept. 2010 - Post-processed ADV data, sampling rate: 64 Hz
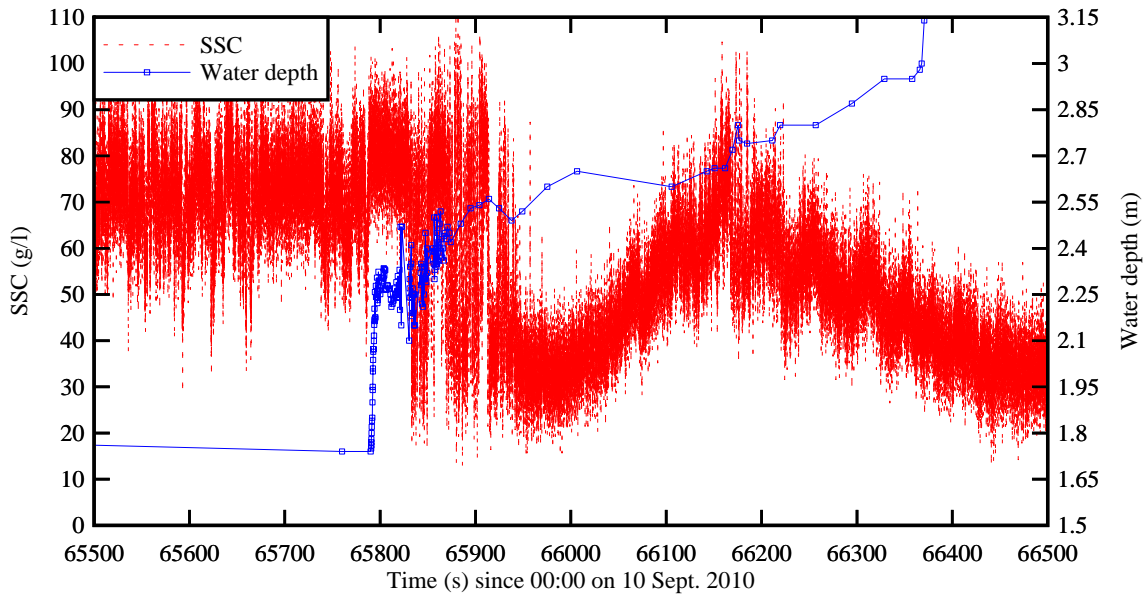
(A) On 10 Sept. 2010
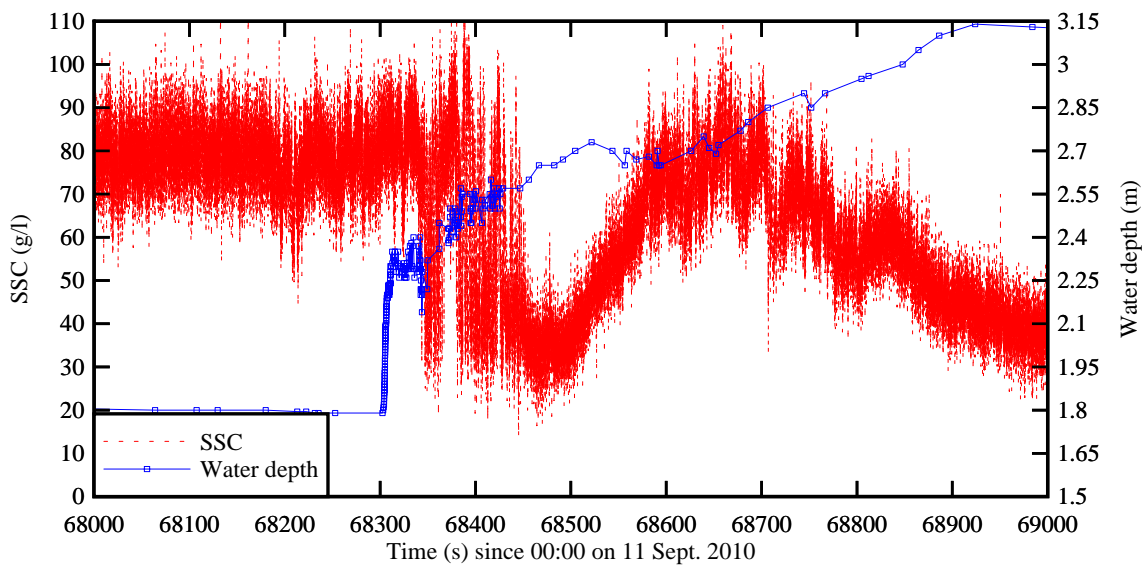
(B) On 11 Sept. 2010

Fig. 5-4 - Water depth and suspended sediment concentration (SSC) shortly after the tidal bore on 10 and 11 Sept. 2010 - Post-processed ADV data, sampling rate: 64 Hz

(A) Murky flood flow past the ADV - Flood flow direction from left to right

(B) Turbulent patches of sediment at the free-surface just downstream of the pontoon

Fig. 5-5 - Photographs of murky waters and sediment patches at the water surface about 50 minutes after the tidal bore on 10 Sept. 2010

5.3 SUSPENDED SEDIMENT FLUX

The present results were used to estimate the instantaneous advective suspended sediment flux per unit area q_s calculated as:

$$q_s = SSC \times V_x \tag{5-4}$$

where q_s and V_x are positive in the downstream direction. In Equation (5-4), the suspended sediment concentration SSC is in kg/m^3, the longitudinal velocity component V_x is in m/s and the sediment flux per unit area is in $kg/m^2/s$. The suspended sediment concentration (SSC) was calculated using Equation (5-3) applied to the post-processed backscatter amplitude signal. The

results are presented in Figure 5-6 in terms of the instantaneous sediment flux q_s.

The sediment flux data showed typically a downstream positive suspended sediment flux during the end of the ebb tide prior to the tidal bore (Fig. 5-6). The arrival of the tidal bore was characterised by a rapid flow reversal and the suspended sediment fluxes were negative during the flood tide after the tidal bore passage. The instantaneous sediment flux data q_s showed some large and rapid time-fluctuations that derived from a combination of velocity and suspended sediment concentration fluctuations. The suspended sediment flux data demonstrated some high-frequency fluctuations with some form of sediment flux bursts that were likely linked to and caused by some turbulent bursting phenomena next to the boundaries. Some low-frequency fluctuations in sediment flux were also observed (Fig. 5-6).

For the study, the sediment flux data were integrated with respect of time. The result gives the net sediment mass transfer per unit area during a period T:

$$\int_T SSC \times V_x \times dt \tag{5-5}$$

Prior the tidal bore ($65{,}000 < t < 68{,}200$ s), the net sediment mass transfer per area was positive and Equation (5-5) yielded $+4{,}770$ kg/m^2 during the 53 minutes of data prior the tidal bore. Immediately after the passage of the bore, the net sediment mass transfer per unit area was negative and equal to $186{,}120$ kg/m^2 for $68{,}300 < t < 72{,}500$ s (i.e. 70 minutes). That is, the net sediment flux was about 30 times larger in magnitude than the sediment flux prior to the tidal bore.
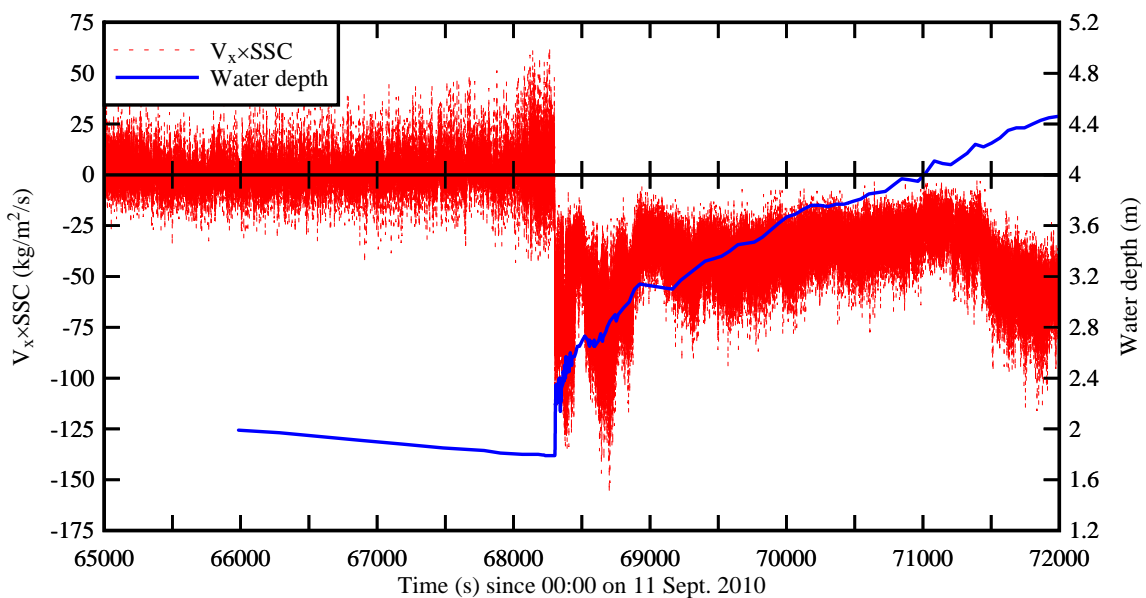
Fig. 5-6 - Time variations of the suspended sediment flux per unit area (SSC×V$_x$) and water depth on 11 Sept. 2010 - Post-processed ADV data, sampling rate: 64 Hz

Discussion

The effects of tidal bores on sediment processes were studied in Alaska, China and France in particular (CHEN et al. 1990, TESSIER and TERWINDT 1994, GREB and ARCHER 2007). Some anecdotal evidences encompassed KJERFVE and FERREIRA (1993) in the Rio Mearim (Brazil), and CHANSON (2001,2008) in the Dordogne River (France). Altogether past studies indicated that the arrival of the bore front was associated with intense bed material mixing and with upstream advection of suspended material behind the bore front. The present data set supported the same trend (Fig. 5-6).

A striking feature of the analysed data set was the large and rapid fluctuations in suspended sediment flux during the tidal bore and flood flow. This feature was not documented, but an important difference between the ADV data set used in this study from earlier reported field measurements was that the present data were collected continuously at relatively high frequency (64 Hz) during a relatively long period (at least 2 hours). It is however acknowledged that the present investigation was a point measurement about 0.8 m beneath the free-surface. Any extrapolation would imply that the sampling volume was representative of the entire channel cross-section.

6. CONCLUSION

Some detailed turbulence field measurements were conducted continuously at high-frequency (64 Hz) prior to, during and after the tidal bore of the Garonne River in September 2010. The turbulent velocity components were sampled with an acoustic Doppler velocimeter (ADV) with its sampling volume about 0.8 m beneath the free-surface. The field site was located in the Arcins channel that is about 1.8 km long, 70 m wide and about 1.1 to 2.5 m deep at low tide.

The tidal bore propagation in the Arcins channel was observed on both 10 and 11 Sept. 2010. The tidal bore was undular as it passed in front of the sampling site. The passage of the tidal bore was characterised by a pseudo-chaotic wave motion lasting for several minutes after the bore. At the sampling location, the free-surface elevation rose very rapidly by 0.50 m and 0.41 m in the first 5 seconds on 10 and 11 Sept. 2010 respectively. For the next 35 minutes, the water elevation rose further by 1.69 m and 1.59 m on 10 and 11 Sept. 2010 respectively. The tidal bore Froude number was estimated from the channel bathymetry and tidal bore observations. It was equal to 1.30 and 1.20 on 10 and 11 Sept. 2010 respectively.

The turbulent velocity data showed the marked impact of the tidal bore propagation. The longitudinal velocity component highlighted some rapid flow deceleration during the passage of the tidal bore, associated with a sudden rise in the free surface elevation, and a flow reversal after the tidal bore front passage. The observations were consistent with the earlier field and laboratory results. The tidal bore passage was further characterised by some large fluctuations of all three turbulent velocity components. The Reynolds stress data indicated some large and rapid turbulent stress fluctuations during the tidal bore and flood flow. The Reynolds stress magnitudes were significantly larger than during the ebb tide, and some substantial normal and tangential stress fluctuations were observed.

The ADV backscatter intensity was calibrated in terms of the suspended sediment concentration in laboratory using the soft mud bed material. The results provided an unique characterisation of the turbulence and sediment flux beneath to the free-surface during the tidal bore. The sediment flux data showed a downstream positive suspended sediment flux during the end of the ebb tide prior to the tidal bore. The arrival of the tidal bore was characterised by a rapid reversal and the suspended sediment fluxes were negative during the flood tide. Prior the tidal bore, the net sediment mass transfer per area was positive. After the passage of the bore, the net sediment mass transfer per unit area was negative and its magnitude was 30 times larger than the ebb tide net flux.

A striking feature of the present field data set was the large and rapid fluctuations in turbulent velocities and suspended sediment flux during the tidal bore and flood flow. This was not documented to date, but an important difference between the ADV data set used herein from earlier

reported field measurements was that the present data were collected continuously at relatively high frequency (64 Hz) during a relatively long period (at least 2 hours). However the present investigation was a point measurement 0.8 m beneath the free-surface, and any extrapolation to the entire channel cross-section would be inappropriate.

This study must be complemented by further field works conducted in the same system under different tidal and fluvial conditions. These studies may include several ADV systems located at different transverse and vertical locations. Further new studies should be conducted in different estuarine systems, including shallow water bays, with different topographies and different sediment materials (cohesive and non-cohesive). Importantly any future studies should include a detailed characterisation of the water physical properties before, during and after the tidal bore, including water temperature, conductivity, turbidity, pH, dissolved oxygen... These measurements should be performed at different vertical elevations.

7. ACKNOWLEDGEMENTS

APPENDIX A - LIST OF FIELD WORK PARTICIPANTS (FIELD STUDY G10, 10 AND 11 SEPTEMBER 2010)

FRIDAY 10 SEPT. 2010

       Hubert CHANSON

       Pierre LUBIN

       Bruno SIMON

       Cedric LE BOT

       Stephane GLOCKNER

       Etienne AHUSBORDE

       Arthur SARTHOU

       Frederic DANEY

       Patrick VIALLE

       Valérie THOUARD

SATURDAY 11 SEPT. 2010

       Hubert CHANSON

       Pierre LUBIN

       Bruno SIMON

       Cedric LE BOT

       Stephane GLOCKNER + Andrea

       Arthur SARTHOU

       Stephen VINCENT + Christelle

       David REUNGOAT + Wife & Family

       Valérie THOUARD + Husband & Family

(A) On 10 Sept. 2010 before the tidal bore - From left to right: Cedric LE BOT, Etienne AHUSBORDE, Stephane GLOCKNER, Bruno SIMON and Pierre LUBIN behind the pylon

(B) Channel cross-section surveying by Arthur SARTHOU and Frederic DANEY (from left to right) on 10 Sept. 2010

(C, Left) Patrick VIALLE on 10 Sept. 2010

(D, Right) On 11 Sept. 2010 before the tidal bore - From left to right: David REUNGOAT, Christelle, Stephane GLOCKNER, Pierre LUBIN (in the water), Bruno SIMON, Cedric LE BOT

(E) David REUNGOAT measuring the surface velocity on 11 Sept. 2010 after the tidal bore

(F) On 11 Sept. 2010 looking downstream with Pont François Mitterand in the background - From left to Right: Stephane GLOCKNER, Stephane VINCENT, Pierre LUBIN, Christelle, Cedric LE BOT, Arthur SARTHOU

Fig. A-1 - Photographs of the participants

APPENDIX B - PHOTOGRAPHS OF THE FIELD STUDY G10 (10 AND 11 SEPTEMBER 2010)

(A) Looking upstream at the *Bras d'Arcins* with *Île d'Arcins* on the right on 9 Sept. 2010 at low tide - The ADV was fixed on the pontoon on the left next to the right bank - Photograph taken from Pont Mitterand

(B) Looking downstream at the *Bras d'Arcins* with *Île d'Arcins* on the left on 11 Sept. 2010 at low tide with Pont Mitterand in the background - The ADV was fixed on the pontoon on the right next to the right bank

(C) View from the right bank on 11 Sept. 2010 at 16:30 - The ADV was fixed between the two hulls of the pontoon in front of the pylon

(D) Details of the ADV - On 10 Sept. 2010 at 19:05 about 50 minutes after the tidal bore - Flow velocity from left to right - Note the dark brown colour of the waters highlighting the large suspended sediment load

Fig. B-1 - Sampling site on the Garonne River between *Île d'Arcins* and Latresne

(A) Bore formation at the channel downstream end at 18:12:50

(B) At 18:13:00

(C) Breaking bore front at 18:13:55

(D) At 18:15:45

(E) Tidal bore at 18:17:06 - Note the undular bore front but close to Île d'Arcins - Frederic DANEY is surfing the bore at the "shoulder" between the breaking and undular front

(F) Tidal bore passing the sampling site at 18:17:40 - Note Frederic DANEY surfing the bore close to Île d'Arcins - On the right, Pierre LUBIN hold the survey staff used to record the water level

(G) At 18:17:45

(H) Whelps at the sampling site at 18:18:30- On the right, Pierre LUBIN hold the survey staff used to record the water level and the ADV is behind him in between the hulls the pontoon

Fig. B-2 - Tidal bore on 10 Sept. 2010
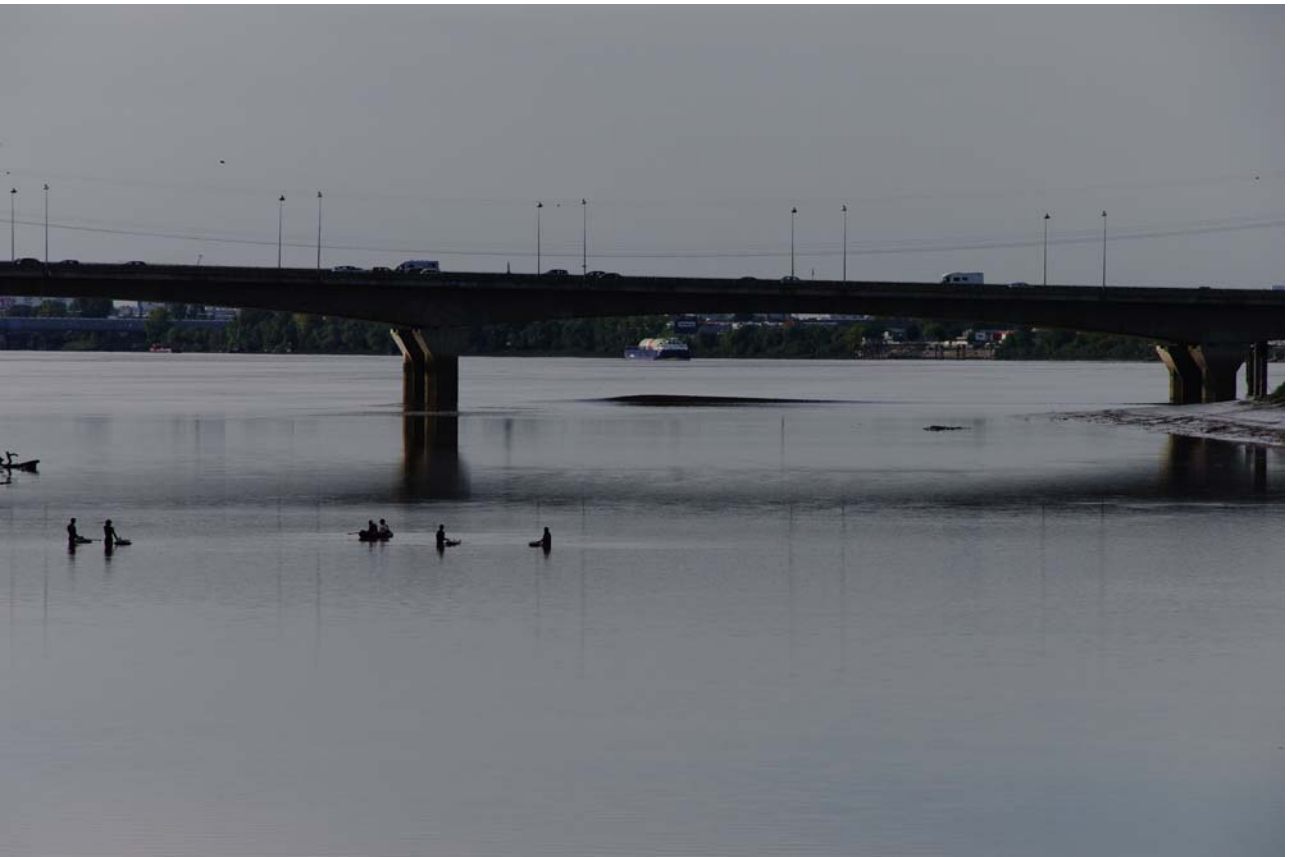
(A) Bore formation at the channel downstream end at 18:54:20

(B) At 18:54:50 - Note the Airbus barge in the background travelling upstream to Langon behind the tidal bore, and the surfers in the foreground standing next to their surf boards

(C) Breaking bore front at 18:55:50

(D) Surfing the bore at 18:58:10

(E) Undular bore but close to *Île d'Arcins* at 18:59:17

(F) Tidal bore passing the sampling site at 18:59:30 - Note the surfers close to *Île d'Arcins*

(G) At 18:59:37

(H) Whelps at 18:59:51 - Stephane VINCENT held the survey staff used to record the water level, with Pierre LUBIN behind him

(I) Whelps at 19:01:41 - Stephane VINCENT held the survey staff and discussed with Pierre LUBIN on his left

Fig. B-3 - Tidal bore on 11 Sept. 2010

APPENDIX C - ACOUSTIC DOPPLER VELOCIMETER CONFIGURATIONS (FIELD STUDY G10, 10 AND 11 SEPTEMBER 2010)

C.1 PRESENTATION

During the field investigation, a Nortek^{TM} Vector ADV (6 MHz, serial number VEC3332) was deployed. The ADV was equipped with a 3D downlooking head (Head ID VEC4665). The ADV V_x direction (receiver head with red mark) was pointed downstream.

The ADV was fixed at the downstream end of a 23.55 m long heavy, sturdy pontoon and it was self logging. The probe was located between the hulls and the sampling volume was 0.8 m below the free-surface. Figure C-1 shows the turbulent velocity data sets. The paragraphs C.2 and C.3 list the ADV settings for the 10 and 11 Sept. 2010 respectively.

Discussion

The main difference between the two configurations was the control volume size: 3.5 mm on 10 Sept. 2010 and 6.6 mm on 11 Sept. 2010. The present experience showed that the original ADV settings (10 Sept. 2010) yielded some very noisy and spiky velocity data, although the signal amplitude, SNR and backscatter data appeared to be correct. A spectral analysis of all velocity components indicated some significant noise for frequencies larger than 0.02 to 0.1 Hz (Fig. C-2). This is seen in Figure C-2 where the power spectrum density functions for the longitudinal velocity component are compared.

As a result, a slightly different set-up was selected on 11 Sept. 2010 with a 6.6 mm control volume size. The change yielded a good quality data set including for the turbulent velocity. Figure C-1 illustrates the contrast in terms of un-processed velocity components. In Figure C-1B, the passage of the tidal bore is seen to be associated with a rapid flow reversal.

While the exact cause of the problem remains unknown, it is thought that the ADV system was overloaded with the smaller control volume on 10 Sept. 2010.
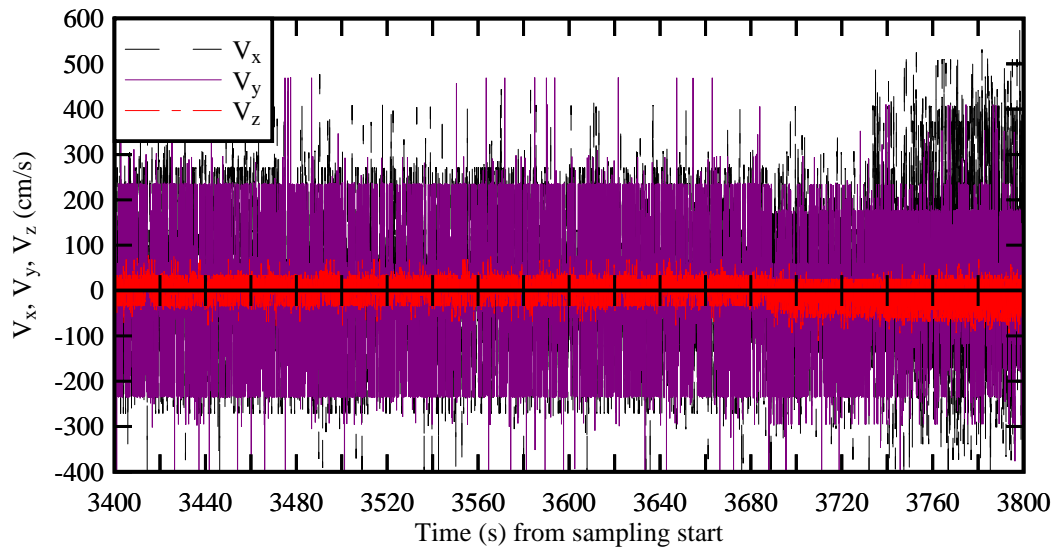
(A) Raw data on 10 Sept. 2010
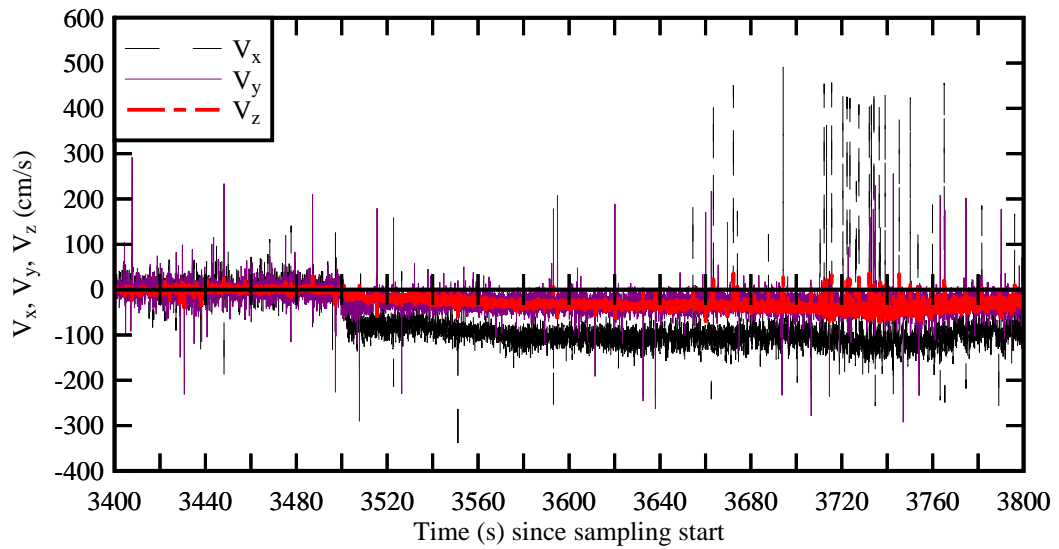
(B) Raw data on 11 Sept. 2010

Fig. C-1 - ADV turbulent velocity components
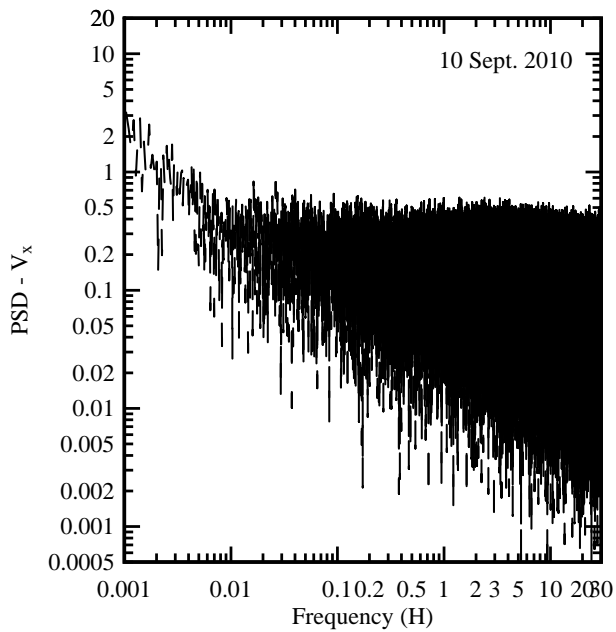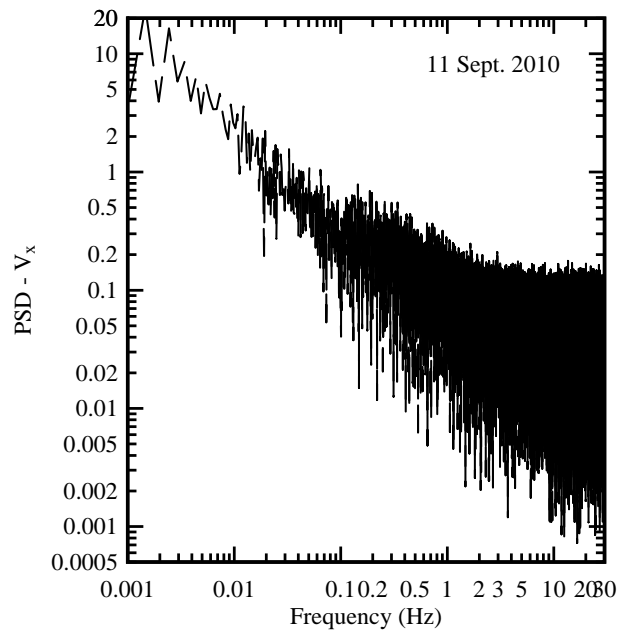
(A, Left) 10 Sept. 2010   (B, Right) 11 Sept. 2010

Fig. C-2 - Power density spectrum of the longitudinal velocity component V_x - Post-processed data

C.2 CONFIGURATION FRIDAY 10 SEPT. 2010

<u>User setup</u>

Sampling rate 64 Hz

Nominal velocity range 2.00 m/s

Burst interval CONTINUOUS

Samples per burst N/A

Sampling volume 3.5 mm

Measurement load 178 %

Transmit length 2.0 mm

Receive length 0.00 m

Output sync VECTOR

Analog output DISABLED

Analog input 1 NONE

Analog input 2 NONE

Power output DISABLED

Output format VECTOR

Velocity scaling 1 mm

Powerlevel HIGH

Coordinate system XYZ

Sound speed MEASURED

Salinity 0.0 ppt

Distance between pings 1.01 m

Number of beams 3

Software version 1.32

Wrap mode OFF

Deployment time 10/09/2010 5:15:00 PM

Hardware configuration

Serial number VEC 3332

Internal code version 13

Revision number 60

Recorder size 154 MByte

Firmware version 1.21

Head configuration

Pressure sensor YES

Compass YES

Tilt sensor YES

System 1 0

Head frequency 6000 kHz

Serial number VEC 4665

Transformation matrix 2.7312 -1.3479 -1.3835

0.0217 2.3530 -2.3708

0.3440 0.3389 0.3479

Pressure sensor calibration 0 0 4472 24558

Number of beams 3

C.3 CONFIGURATION SATURDAY 11 SEPT. 2010

User setup

Sampling rate 64 Hz

Nominal velocity range 2.00 m/s

Burst interval CONTINUOUS

Samples per burst N/A

Sampling volume 6.6 mm

Measurement load 62 %

Transmit length 2.0 mm

Receive length 0.00 m

Output sync VECTOR

Analog output DISABLED

Analog input 1 NONE

Analog input 2 NONE

Power output DISABLED

Output format VECTOR

Velocity scaling 1 mm

Powerlevel HIGH

Coordinate system XYZ

Sound speed MEASURED

Salinity 0.0 ppt

Distance between pings 1.01 m

Number of beams 3

Software version 1.32

Wrap mode OFF

Deployment time 11/09/2010 18:00:00

Hardware configuration

Serial number VEC 3332

Internal code version 13

Revision number 60

Recorder size 154 MByte

Firmware version 1.21

Head configuration

Pressure sensor YES

Compass YES

Tilt sensor YES

System 1 0

Head frequency 6000 kHz

Serial number VEC 4665

Transformation matrix 2.7312 -1.3479 -1.3835

0.0217 2.3530 -2.3708

0.3440 0.3389 0.3479

Pressure sensor calibration 0 0 4472 24558

Number of beams 3

APPENDIX D - EXPERIMENTAL DATA: ACOUSTIC BACKSCATTER INTENSITY VERSUS SUSPENDED SEDIMENT CONCENTRATION

D.1 PRESENTATION

Some Garonne River bed materials were collected at low tide on 11 September 2010 next to the right bank at Arcins. The soil sample consisted of fine mud and silt materials collected on the stream bed just above the low water mark. The mud sample was soft and could be considered somehow as a form of mud cream (*crème de vase*), although the granulometry was not tested. A series of laboratory tests were conducted with the Nortek™ Vector ADV (6 MHz, serial number VEC3332) system using the same settings as for the field observations on 10 and 11 Sept. 2010 (App. C). The ADV was calibrated by measuring the signal amplitude of known, artificially produced concentrations of material obtained from the bed material sample, diluted in tap water and thoroughly mixed. For each test, a known mass of sediment was introduced in the water tank which was stirred continuously with two propeller mixers (Fig. D-1). The mixers' blades were located at 85 and 60 mm above the tank bottom, and the ADV sampling volume was 57 mm above the tank bottom. The tank was strongly agitated by the two mixers. Typically the standard deviations of the velocity components were: $v_x' \approx 0.25\text{-}1.0$ m/s, $v_y' \approx 0.25\text{-}1.0$ m/s, and $v_z' \approx 0.10\text{-}0.24$ m/s depending upon the experimental conditions.

The mass of wet sediment was measured with a Mettler™ Type PM200 (Serial 86.1.06.627.9.2) balance, and the error was less than 0.01 g. The mass concentration was deduced from the measured mass of wet sediment and the measured water tank volume. The acoustic backscatter amplitude measurements were conducted with the ADV (6 MHz) system using the same configuration employed in the field (pulse length, scan rate, velocity range). The ADV signal outputs were scanned at 64 Hz for 3 minutes for each test. The average amplitude measurements represented the average signal strength of the three ADV receivers. They were measured in counts, with one count equal to 0.45 dB (Nortek 2005). The backscatter intensity was deduced from the average amplitude as:

$$\text{BSI} = 10^{-5} \times 10^{0.043 \times \text{Ampl}} \tag{D-1}$$

where the backscatter intensity BSI is dimensionless and the average amplitude Ampl is in counts. The coefficient 10^{-5} is a value introduced to avoid large values of backscatter intensity (NIKORA and GORING 2002, CHANSON et al. 2008). Note that the ADV data were post-processed with the removal of average signal to noise ratio data less than 15 dB, average correlation values less than 60%, and communication errors. No further processing was performed.
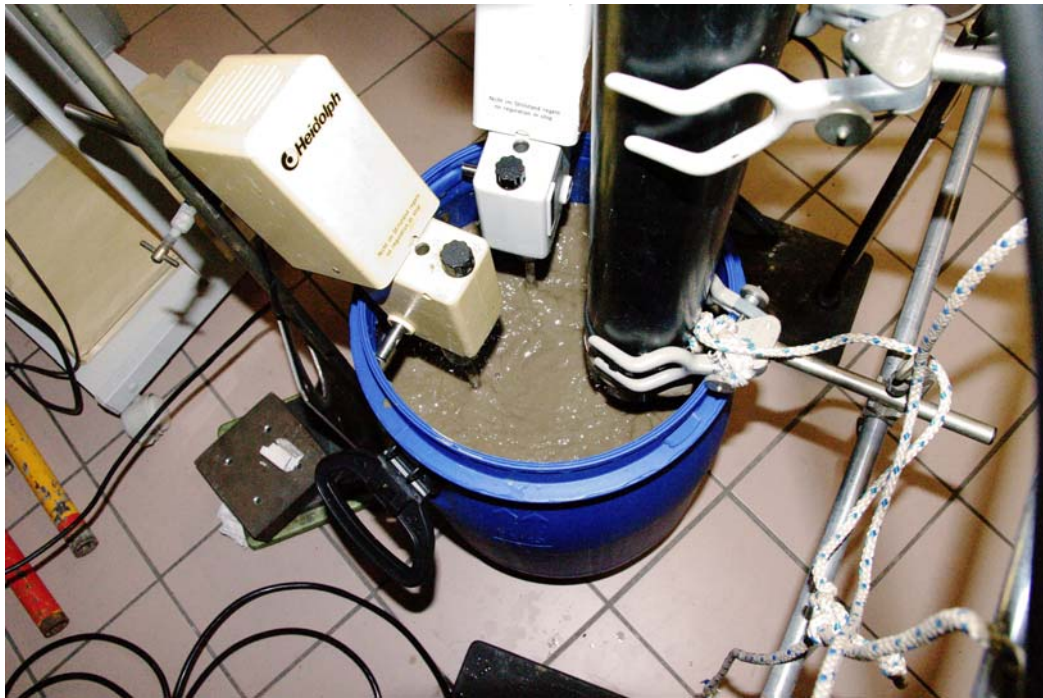
Fig. D-1 - Photograph of the laboratory experiment with the ADV on the right and the two mixers on the centre and left - SSC = 60.8 g/l

D.2 EXPERIMENTAL RESULTS

Location :	The University of Bordeaux (France)
Dates :	13-15 September 2010
Experiments by :	H. CHANSON and D. REUNGOAT
Data processing by:	H. CHANSON
Soil and water samples :	Tap water. Mud samples collected in the Arcins channel (Garonne River, France) next to the right bank just above the low water line on 11 Sept. 2010 at about 18:15 before the tidal bore passage.
Instrumentation :	Nortek™ Vector ADV (6 MHz, serial number VEC3332) with a three-dimensional down-looking head (Head ID VEC4665) scanned at 64 Hz for 3 minutes for each test. ADV settings: 10 Sept. 2010 & 11 Sept. 2010 (App. C).
Comments :	Soil sample collection on a sunny day. All the samples were kept in sealed, water tight containers until testing. Water temperature: 17 to 20.5 C.

Laboratory tests - Vector ADV system measurements - Configuration Friday 10 Sept. 2010

Test	SSC	Avg Ampl	Avg BSI	Avg Correl	Avg SNR	Percent. good samples	Avg V_x	Avg V_y	Avg V_z	Std V_x	Std V_y	Std V_z
	g/l	counts	Eq. (B-1)	%	dB	%	cm/s	cm/s	cm/s	cm/s	cm/s	cm/s
4	0.00	163.7	109.9	97.7	70.4	93.9	-11.18	10.98	-4.96	202.7	212.1	37.2
5	0.02	162.6	97.6	97.7	69.9	93.9	-5.83	7.63	-4.70	206.7	211.2	37.2
12	0.06	168.6	177.4	97.7	72.5	93.9	-10.12	6.27	-3.93	204.9	209.2	37.2
13	0.13	168.3	173.1	97.7	72.4	93.9	-9.32	9.99	-3.68	208.2	209.9	37.2
20	0.27	168.2	171.5	97.7	72.3	93.9	-9.89	4.42	-6.82	207.1	212.9	36.6
21	0.48	175.4	347.5	97.8	75.4	93.9	-12.94	8.32	-7.63	200.9	204.4	36.3
25	0.87	174.2	310.7	97.7	74.9	93.9	-9.25	17.58	-4.22	201.2	203.7	36.8
28	1.58	174.7	323.6	97.8	75.1	93.9	-12.42	13.25	-4.10	198.9	203.9	36.1
29	2.92	173.8	298.3	97.7	74.8	93.9	-13.15	16.81	-4.26	198.4	202.2	36.5
32	4.79	174.6	321.0	97.7	75.1	93.9	-16.45	18.11	-5.00	185.7	190.0	33.9
33	7.61	172.9	272.4	97.7	74.4	93.9	-12.02	19.11	-4.75	185.1	183.0	33.4
36	13.52	169.8	199.6	97.7	73.0	93.9	-16.55	22.41	-5.00	178.6	180.4	32.2
37	18.09	167.1	153.1	97.7	71.9	93.9	-15.26	21.72	-5.83	175.5	176.8	31.8
50	18.09	167.2	154.3	97.7	71.9	93.9	-15.72	13.59	-5.59	173.2	182.7	32.1
53	23.37	164.5	118.2	97.7	70.7	93.9	-17.68	19.05	-11.62	127.7	130.4	24.9
54	33.35	161.4	86.8	97.7	69.4	93.9	-17.02	19.18	-10.86	127.8	132.2	25.3
57	46.50	156.2	51.9	97.8	67.2	93.9	-16.02	18.59	-11.87	125.4	128.3	24.5
58	60.83	148.6	24.4	97.8	63.9	93.9	-19.97	19.95	-10.90	134.3	140.1	26.0
61	73.79	143.5	14.8	97.8	61.7	93.9	-13.89	18.30	-10.49	125.1	128.1	25.1

Notes: 3D Vector ADV data scanned at 64 Hz for 3 minutes; Ampl: acoustic backscatter amplitude (counts); Avg: time-averaged; Correl: correlation; Percent. good samples: percentage of good ADV samples after post-processing; SNR: signal to noise ratio; Std: standard deviation.

Laboratory tests - Vector ADV system measurements - Configuration Saturday 11 Sept. 2010

Test	SSC	Avg Ampl	Avg BSI	Avg Correl	Avg SNR	Percent. good samples	Avg V_x	Avg V_y	Avg V_z	Std V_x	Std V_y	Std V_z
	g/l	counts	Eq. (B-1)	%	dB	%	cm/s	cm/s	cm/s	cm/s	cm/s	cm/s
3	0.00	165.3	128.2	88.0	71.1	99.1	-14.88	12.54	-4.38	130.2	137.5	24.3
6	0.02	162.3	95.4	86.8	69.8	98.7	-14.13	15.06	-3.54	137.6	147.0	25.5
11	0.06	169.2	187.9	88.3	72.7	99.1	-13.54	10.84	-2.34	121.1	126.2	22.6
14	0.13	168.7	179.2	89.0	72.5	99.2	-14.23	10.16	-2.31	122.0	127.3	22.8
19	0.27	168.5	176.3	86.2	72.5	98.5	-22.66	11.66	-7.81	128.3	136.2	24.4
22	0.48	175.6	356.5	83.8	75.5	96.7	-23.05	11.15	-9.95	120.0	124.8	23.1
26	0.87	174.7	324.8	85.2	75.1	97.9	-16.80	19.52	-2.96	114.3	117.2	21.4
27	1.58	174.8	326.8	84.9	75.1	97.6	-17.93	21.91	-3.77	112.4	114.4	21.1
30	2.92	174.7	324.8	84.3	75.1	96.8	-17.38	22.86	-3.23	102.8	105.9	19.7
31	4.79	173.4	285.6	82.6	74.6	94.9	-13.06	24.32	-5.26	99.9	100.5	20.0
34	7.61	172.6	263.3	80.8	74.2	93.0	-18.85	26.60	-5.76	83.2	84.0	17.0
35	13.52	169.8	200.4	81.5	73.0	93.7	-20.01	27.80	-6.47	73.0	74.9	15.5
38	18.09	167.1	152.9	81.5	71.9	93.8	-18.85	26.34	-6.68	66.5	68.3	14.8
51	18.09	166.1	138.9	83.2	71.4	95.9	-23.67	19.34	-11.36	49.6	52.6	13.2
52	23.37	164.4	117.0	84.5	70.7	97.4	-21.36	18.38	-11.57	29.7	29.5	10.9
55	33.35	161.2	85.6	85.7	69.3	98.0	-19.70	15.79	-10.63	28.7	27.6	10.6
56	46.50	156.1	51.7	86.8	67.1	98.6	-14.50	15.63	-7.56	26.2	25.7	10.0
59	60.83	143.6	14.9	77.8	61.7	87.0	-24.63	24.57	-9.58	55.9	58.0	13.9
60	73.79	141.4	12.0	80.8	60.8	92.6	-26.40	21.87	-11.89	40.2	40.6	12.7

Notes: 3D Vector ADV data scanned at 64 Hz for 3 minutes; Ampl: acoustic backscatter amplitude (counts); Avg: time-averaged; Correl: correlation; Percent. good samples: percentage of good ADV samples after post-processing; SNR: signal to noise ratio; Std: standard deviation.

D.3 DISCUSSION

The experimental data showed that the results were basically independent of the ADV settings for the two selected configurations (App. C). Further the data showed a monotonic increase in ADV amplitude counts with increasing SSC up to 0.48 g/l. The trend was consistent with earlier results with cohesive sediments including CHANSON et al. (2008) and HA et al. (2009).

For larger suspended sediment concentrations (SSC > 0.48 g/l), some signal amplitude attenuation was observed and believed to be linked multiple scattering and associated sound absorption. The ADV backscatter intensity was saturated and decreased with increasing SSC.

APPENDIX E - UNSTEADY TURBULENT REYNOLDS STRESSES DURING THE TIDAL BORE ON 11 SEPT. 2010

E.1 PRESENTATION

Some detailed turbulence field measurements were conducted continuously at high-frequency (64 Hz) prior to, during and after the tidal bore of the Garonne River on 11 September 2010. An acoustic Doppler velocimeter (ADV) was fixed on a large, heavy pontoon and the instrument sampled the turbulent velocity components about 0.8 m beneath the free-surface. The ADV data underwent a thorough post-processing procedure to eliminate any erroneous or corrupted data from the data sets to be analysed. The post processing was conducted with the software WinADV[TM] version 2.026, and it included the removal of communication errors, the removal of average signal to noise ratio data less than 15 dB and the removal of average correlation values less than 60%. In addition, the phase-space thresholding technique developed by GORING and NIKORA (2002) was applied to remove spurious points.

The turbulent Reynolds stresses characterise a transport effect resulting from turbulent motion induced by velocity fluctuations with its subsequent increase of momentum exchange and of mixing (BRADSHAW 1971, PIQUET 1999). The Reynolds stresses are proportional to the product of two velocity fluctuations, where the turbulent velocity fluctuation is the deviation of the instantaneous velocity from a low-pass filtered velocity component, also called the variable interval time average VITA. The VITA method was applied using a cut-off frequency derived upon a sensitivity analysis conducted between an upper limit of the filtered signal (herein 32 Hz, the Nyquist frequency) and a lower limit corresponding to a period of about 1-2 s of some residual undulations. The results yielded an optimum threshold of $F_{cutoff} = 1$ Hz, and the filtering was applied to all velocity components. Note that KOCH and CHANSON (2008) and DOCHERTY and CHANSON (2010) selected similarly a cutoff period $1/F_{cutoff}$ that was between the undulation period and half the undulation period, as in the present study. The filtering was applied to all velocity components ([1]), and the turbulent Reynolds stresses were calculated from the high-pass filtered signals.

The experimental results are presented in the next section.

---

[1] Prior to the filtering, the erroneous data points were replaced by linear interpolation between the end points of the removed data interval.

E.2 EXPERIMENTAL RESULTS

E.2.1 Normal Reynolds stresses
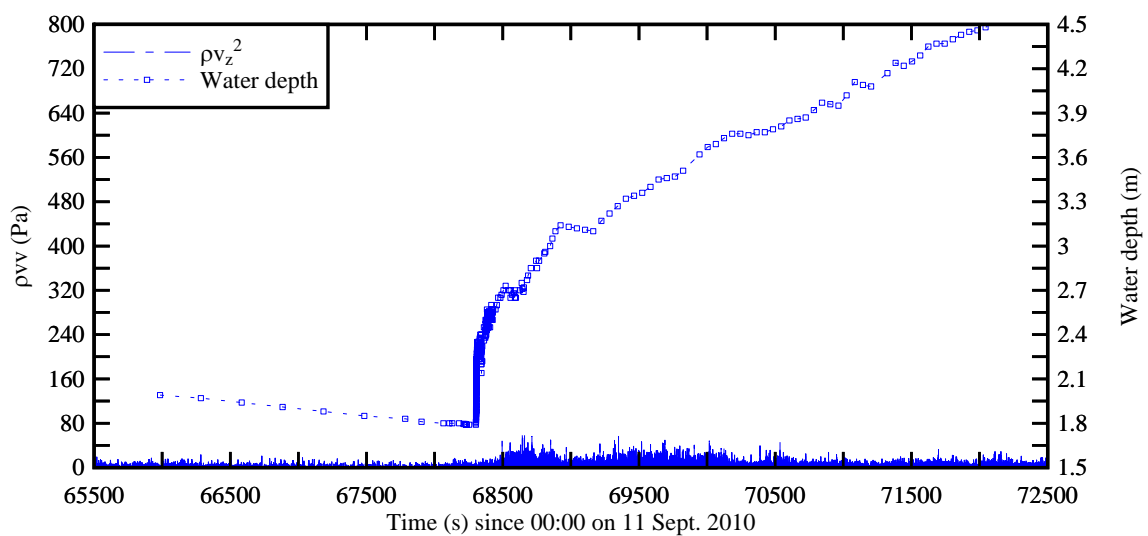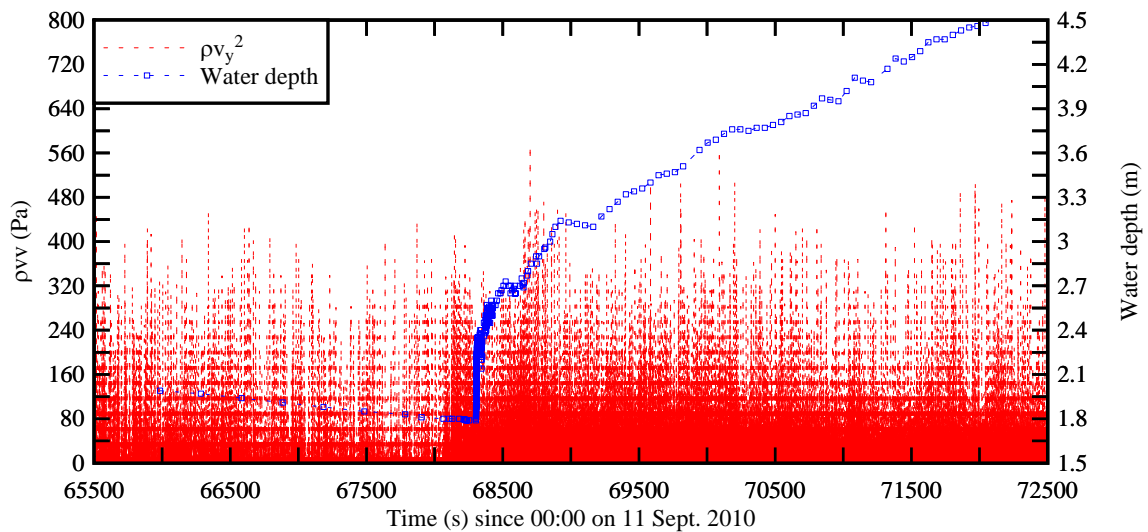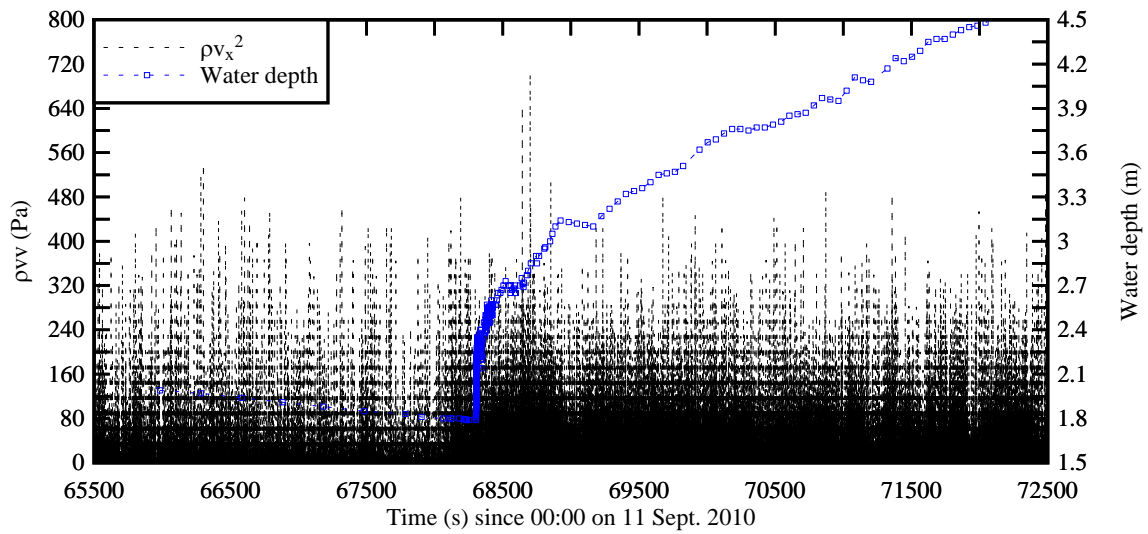
E2.2 Tangential Reynolds stresses
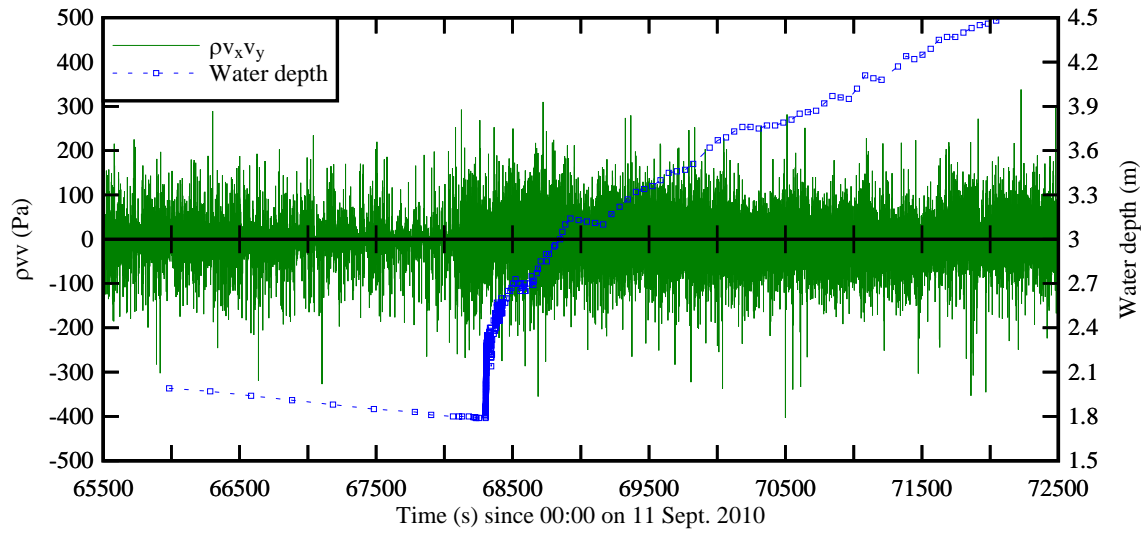
APPENDIX F - APPLICATION OF THE CONTINUITY AND MOMENTUM PRINCIPLES TO A TIDAL BORE PROPAGATING IN A CHANNEL OF IRREGULAR CROSS-SECTIONAL SHAPE (BY H. CHANSON)

F.1 PRESENTATION

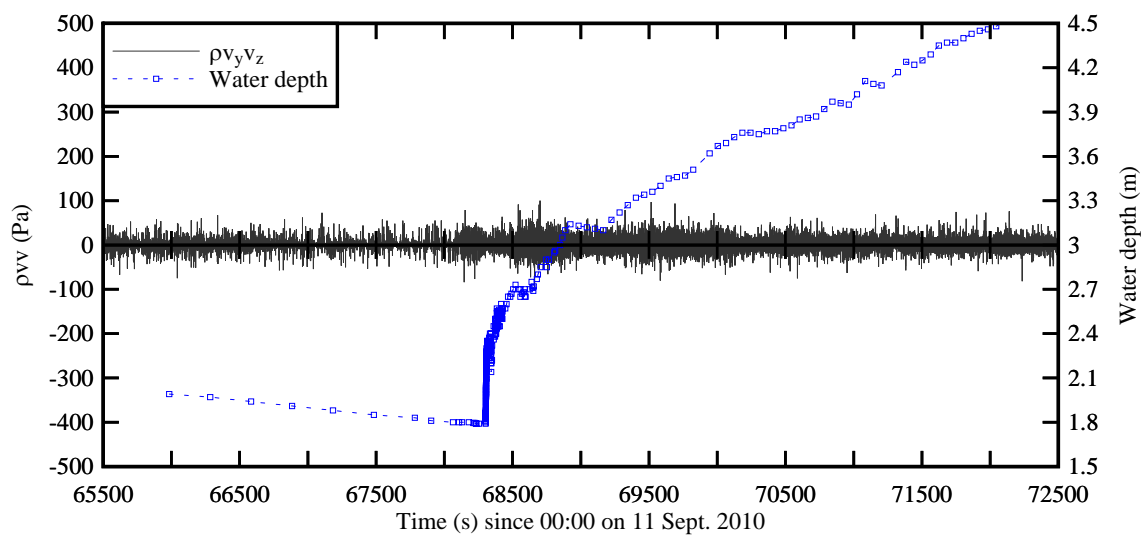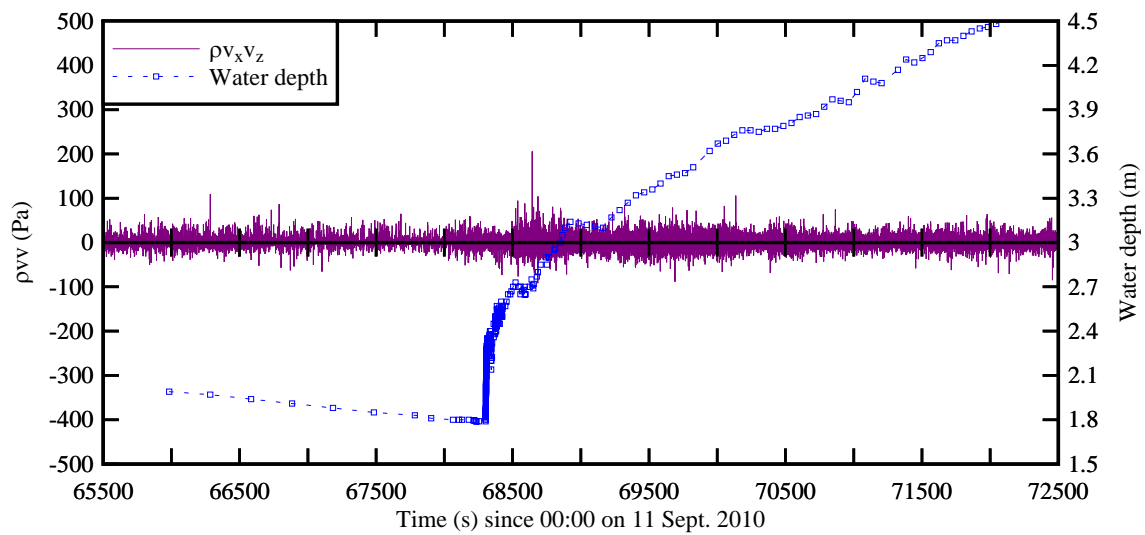A tidal bore is a hydraulic jump in translation. Its front is characterised by a sudden rise in free-surface elevation and a discontinuity of the pressure and velocity fields: it is a hydrodynamic shock (LIGHTHILL 1978). In a tidal bore, the flow properties immediately before and after the bore front must satisfy the equations of conservation of mass and momentum (HENDERSON 1966, LIGGETT 1994, CHANSON 2004). In the system of reference in translation with the bore front, the integral form of the equations of conservation of mass and momentum gives a series of relationships between the flow properties in front of and behind the bore:

$$(V_1 + U) \times A_1 = (V_2 + U) \times A_2 \tag{F-1}$$

$$\rho \times (V_1 + U) \times A_1 \times (\beta_1 \times (V_1 + U) - \beta_2 \times (V_2 + U)) = \iint_{A_2} P \times dA - \iint_{A_1} P \times dA + F_{fric} \tag{F-2}$$

where ρ is the water density, g is the gravity acceleration, U is the bore celerity for an observer standing on the bank, positive upstream, V is the cross-sectional averaged velocity positive downstream towards the river mouth, A is the flow cross-section, β is a momentum correction coefficient, P is the pressure, the subscript 1 refers to the initial flow conditions and the subscript 2 refers to the flow conditions immediately after the passage of the front, and F_{fric} is the flow resistance force.

Fig. F-1 - Definition sketch of a tidal bore propagation in a natural channel

Neglecting the flow resistance ($F_{fric} = 0$) and the effect of the velocity distribution ($\beta_1 = \beta_2 = 0$), the momentum principle becomes:

$$\rho \times (V_1 + U) \times A_1 \times (V_1 - V_2) = \iint\limits_{A_2} P \times dA - \iint\limits_{A_1} P \times dA \qquad \text{(F-3)}$$
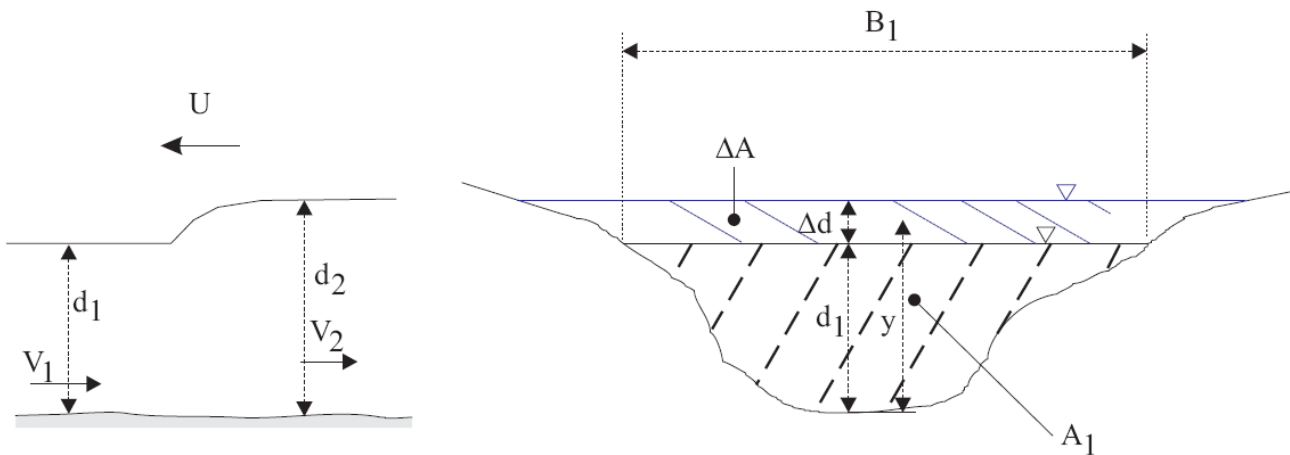
The difference in pressure forces may be derived assuming a hydrostatic pressure distribution in front of and behind the tidal bore front. The net pressure force resultant consists of the increase of pressure $\rho \times g \times (d_2 - d_1)$ applied to the initial flow cross-section A_1 plus the pressure force on the area $\Delta A = A_2 - A_1$:

$$\iint\limits_{A_1}^{A_2} \rho \times g \times (d_2 - y) \times dA = \frac{1}{2} \times \rho \times g \times (d_2 - d_1)^2 \times B' \qquad \text{(F-4)}$$

where y is the distance normal to the bed, d_1 and d_2 are the initial and new flow depths (Fig. F-1), and B' is characteristic free-surface width.

Equation (F-3) may be rewritten:

$$\rho \times (V_1 + U) \times A_1 \times (V_1 - V_2) = \rho \times g \times (d_2 - d_1) \times A_1 + \frac{1}{2} \times \rho \times g \times (d_2 - d_1)^2 \times B' \qquad \text{(F-5)}$$

Let us note that

$$\iint\limits_{A_1}^{A_2} dA = A_2 - A_1 = (d_2 - d_1) \times B \qquad \text{(F-6)}$$

where B is another characteristic free-surface width.

F.2 GENERAL SOLUTION

In the general case, the momentum principle becomes:

$$\rho \times (V_1 + U) \times A_1 \times (V_1 - V_2) = \frac{1}{2} \times \rho \times g \times \frac{(A_2 - A_1)}{B} \times \left(\left(2 - \frac{B'}{B} \right) \times A_1 + \frac{B'}{B} \times A_2 \right) \qquad \text{(F-7)}$$

Since the continuity equation may be rewritten:

$$(V_1 - V_2) = (V_1 + U) \times \frac{A_2 - A_1}{A_2} \qquad \text{(F-8)}$$

the combination of the continuity and momentum principle gives:

$$(U + V_1)^2 = \frac{1}{2} \times \frac{g \times A_2}{A_1 \times B} \times \left(\left(2 - \frac{B'}{B} \right) \times A_1 + \frac{B'}{B} \times A_2 \right) \qquad \text{(F-9)}$$

$$(V_1 - V_2)^2 = \frac{1}{2} \times \frac{g \times (A_2 - A_1)^2}{B \times A_1 \times A_2} \times \left(\left(2 - \frac{B'}{B} \right) \times A_1 + \frac{B'}{B} \times A_2 \right) \qquad \text{(F-10)}$$

Equation (F-9) may be transformed into:

$$\frac{(U + V_1)^2}{g \times \dfrac{A_1}{B_1}} = \frac{1}{2} \times \frac{A_2}{A_1} \times \frac{B_1}{B} \times \left(\left(2 - \frac{B'}{B} \right) + \frac{B'}{B} \times \frac{A_2}{A_1} \right) \qquad \text{(F-11)}$$

where B_1 is the initial free-surface width (Fig. F-1). Equation (F-11) gives an analytical solution of the square of the tidal bore Froude number (Fr_1^2) as a function of the cross-sectional ratio A_2/A_1, the ratio B'/B and the ratio B_1/B.

Equation (F-11) may be rewritten in the form of the cross-sectional ratio A_2/A_1 as a function of the tidal bore Froude number Fr_1:

$$\frac{A_2}{A_1} = \frac{1}{2} \times \frac{\sqrt{\left(2 - \frac{B'}{B}\right)^2 + 8 \times \frac{B'/B}{B_1/B} \times Fr_1^2} - \left(2 - \frac{B'}{B}\right)}{\frac{B'}{B}} \qquad (F-12)$$

F.3 PARTICULAR CASE $B \approx B' \approx B_1$

In some particular cases, the approximation $B \approx B' \approx B_1$ may hold. These include a relatively small bore (($A_2 - A_1)/A_1 \ll 1$)), a rectangular channel, or a channel cross-sectional shape such as $B(d_1 < y < d_2) = B_1 = B_2$. The latter situation corresponds to a channel with parallel walls next to the waterline.

For $B \approx B' \approx B_1$, the momentum principle may be simplified into:

$$\rho \times (V_1 + U) \times A_1 \times (V_1 - V_2) = \frac{1}{2} \times \rho \times g \times \frac{(A_1 + A_2) \times (A_2 - A_1)}{B} \qquad (F-13)$$

Using Equation (F-8), the combination of the continuity and momentum principle gives:

$$(U + V_1)^2 = \frac{1}{2} \times \frac{g}{A_1} \times \frac{(A_1 + A_2) \times A_2}{B} \qquad (F-14)$$

$$(V_1 - V_2)^2 = \frac{1}{2} \times \frac{g \times (A_1 + A_2) \times (A_2 - A_1)^2}{B \times A_1 \times A_2} \qquad (F-15)$$

The solution (Eq. (F-13) and (F-14)) is a rewriting of the development of LIGHTHILL (1978). Equation (F-14) yields the simplified expression:

$$\frac{(U + V_1)^2}{g \times \frac{A_1}{B_1}} = \frac{1}{2} \times \frac{A_2}{A_1} \times \frac{B_1}{B} \times \left(1 + \frac{A_2}{A_1}\right) \qquad (F-16)$$

Equation (F-16) may be rewritten:

$$\frac{A_2}{A_1} = \frac{1}{2} \times \left(\sqrt{1 + 8 \times Fr_1^2} - 1\right) \qquad (F-17)$$

Remark

Note that, for a small tidal bore ($A_2 - A_1)/A_1 \ll 1$), the bore may be undular and the approximation

of hydrostatic pressure distribution does not hold.

For a rectangular channel, Equation (F-17) yields:

$$\frac{d_2}{d_1} = \frac{1}{2} \times \left(\sqrt{1 + 8 \times Fr_1{}^2} - 1 \right) \qquad \text{Rectangular channel} \quad \text{(F-18)}$$

F.4 EFFETS OF FLOW RESISTANCE

In presence of some flow resistance, the momentum principle yields:

$$\rho \times (V_1 + U) \times A_1 \times (V_1 - V_2) = \frac{1}{2} \times \rho \times g \times \frac{(A_2 - A_1)}{B} \times \left(\left(2 - \frac{B'}{B} \right) \times A_1 + \frac{B'}{B} \times A_2 \right) + F_{\text{fric}}$$

$$\text{(F-19)}$$

The combination of the continuity and momentum principle gives:

$$(U + V_1)^2 = \frac{1}{2} \times \frac{g \times A_2}{A_1 \times B} \times \left(\left(2 - \frac{B'}{B} \right) \times A_1 + \frac{B'}{B} \times A_2 \right) + \frac{A_2}{A_2 - A_1} \times \frac{F_{\text{fric}}}{\rho \times A_1} \qquad \text{(F-20)}$$

$$(V_1 - V_2)^2 = \frac{1}{2} \times \frac{g \times (A_2 - A_1)^2}{B \times A_1 \times A_2} \times \left(\left(2 - \frac{B'}{B} \right) \times A_1 + \frac{B'}{B} \times A_2 \right) + \frac{A_2}{A_2 - A_1} \times \frac{F_{\text{fric}}}{\rho \times g \times \frac{A_1{}^2}{B}}$$

$$\text{(F-21)}$$

Equation (F-20) may be transformed into:

$$\frac{(U + V_1)^2}{g \times \frac{A_1}{B_1}} = \frac{1}{2} \times \frac{A_2}{A_1} \times \frac{B_1}{B} \times \left(\left(2 - \frac{B'}{B} \right) + \frac{B'}{B} \times \frac{A_2}{A_1} \right) + \frac{A_2}{A_2 - A_1} \times \frac{F_{\text{fric}}}{\rho \times g \times \frac{A_1{}^2}{B}} \qquad \text{(F-22)}$$

REFERENCES

BAZIN, H. (1865). "Recherches Expérimentales sur la Propagation des Ondes." *Mémoires présentés par divers savants à l'Académie des Sciences*, Paris, France, Vol. 19, pp. 495-644 (in French).

BÉLANGER, J.B. (1828). "Essai sur la Solution Numérique de quelques Problèmes Relatifs au Mouvement Permanent des Eaux Courantes." ('Essay on the Numerical Solution of Some Problems relative to Steady Flow of Water.') *Carilian-Goeury*, Paris, France, 38 pages & 5 tables (in French).

BÉLANGER, J.B. (1841). "Notes sur l'Hydraulique." ('Notes on Hydraulic Engineering.') *Ecole Royale des Ponts et Chaussées*, Paris, France, session 1841-1842, 223 pages (in French).

BOSSUT, Abbé C. (1772). "Traité Elémentaire d'Hydrodynamique." (Elementary Treaty on Hydrodynamics.') *Imprimerie Chardon*, Paris, France, 1st ed. (in French). (2nd ed. : 1786, Paris, France; 3rd ed. : 1796, Paris, France.)

BRADSHAW, P. (1971). "An Introduction to Turbulence and its Measurement." *Pergamon Press*, Oxford, UK, The Commonwealth and International Library of Science and technology Engineering and Liberal Studies, Thermodynamics and Fluid Mechanics Division, 218 pages.

BRANNER, J.C. (1884). "The Pororoca, or Bore, of the Amazon." *Science*, Vol. 4, No. 95, 28 Nov., pp. 488-492. (Also 1885, Rand, Avery & Co, Boston, USA, pp. 3-12. Also 1903, List of Publications by Members of the Department of Geology, Stanford University, USA.)

BRESSE, J.A. (1860). "Cours de Mécanique Appliquée Professé à l'Ecole des Ponts et Chaussées." ('Course in Applied Mechanics lectured at the Pont-et-Chaussées Engineering School.') *Mallet-Bachelier*, Paris, France (in French).

BROWN, G.O. (2002). "The History of the Darcy-Weisbach Equation for Pipe Flow Resistance." in Environmental and Water Resources History, Proc. ASCE 150th Anniversary (1852-2002), ASCE Civil Eng. Conf. and Expo., .Washington DC, J.R. ROGERS and A.J. FREDRICH Eds., pp. 34-43.

BUAT, P.L.G. du (1779). "Principes d'Hydraulique, vérifiés par un grand nombre d'expériences faites par ordre du gouvernement." ('Hydraulic Principles, verified by a large number of experiments.') *Imprimerie de Monsieur*, Paris, France, 1st ed. (in French). (2nd ed.: 1786, Paris, France, 2 volumes; 3rd ed.: 1816, Paris, France, 3 volumes)

BUTCHER, J.G. (2004). "The Closing of the Frontier. A History of the Marine Fisheries of Southeast Asia c. 1850-2000." *KITLV Press*, Leiden, The Netherlands, A Modern Economic History of Southeast Asia Series, 442 pages.

CANCINO, L., and NEVES, R. (1999). "Hydrodynamic and Sediment Suspension Modelling in Estuarine Systems. Part II: Application to the Western Scheldt and Gironde Estuaries." *Jl of Marine Systems*, Vol. 22, pp. 117-131.

CHANSON, H. (2001). "Flow Field in a Tidal Bore: a Physical Model." *Proc. 29th IAHR Congress*, Beijing, China, Theme E, Tsinghua University Press, Beijing, G. LI Ed., pp. 365-373. (CD-ROM, Tsinghua University Press.)

CHANSON, H. (2004). "Environmental Hydraulics of Open Channel Flows." *Elsevier Butterworth-Heinemann*, Oxford, UK, 483 pages.

CHANSON, H. (2007). "Le Potentiel de Vitesse pour les Ecoulements de Fluides Réels: la Contribution de Joseph-Louis Lagrange." ('Velocity Potential in Real Fluid Flows: Joseph-Louis Lagrange's Contribution.') *Jl La Houille Blanche*, No. 5, pp. 127-131 (DOI: 10.1051/lhb:2007072) (in French).

CHANSON, H. (2008). "Photographic Observations of Tidal Bores (Mascarets) in France." *Hydraulic Model Report No. CH71/08*, Div. of Civil Engineering, The University of Queensland, Brisbane, Australia, 104 pages, 1 movie and 2 audio files (ISBN 9781864999303).

CHANSON, H. (2009). "Development of the Bélanger Equation and Backwater Equation by Jean-Baptiste Bélanger (1828)." *Journal of Hydraulic Engineering*, ASCE, Vol. 135, No. 3, pp. 159-163 (DOI: 10.1061/(ASCE)0733-9429(2009)135:3(159)).

CHANSON, H. (2010). "Unsteady Turbulence in Tidal Bores: Effects of Bed Roughness." *Journal of Waterway, Port, Coastal, and Ocean Engineering*, ASCE, Vol. 136, No. 5, pp. 247-256 (DOI: 10.1061/(ASCE)WW.1943-5460.0000048).

CHANSON, H., JARNY, S., and COUSSOT, P. (2006). "Dam Break Wave of Thixotropic Fluid." *Journal of Hydraulic Engineering*, ASCE, Vol. 132, No. 3, pp. 280-293 (DOI: 10.1061/(ASCE)0733-9429(2006)132:3(280)).

CHANSON, H., TAKEUCHI, M., and TREVETHAN, M. (2008). "Using Turbidity and Acoustic Backscatter Intensity as Surrogate Measures of Suspended Sediment Concentration in a Small Sub-Tropical Estuary." *Journal of Environmental Management*, Vol. 86, No. 4, pp. 1406-1416 (DOI: 10.1016/j.jenvman.2007.07.009).

CHANSON, H., and TAN, K.K. (2010). "Particle Dispersion under Tidal Bores: Application to Sediments and Fish Eggs." *Proc. 7th International Conference on Multiphase Flow ICMF 2010*, Tampa FL, USA, May 30-June 4, Paper No. 12.7.3, 9 pages.

CHEN, Jiyu, LIU, Cangzi, ZHANG, Chongle, and WALKER, H.J. (1990). "Geomorphological Development and Sedimentation in Qiantang Estuary and Hangzhou Bay." *Jl of Coastal Res.*, Vol. 6, No. 3, pp. 559-572.

CHEN, S. (2003). "Tidal Bore in the North Branch of the Changjiang Estuary." *Proc. Intl Conf. on Estuaries & Coasts ICEC-2003*, Hangzhou, China, Nov. 8-11, Intl Research & Training Center on Erosion & Sedimentation Ed., Vol. 1, pp. 233-239.

DARCY, H.P.G. (1856). "Les Fontaines Publiques de la Ville de Dijon." ('The Public Fountains of the City of Dijon.') *Victor Dalmont*, Paris, France, 647 pages (in French).

DARCY, H. (1856). "The Public Fountains of the City of Dijon. Exposition and Application of principles to Follow and Formulas to use in Questions of Water Distribution." *Kendal/Hunt Publ.*, Dubuque, Iowa, English Translation by P. BOBECK.

DARCY, H.P.G. (1858). "Recherches Expérimentales relatives aux Mouvements de l'Eau dans les Tuyaux." ('Experimental Research on the Motion of Water in Pipes.') *Mémoires Présentés à l'Académie des Sciences de l'Institut de France*, Vol. 14, p. 141 (in French).

DARCY, H.P.G., and BAZIN, H. (1865). "Recherches Hydrauliques." ('Hydraulic Research.') *Imprimerie Impériales*, Paris, France, Parties 1ère et 2ème (in French).

DOCHERTY, N.J., and CHANSON, H. (2010). "Characterisation of Unsteady Turbulence in Breaking Tidal Bores including the Effects of Bed Roughness." *Hydraulic Model Report No. CH76/10*, School of Civil Engineering, The University of Queensland, Brisbane, Australia, 112 pages.

DOXARAN, D., FROIDEFOND, J.M., CASTAING, P., and BABIN, M. (2009). "Dynamics of the Turbidity in a Macrotidal Estuary (the Gironde, France): Observations from Field and MODIS Satellite Data." *Estuarine, Coastal and Shelf Science*, Vol. 81, pp. 321-332.

DUPUIT, A.J.E. (1848). "Etudes Théoriques et Pratiques sur le Mouvement des Eaux Courantes." *Dunod*, Paris, France (in French).

FAWER, C. (1937). "Etude de Quelques Ecoulements Permanents à Filets Courbes." *Thesis*, Lausanne, Switzerland, Imprimerie La Concorde, 127 pages (in French).

FROUDE, W. (1872). "Experiments on the Surface-friction experienced by a Plane moving through Water." *British Association for the Advancement of Science*, 42nd meeting.

FUGATE, D.C., and FRIEDRICHS, C.T. (2002). "Determining Concentration and Fall Velocity of Estuarine Particle Populations using ADV, OBS and LISST." *Continental Shelf Research*, Vol. 22, pp. 1867-1886.

GORING, D.G., and NIKORA, V.I. (2002). "Despiking Acoustic Doppler Velocimeter Data." *Jl of Hyd. Engrg.*, ASCE, Vol. 128, No. 1, pp. 117-126. Discussion: Vol. 129, No. 6, pp. 484-489.

GRAF, W.H. (1971). "Hydraulics of Sediment Transport". *McGraw-Hill*, New York, USA.

GREB, S.F., and ARCHER, A.W. (2007). "Soft-Sediment Deformation Produced by Tides in a Meizoseismic Area, Turnagain Arm, Alaska." *Geology*, Vol. 35, No. 5, pp. 435-438.

HA, H.K., HSU, W.Y., MAA, J.P.Y., SHAO, Y.Y., and HOLLAND, C.W. (2009). "Using ADV Backscatter Strength for Measuring Suspended Cohesive Sediment Concentration." *Continental Shelf Research*, Vol. 29, pp. 1310-1316.

HENDERSON, F.M. (1966). "Open Channel Flow." *MacMillan Company*, New York, USA.

HORNUNG, H.G., WILLERT, C., and TURNER, S. (1995). "The Flow Field Downstream of a Hydraulic Jump." *Jl of Fluid Mech.*, Vol. 287, pp. 299-316.

HUANG, X., and GARCIA, M. (1998). "A Herschel-Bulkley Model for Mud Flow Down a Slope." *Jl of Fluid Mech.*, Vo. 374, pp. 305-333.

JULIEN, P.Y. (1995). "Erosion and Sedimentation." *Cambridge University Press*, Cambridge, UK, 280 pages.

KAWANISI, K., and YOKOSI, S. (1997). "Characteristics of Suspended Sediment and Turbulence in a Tidal Boundary Layer." *Estuarine, Coastal and Shelf Science*, Vol. 38, pp. 447-469.

KJERFVE, B., and FERREIRA, H.O. (1993). "Tidal Bores: First Ever Measurements." *Ciência e Cultura (Jl of the Brazilian Assoc. for the Advancement of Science)*, Vol. 45, No. 2, March/April, pp. 135-138.

KOCH, C., and CHANSON, H. (2009). "Turbulence Measurements in Positive Surges and Bores." *Journal of Hydraulic Research*, IAHR, Vol. 47, No. 1, pp. 29-40 (DOI: 10.3826/jhr.2009.2954).

LEFEUVRE, J.C., and BOUCHARD, V. (2002). "From a Civil Engineering Project to an Ecological Engineering Project: An Historical Perspective from the Mont Saint Michel Bay (France)." *Ecological Engineering*, Vol. 18, pp. 593-606.

LEWIS, A.W. (1972). "Field Studies of a Tidal Bore in the River Dee." *M.Sc. thesis*, Marine Science Laboratories, University College of North Wales, Bangor, UK.

LIGGETT, J.A. (1994). "Fluid Mechanics." *McGraw-Hill*, New York, USA.

LIGHTHILL, J. (1978). "Waves in Fluids." *Cambridge University Press*, cambridge, UK, 504 pages.

MALANDAIN, J.J. (1988). "La Seine au Temps du Mascaret." ('The Seine River at the Time of the Mascaret.') *Le Chasse-Marée*, No. 34, pp. 30-45 (in French).

McLELLAND, S.J., and NICHOLAS, A.P. (2000). "A New Method for Evaluating Errors in High-Frequency ADV Measurements." *Hydrological Processes*, Vol. 14, pp. 351-366.

NAVARRE, P. (1995). "Aspects Physiques du Caractère Ondulatoire du Macaret en Dordogne." ('Physical Features of the Undulations of the Dordogne River Tidal Bore.') *D.E.A. thesis*, Univ. of Bordeaux, France, 72 pages (in French).

Nortek (2005). "Vector Current Meter. User Manual" *Nortek AS*, Revision H, 86 pages.

PIQUET, J. (1999). "Turbulent Flows: Models and Physics." *Springer*, Berlin, Germany, 761 pages.

REECH, F. (1852). "Cours de Mécanique d'après la Nature Genéralement Flexible et Elastique des Corps." *Carilian-Goeury*, Paris, France (in French).

ROUSSEL, N., LE ROY, R., and COUSSOT, P. (2004). "Thixotropy Modelling at Local and Macroscopic Scales." *Jl of Non-Newtonian Fluid Mech.*, Vol. 117, No. 2-3, pp. 85-95.

RULIFSON, R.A., and TULL, K.A. (1999). "Striped Bass Spawning in a Tidal Bore River : the Shubenacadie Estuary, Atlantic Canada." *Trans. American Fisheries Soc.*, Vol. 128, pp. 613-624.

SIMPSON, J.H., FISHER, N.R., and WILES, P. (2004). "Reynolds Stress and TKE Production in an Estuary with a Tidal Bore." *Estuarine, Coastal and Shelf Science*, Vol. 60, No. 4, pp. 619-627.

SOTTOLOCHIO, A., and CASTAING, P. (1999). "A Synthesis on Seasonal Dynamics of Highly-Concentrated Structures in the Gironde Estuary." *C.R. Acad. Sci. Paris, Earth & Planetary Sciences*, Vol. 329, pp. 795-800.

TESSIER, B., and TERWINDT, J.H.J. (1994). "An Example of Soft-Sediment Deformations in an intertidal Environment - The Effect of a Tidal Bore". *Comptes-Rendus de l'Académie des Sciences*, Série II, Vol. 319, No. 2, Part 2, pp. 217-233 (in French).

TRICKER, R.A.R. (1965). "Bores, Breakers, Waves and Wakes." *American Elsevier Publ. Co.*, New York, USA.

TULL, K.A. (1997). "Spawning Activity of triped Bass in a Tidal Bore River: the Shubenacadie-Stewiacke System, Nova Scotia." *M.Sc. thesis*, University of East Carolina, Dept of Biology, 140 pages.

WILSON, S.D.R., and BURGESS, S.L. (1998). "The Steady, Speading Flow of a Rivulet of Mud." *Jl Non-Newtonian Fluid Mech.*, Vol. 79, pp. 77-85.

WOLANSKI, E., MOORE, K., SPAGNOL, S., D'ADAMO, N., and PATTIERATCHI, C. (2001). "Rapid, Human-Induced Siltation of the Macro-Tidal Ord River Estuary, Western Australia." *Estuarine, Coastal and Shelf Science*, Vol. 53, pp. 717-732.

WOLANSKI, E., WILLIAMS, D., SPAGNOL, S., and CHANSON, H. (2004). "Undular Tidal Bore Dynamics in the Daly Estuary, Northern Australia." *Estuarine, Coastal and Shelf Science*, Vol. 60, No. 4, pp. 629-636.

Internet bibliography

VigiCrue	{http://www.vigicrues.gouv.fr/}
VigiCrue Bordeaux	{http://www.vigicrues.gouv.fr/niveau3.php?idspc=13&idstation=1429}
SHOM	{http://www.shom/fr}
SHOM - Reference Altitudes	{http://www.shom.fr/fr_page/fr_act_oceano/RAM/RAM_P1.htm#Contexte%20et%20aspects%20r%C3%A9glementaires}
SHOM - Reference Altitude: Zone Sud Gascogne	{http://www.shom.fr/fr_page/fr_act_oceano/RAM/RAM_SG_2010.pdf}
The tidal bore of the Seine River	{http://www.uq.edu.au/~e2hchans/mascaret.html}
Tidal bores, Mascaret, Pororoca. Myths, Fables and Reality !!!	{http://www.uq.edu.au/~e2hchans/tid_bore.html}
Mascaret, Aegir, Pororoca, Tidal Bore. Quid? Où? Quand? Comment? Pourquoi?	{http://espace.library.uq.edu.au/view.php?pid=UQ:9447}
The Rumble Sound Generated by a Tidal Bore Event in the Baie du Mont Saint Michel	{http://espace.library.uq.edu.au/view/UQ:178445}

Open Access Repositories

OAIster	{http://www.oaister.org/}
UQeSpace	{http://espace.library.uq.edu.au/}

Bibliographic reference of the Report CH79/10
The Hydraulic Model research report series CH is a refereed publication published by the School of
Civil Engineering at the University of Queensland, Brisbane, Australia.

The bibliographic reference of the present report is:

CHANSON, H., LUBIN, P., SIMON, B., and REUNGOAT, D. (2010). "Turbulence and Sediment
    Processes in the Tidal Bore of the Garonne River: First Observations." *Hydraulic Model Report
    No. CH79/10*, School of Civil Engineering, The University of Queensland, Brisbane, Australia,
    97 pages (ISBN 9781742720104).

The Report CH79/10 is available, in the present form, as a PDF file on the Internet at UQeSpace:

http://espace.library.uq.edu.au/

It is listed at:

http://espace.library.uq.edu.au/list/author_id/193/

HYDRAULIC MODEL RESEARCH REPORT CH

The Hydraulic Model Report CH series is published by the School of Civil Engineering at the University of Queensland. Orders of any reprint(s) of the Hydraulic Model Reports should be addressed to the School Secretary.

School Secretary, School of Civil Engineering, The University of Queensland

Brisbane 4072, Australia - Tel.: (61 7) 3365 3619 - Fax : (61 7) 3365 4599

Url: http://www.eng.uq.edu.au/civil/ Email: hodciveng@uq.edu.au

Report CH	Unit price	Quantity	Total price
CHANSON, H., LUBIN, P., SIMON, B., and REUNGOAT, D. (2010). "Turbulence and Sediment Processes in the Tidal Bore of the Garonne River: First Observations." *Hydraulic Model Report No. CH79/10*, School of Civil Engineering, The University of Queensland, Brisbane, Australia, 97 pages (ISBN 9781742720104).	AUD$60.00		
CHACHEREAU, Y., and CHANSON, H., (2010). "Free-Surface Turbulent Fluctuations and Air-Water Flow Measurements in Hydraulics Jumps with Small Inflow Froude Numbers." *Hydraulic Model Report No. CH78/10*, School of Civil Engineering, The University of Queensland, Brisbane, Australia, 133 pages (ISBN 9781742720036).	AUD$60.00		
CHANSON, H., BROWN, R., and TREVETHAN, M. (2010). " Turbulence Measurements in a Small Subtropical Estuary under King Tide Conditions." *Hydraulic Model Report No. CH77/10*, School of Civil Engineering, The University of Queensland, Brisbane, Australia, 82 pages (ISBN 9781864999969).	AUD$60.00		
DOCHERTY, N.J., and CHANSON, H. (2010). "Characterisation of Unsteady Turbulence in Breaking Tidal Bores including the Effects of Bed Roughness." *Hydraulic Model Report No. CH76/10*, School of Civil Engineering, The University of Queensland, Brisbane, Australia, 112 pages (ISBN 9781864999884).	AUD$60.00		
CHANSON, H. (2009). "Advective Diffusion of Air Bubbles in Hydraulic Jumps with Large Froude Numbers: an Experimental Study." *Hydraulic Model Report No. CH75/09*, School of Civil Engineering, The University of Queensland, Brisbane, Australia, 89 pages & 3 videos (ISBN 9781864999730).	AUD$60.00		
CHANSON, H. (2009). "An Experimental Study of Tidal Bore Propagation: the Impact of Bridge Piers and Channel Constriction." *Hydraulic Model Report No. CH74/09*, School of Civil Engineering, The University of Queensland, Brisbane, Australia, 110 pages and 5 movies (ISBN 9781864999600).	AUD$60.00		
CHANSON, H. (2008). "Jean-Baptiste Charles Joseph BÉLANGER (1790-1874), the Backwater Equation and the Bélanger Equation." *Hydraulic Model Report No. CH69/08*, Div. of Civil Engineering, The University of Queensland, Brisbane, Australia, 40 pages (ISBN 9781864999211).	AUD$60.00		

GOURLAY, M.R., and HACKER, J. (2008). "Reef-Top Currents in Vicinity of Heron Island Boat Harbour, Great Barrier Reef, Australia: 2. Specific Influences of Tides Meteorological Events and Waves." *Hydraulic Model Report No. CH73/08*, Div. of Civil Engineering, The University of Queensland, Brisbane, Australia, 331 pages (ISBN 9781864999365).	AUD$60.00		
GOURLAY, M.R., and HACKER, J. (2008). "Reef Top Currents in Vicinity of Heron Island Boat Harbour Great Barrier Reef, Australia: 1. Overall influence of Tides, Winds, and Waves." *Hydraulic Model Report CH72/08*, Div. of Civil Engineering, The University of Queensland, Brisbane, Australia, 201 pages (ISBN 9781864999358).	AUD$60.00		
LARRARTE, F., and CHANSON, H. (2008). "Experiences and Challenges in Sewers: Measurements and Hydrodynamics." *Proceedings of the International Meeting on Measurements and Hydraulics of Sewers*, Summer School GEMCEA/LCPC, 19-21 Aug. 2008, Bouguenais, Hydraulic Model Report No. CH70/08, Div. of Civil Engineering, The University of Queensland, Brisbane, Australia (ISBN 9781864999280).	AUD$60.00		
CHANSON, H. (2008). "Photographic Observations of Tidal Bores (Mascarets) in France." *Hydraulic Model Report No. CH71/08*, Div. of Civil Engineering, The University of Queensland, Brisbane, Australia, 104 pages, 1 movie and 2 audio files (ISBN 9781864999303).	AUD$60.00		
CHANSON, H. (2008). "Turbulence in Positive Surges and Tidal Bores. Effects of Bed Roughness and Adverse Bed Slopes." *Hydraulic Model Report No. CH68/08*, Div. of Civil Engineering, The University of Queensland, Brisbane, Australia, 121 pages & 5 movie files (ISBN 9781864999198)	AUD$70.00		
FURUYAMA, S., and CHANSON, H. (2008). "A Numerical Study of Open Channel Flow Hydrodynamics and Turbulence of the Tidal Bore and Dam-Break Flows." *Report No. CH66/08*, Div. of Civil Engineering, The University of Queensland, Brisbane, Australia, May, 88 pages (ISBN 9781864999068).	AUD$60.00		
GUARD, P., MACPHERSON, K., and MOHOUPT, J. (2008). "A Field Investigation into the Groundwater Dynamics of Raine Island." *Report No. CH67/08*, Div. of Civil Engineering, The University of Queensland, Brisbane, Australia, February, 21 pages (ISBN 9781864999075).	AUD$40.00		
FELDER, S., and CHANSON, H. (2008). "Turbulence and Turbulent Length and Time Scales in Skimming Flows on a Stepped Spillway. Dynamic Similarity, Physical Modelling and Scale Effects." *Report No. CH64/07*, Div. of Civil Engineering, The University of Queensland, Brisbane, Australia, March, 217 pages (ISBN 9781864998870).	AUD$60.00		
TREVETHAN, M., CHANSON, H., and BROWN, R.J. (2007). "Turbulence and Turbulent Flux Events in a Small Subtropical Estuary." Report No. CH65/07, Div. of Civil Engineering, The University of Queensland, Brisbane, Australia, November, 67 pages (ISBN 9781864998993)	AUD$60.00		
MURZYN, F., and CHANSON, H. (2007). "Free Surface, Bubbly flow and Turbulence Measurements in Hydraulic Jumps." *Report CH63/07*, Div. of Civil Engineering, The University of Queensland, Brisbane, Australia, August, 116 pages (ISBN 9781864998917).	AUD$60.00		
KUCUKALI, S., and CHANSON, H. (2007). "Turbulence in Hydraulic Jumps: Experimental Measurements." *Report No. CH62/07*, Div. of Civil Engineering, The University of Queensland, Brisbane, Australia, July, 96 pages (ISBN 9781864998825).	AUD$60.00		
CHANSON, H., TAKEUCHI, M, and TREVETHAN, M. (2006). "Using Turbidity and Acoustic Backscatter Intensity as Surrogate Measures of Suspended Sediment Concentration. Application to a Sub-Tropical Estuary (Eprapah Creek)." *Report No. CH60/06*, Div. of Civil Engineering, The University of Queensland, Brisbane, Australia, July, 142 pages (ISBN 1864998628).	AUD$60.00		

CAROSI, G., and CHANSON, H. (2006). "Air-Water Time and Length Scales in Skimming Flows on a Stepped Spillway. Application to the Spray Characterisation." *Report No. CH59/06*, Div. of Civil Engineering, The University of Queensland, Brisbane, Australia, July (ISBN 1864998601).	AUD$60.00		
TREVETHAN, M., CHANSON, H., and BROWN, R. (2006). "Two Series of Detailed Turbulence Measurements in a Small Sub-Tropical Estuarine System." *Report No. CH58/06*, Div. of Civil Engineering, The University of Queensland, Brisbane, Australia, Mar. (ISBN 1864998520).	AUD$60.00		
KOCH, C., and CHANSON, H. (2005). "An Experimental Study of Tidal Bores and Positive Surges: Hydrodynamics and Turbulence of the Bore Front." *Report No. CH56/05*, Dept. of Civil Engineering, The University of Queensland, Brisbane, Australia, July (ISBN 1864998245).	AUD$60.00		
CHANSON, H. (2005). "Applications of the Saint-Venant Equations and Method of Characteristics to the Dam Break Wave Problem." *Report No. CH55/05*, Dept. of Civil Engineering, The University of Queensland, Brisbane, Australia, May (ISBN 1864997966).	AUD$60.00		
CHANSON, H., COUSSOT, P., JARNY, S., and TOQUER, L. (2004). "A Study of Dam Break Wave of Thixotropic Fluid: Bentonite Surges down an Inclined plane." *Report No. CH54/04*, Dept. of Civil Engineering, The University of Queensland, Brisbane, Australia, June, 90 pages (ISBN 1864997710).	AUD$60.00		
CHANSON, H. (2003). "A Hydraulic, Environmental and Ecological Assessment of a Sub-tropical Stream in Eastern Australia: Eprapah Creek, Victoria Point QLD on 4 April 2003." *Report No. CH52/03*, Dept. of Civil Engineering, The University of Queensland, Brisbane, Australia, June, 189 pages (ISBN 1864997044).	AUD$90.00		
CHANSON, H. (2003). "Sudden Flood Release down a Stepped Cascade. Unsteady Air-Water Flow Measurements. Applications to Wave Run-up, Flash Flood and Dam Break Wave." *Report CH51/03*, Dept of Civil Eng., Univ. of Queensland, Brisbane, Australia, 142 pages (ISBN 1864996552).	AUD$60.00		
CHANSON, H,. (2002). "An Experimental Study of Roman Dropshaft Operation : Hydraulics, Two-Phase Flow, Acoustics." *Report CH50/02*, Dept of Civil Eng., Univ. of Queensland, Brisbane, Australia, 99 pages (ISBN 1864996544).	AUD$60.00		
CHANSON, H., and BRATTBERG, T. (1997). "Experimental Investigations of Air Bubble Entrainment in Developing Shear Layers." *Report CH48/97*, Dept. of Civil Engineering, University of Queensland, Australia, Oct., 309 pages (ISBN 0 86776 748 0).	AUD$90.00		
CHANSON, H. (1996). "Some Hydraulic Aspects during Overflow above Inflatable Flexible Membrane Dam." *Report CH47/96*, Dept. of Civil Engineering, University of Queensland, Australia, May, 60 pages (ISBN 0 86776 644 1).	AUD$60.00		
CHANSON, H. (1995). "Flow Characteristics of Undular Hydraulic Jumps. Comparison with Near-Critical Flows." *Report CH45/95*, Dept. of Civil Engineering, University of Queensland, Australia, June, 202 pages (ISBN 0 86776 612 3).	AUD$60.00		
CHANSON, H. (1995). "Air Bubble Entrainment in Free-surface Turbulent Flows. Experimental Investigations." *Report CH46/95*, Dept. of Civil Engineering, University of Queensland, Australia, June, 368 pages (ISBN 0 86776 611 5).	AUD$80.00		
CHANSON, H. (1994). "Hydraulic Design of Stepped Channels and Spillways." *Report CH43/94*, Dept. of Civil Engineering, University of Queensland, Australia, Feb., 169 pages (ISBN 0 86776 560 7).	AUD$60.00		
POSTAGE & HANDLING (per report)	AUD$10.00		
GRAND TOTAL			

OTHER HYDRAULIC RESEARCH REPORTS

Reports/Theses	Unit price	Quantity	Total price
TREVETHAN, M. (2008). "A Fundamental Study of Turbulence and Turbulent Mixing in a Small Subtropical Estuary." Ph.D. thesis, Div. of Civil Engineering, The University of Queensland, 342 pages.	AUD$100.00		
GONZALEZ, C.A. (2005). "An Experimental Study of Free-Surface Aeration on Embankment Stepped Chutes." *Ph.D. thesis*, Dept of Civil Engineering, The University of Queensland, Brisbane, Australia, 240 pages.	AUD$80.00		
TOOMBES, L. (2002). "Experimental Study of Air-Water Flow Properties on Low-Gradient Stepped Cascades." *Ph.D. thesis*, Dept of Civil Engineering, The University of Queensland, Brisbane, Australia.	AUD$100.00		
CHANSON, H. (1988). "A Study of Air Entrainment and Aeration Devices on a Spillway Model." *Ph.D. thesis*, University of Canterbury, New Zealand.	AUD$60.00		
POSTAGE & HANDLING (per report)	AUD$10.00		
GRAND TOTAL			

CIVIL ENGINEERING RESEARCH REPORT CE

The Civil Engineering Research Report CE series is published by the School of Civil Engineering at the University of Queensland. Orders of any of the Civil Engineering Research Report CE should be addressed to the School Secretary.

School Secretary, School of Civil Engineering, The University of Queensland

Brisbane 4072, Australia

Tel.: (61 7) 3365 3619   Fax : (61 7) 3365 4599

Url: http://www.eng.uq.edu.au/civil/ Email: hodciveng@uq.edu.au

Recent Research Report CE	Unit price	Quantity	Total price
CALLAGHAN, D.P., NIELSEN, P., and CARTWRIGHT, N. (2006). "Data and Analysis Report: Manihiki and Rakahanga, Northern Cook Islands - For February and October/November 2004 Research Trips." *Research Report CE161*, Division of Civil Engineering, The University of Queensland (ISBN No. 1864998318).	AUD$10.00		
GONZALEZ, C.A., TAKAHASHI, M., and CHANSON, H. (2005). "Effects of Step Roughness in Skimming Flows: an Experimental Study." *Research Report No. CE160*, Dept. of Civil Engineering, The University of Queensland, Brisbane, Australia, July (ISBN 1864998105).	AUD$10.00		

CHANSON, H., and TOOMBES, L. (2001). "Experimental Investigations of Air Entrainment in Transition and Skimming Flows down a Stepped Chute. Application to Embankment Overflow Stepped Spillways." *Research Report No. CE158*, Dept. of Civil Engineering, The University of Queensland, Brisbane, Australia, July, 74 pages (ISBN 1 864995297).	AUD$10.00		
HANDLING (per order)	AUD$10.00		
GRAND TOTAL			

Note: Prices include postages and processing.

PAYMENT INFORMATION

1- VISA Card

Name on the card :	
Visa card number :	
Expiry date :	
Amount :	AUD$ ....

2- Cheque/remittance payable to: THE UNIVERSITY OF QUEENSLAND and crossed "Not Negotiable".

N.B. For overseas buyers, cheque payable in Australian Dollars drawn on an office in Australia of a bank operating in Australia, payable to: THE UNIVERSITY OF QUEENSLAND and crossed "Not Negotiable".

Orders of any Research Report should be addressed to the School Secretary.

School Secretary, School of Civil Engineering, The University of Queensland

Brisbane 4072, Australia - Tel.: (61 7) 3365 3619 - Fax : (61 7) 3365 4599

Url: http://www.eng.uq.edu.au/civil/ Email: hodciveng@uq.edu.au